A STUDY OF DEFLAGRATION TO DETIONATION TRANSITION IN A PULSED DETONATION ENGINE

A Thesis
Presented To
The Academic Faculty

By

David M Chapin

In Partial Fulfillment
of the Requirements for the Degree
Masters of Science in the
School of Mechanical Engineering

Georgia Institute of Technology

December, 2005

A Study of Deflagration to Detonation Transition In a Pulsed Detonation Engine

Approved by:

Dr. Tim Lieuwen, Advisor
School of Aerospace Engineering
Georgia Institute of Technology

Dr. Ben T Zinn, Advisor
School of Mechanical Engineering
Georgia Institute of Technology

Dr. Anthony J Dean
Advanced Technology Leader
General Electric Global Research

Dr. William Wepfer
Vice Provost DLPE
Georgia Institute of Technology

Date Approved: November 01, 2005

I would like to dedicate this work
to my family, friends, and coworkers,
who have supported me throughout the course
of this research.

ACKNOWLEDGMENTS

I would like to take this opportunity thank Tony Dean for his support and technical mentoring throughout this project and other projects. I would like to thank Kent Cueman for giving me the chance to show what I could do and for being a great personal mentor. I would like to thank Tim Lieuwen for being my thesis advisor and staying with me through the tougher times. I would like to thank Venkat Tangirala for providing the computational analysis for comparison.

I would also like to thank Benn Zinn and William Wepfer for serving on my thesis reading committee.

Finally, I would like to thank General Electric and the EEDP program for allowing me to perform this research and funding me throughout my post-graduate education.

TABLE OF CONTENTS

LIST OF TABLES

LIST OF FIGURES

LIST OF SYMBOLS

L_T	Integral turbulence length scale
δ	Laminar flame thickness
ρ	Density
σ	$\rho_{reactant}/\rho_{product}$
S_L	Laminar flame speed
c_{sr}	Speed of sound in reactants
c_{sp}	Speed of sound in products
γ_r	Ratio of specific heats of reactants
Le	Lewis number
Ze	Zeldovich number = $E_a(T_b-T_u)/(RT_b^2)$
Ea	Activation Energy
T_b	Adiabatic Flame Temperature
T_u	Unburned Reactants Temperature
T_o	Inner Layer Temperature
λ	Detonation cell size
d/λ	Minimum tube diameter criteria
L/D	Normalized length (length/diameter) also X/D
BR	Blockage Ratio = $(D_{Tube}^2-D_{Orifice}^2)/(D_{Tube}^2)$
CJ	Chapman-Jouguet

SUMMARY

A Pulse Detonation Engine (PDE) is a propulsion device that takes advantage of the pressure rise inherent to the efficient burning of fuel-air mixtures via detonations. Detonation initiation is a critical process that occurs in the cycle of a PDE. A practical method of detonation initiation is Deflagration-to-Detonation Transition (DDT), which describes the acceleration of a subsonic deflagration created using low initiation energies to a supersonic detonation. The DDT process is not well understood due to a wide range of time and length scales involving complex chemistry, turbulence and unsteady pressure waves. This thesis presents the effects of obstacle spacing, blockage ratio, DDT section length, and airflow on DDT in hydrogen-air and ethylene-air mixtures for a repeating PDE. The test rig used was a 2" diameter, 40" long, continuous flow, repeating PDE located at the General Electric Global Research Center in Niskayuna, New York.

A fundamental study of experiments performed on a modular orifice plate obstacle DDT geometry reveals that all three factors tested (obstacle blockage ratio, length of DDT section, and spacing between obstacles) are statistically significant. All of the interactions between the factors except for the interaction of the blockage ratio with the spacing between obstacles are also significant. Flame velocities were obtained using time-of-flight measurements of the pressure wave between two dynamic pressure transducers located at the tail end of the PDE tube. To better characterize the non-linearity of the DDT process, further studies were performed using a measurement technique that utilized a clear polycarbonate detonation chamber and a high-speed camera to capture combustion chemiluminescence and track the leading flame front as it progressed through the PDE. This technique provided higher resolution tracking of the position and acceleration of the combustion front.

Results show that most obstacle configurations hinder the distance and time to transition to detonation if excess obstacles, past what was minimally required to transition to detonation, are present. Data from the experiments reported here provides validation runs for computational simulation. In some cases as little as 20% difference was seen.

The minimum DDT length for 0.15 lb/s hydrogen-air studies was 8 L/D from the spark location, while for ethylene it was 16 L/D. It was also observed that increasing the airflow rate through the tube from 0.1 to 0.3 lbs/sec decreased the time required for DDT by 26%, from 3.9 ms to 2.9 ms while having minimal effect on run-up distance.

CHAPTER I: INTRODUCTION

Pulse detonation engines (PDEs) have emerged as potential devices to better utilize the chemical energy content of reactive fuel/air mixtures [1]. One of the main advantages of PDEs is that detonations create less entropy when they combust a fuel/air mixture than conventional constant pressure combustion processes such as those used in current gas turbines [2], resulting in a more efficient thermodynamic cycle. Establishing whether PDEs can achieve higher operating efficiency than conventional propulsion systems (i.e. gas turbines, ramjets, etc) is the focus of many research groups around the world.

One of the main challenges to make PDEs practical is the requirement for repeated initiation of detonations within the detonation chamber at high frequencies. Pulse detonation engines primarily rely on Deflagration-to-Detonation Transition (DDT) to avoid the high energy required for direct initiation. DDT is the process whereby a deflagration is initiated using a weak energy source (typically tens or hundreds of milliJoules). The subsonic flame is accelerated via a series of gas dynamic processes, eventually transitioning to a supersonic detonation before exiting the combustion tube. A drawback of this approach for practical devices is the necessary length and time for transition to detonation (referred to as the run-up distance and time, respectively), which can limit cycle frequency. One method to reduce the run-up distance is the addition of oxygen in the initiation region [3]. This can greatly reduce the length required for DDT but can add significant complexity, weight, and logistical requirements to a propulsion system. Another method, the focus of this thesis, is to place obstacles inside the

detonation chamber. This has also been shown to significantly reduce run-up distance in fuel-air mixtures with little additional weight or complexity. Optimization for an obstacle-based DDT section is a trade-off between minimizing run-up distance via enhanced turbulence, and minimizing performance loss (pressure losses) via less obstacles or smaller blockage ratio. Little previous research has been found that quantifies the performance effects of obstacle dimensions for single-shot detonation chambers or repeating PDEs.

A bench-scale PDE located at the General Electric Global Research Center in Niskayuna, New York consists of a 2" schedule 40 stainless steel pipe about 40" long, open on one end. Both Hydrogen-Air and Ethylene-Air mixtures were examined. DDT experimentation concentrated around a modular orifice plate obstacle geometry spaced along the length of the DDT section. Characterization of this type of device was obtained by varying the number of obstacles, the distance between the obstacles, and the blockage ratio of each obstacle. This thesis describes the facilities used, the experimental methods employed and the experimental and computational results that were obtained. The key findings are summarized and recommendations are made for optimal DDT designs as well as future DDT experiments.

CHAPTER II: BACKGROUND

Previous Work:

Shepherd et al. [4] characterize the DDT process as having four phases: Deflagration initiation, flame acceleration, formation and amplification of explosion centers, and formation of a detonation wave. Three positive-feedback flame acceleration mechanisms are proposed: Flame interaction with shocked reactants, flame interaction with reflected shocks, and lastly flame interaction with solid based obstacles and gas dynamic jets.

Shepherd also describes DDT as a fundamental change in propagation mechanism. Flame propagation via the diffusive and turbulent mixing processes of low-speed flow are replaced in detonation propagation by the process of convected explosions or reaction waves coupled to initiating shock waves [4].

Chan et al. mentions the existence of a critical Mach number of 1.5 that the flame must reach in order to be able to transition to detonation [5]. He draws the conclusion that the "existence of a critical flame Mach number implies that the dominant mechanism for DDT in H2-[air] mixtures is related to the strength of its precursor shock". This relates to the shock-focusing phenomenon, induced by obstacles or end walls, which can create local hot spots in the mixture that are of high enough temperature to directly initiate detonation. Since there are numerous obstacles in any given DDT section, this creates opportunities for the creation of these hotspots. This supports Shepherd's findings relating to the formation of explosion centers.

One of the challenges facing PDE engines is characterization and optimization of DDT behavior. By transitioning to detonation quickly (< 1 ms), in small length scales, and more reliably, one can achieve higher frequencies, resulting in higher thrust. Many methods have been employed to characterize the DDT process in single shot detonation tubes. However, little work has been performed to study DDT behavior during cyclic operation of a continuous flow PDE. Work by Lee et Al. [6] established the primary obstacle blockage ratio used for this experimentation. His experimentation with various gaseous fuels (H_2, C_2H_2, C_2H_4, C_3H_8, and CH_4) in 18 meter long single-shot tubes of various diameters (5, 15, and 30 cm) concluded that 0.43 was the optimal blockage ratio and 1 diameter was the optimum obstacle spacing to "achieve the maximum flame acceleration and the highest possible terminal flame speeds." He went on to conjecture that "if the obstacles are too close, most likely the burnout time of the pockets of gas between the obstacles is longer than the transit time of the core of the flame through the orifice. For larger obstacle spacing, the accelerated flame beyond each obstacle begins to attenuate before the next obstacle is reached", effectively reducing the cascading effects of the flame acceleration. The full length of Lee's experimental 18-meter long detonation tube contained obstacles. He assumed that this would make sure "adequate stimulus was provided for the flame acceleration process to reach the maximum possible flame speed and maintain it within the available length of the combustion tube".

Another challenge with PDEs is the use of hydrocarbon fuels. To establish methods and a baseline, the initial experiments reported here were conducted with hydrogen-air mixtures. However, in latter experiments heavier hydrocarbons, which are harder to detonate, such as ethylene and ethane were used. Both the cycle time and the

run-up distance to detonation varied greatly between the various fuels as well as the sensitivity to equivalence ratio and the range of ratios that would reliably produce detonations. All the experiments presented in this paper were conducted with a fuel-air equivalence ratio approximately equal to one.

Previous results by Dorofeev [7] have shown the effects of varying hydrogen-Air molar ratios on the flame velocities along the length of a detonation tube. He describes three categories of flames based on their velocities: Slow flame, fast flame, and quasi-detonation (Figure 1).

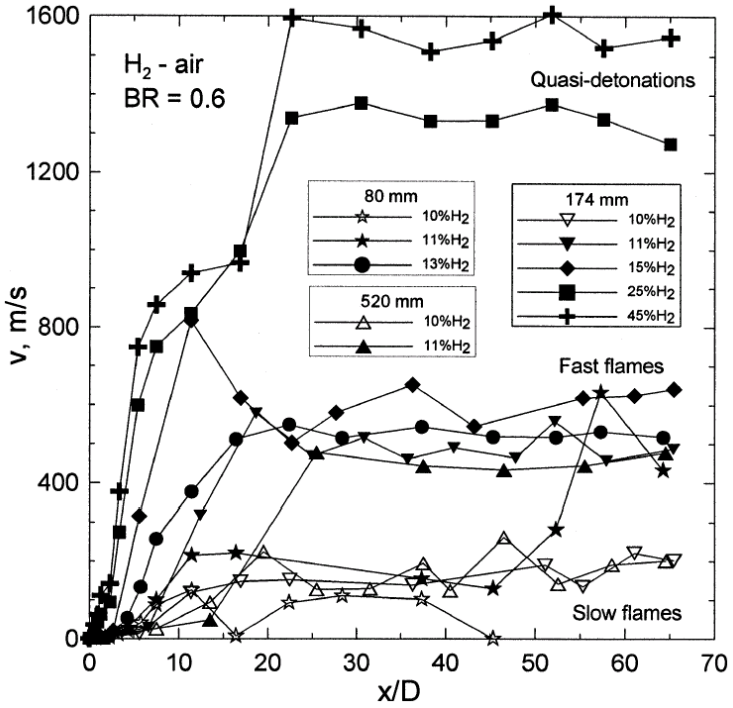

Figure 1: *Flame velocities versus distance for hydrogen-air mixtures (BR=0.6) [Reference 8]*

These results showed the run up distance to a steady state velocity of 1600 m/s was about 22 x/D (normalized length to diameter ratio) for a case with 45% H_2.

However, none of this data showed the characteristic Chapman-Jouguet velocity for detonation in hydrogen-air of 1960 m/s. This could be due to the presence of excess obstacles past what is minimally required to transition to detonation. These excess obstacles could actually prolong the transition to detonation and in some cases, depending on blockage ratio and other factors, prevent it.

Previous work has also been performed with hydrocarbons, specifically propane by Ciccarelli [8], resulting in plots showing acceleration of flame fronts through a 5.5" diameter tube. These results show a large dependence of flame run-up distance on equivalence ratio, while indicating that blockage ratio of the obstacles (ranging from 0.43 to 0.9) has a less significant effect (Figure 2).

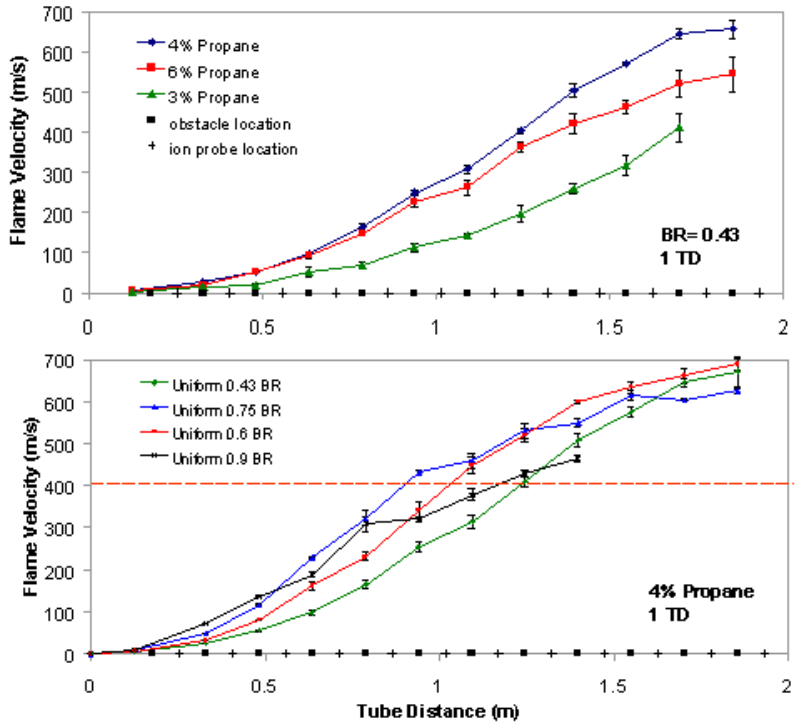

Figure 2: *Acceleration of propane-air flame with varying blockage ratio obstacles and % propane [Reference 9]*

Ciccarelli also presents results indicating the large effects of hydrogen-air composition on flame speed development in a hydrogen-air mixture (Figure 3). These results reveal that none of these compositions reached the characteristic CJ velocity for detonation in hydrogen-air mixtures, however, they do agree closely with the flame velocity bands reported by Dorofeev, mentioned previously.

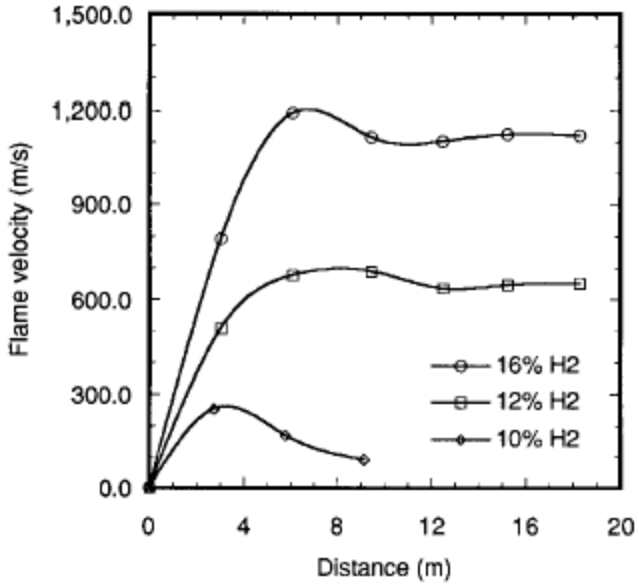

Figure 3: *Flame velocity versus distance for hydrogen-air mixtures at 300K and 0.1 MPa [Reference 9]*

Dorofeev et al. [7] has created an expression relating key dimensionless parameters for flame acceleration and DDT. The following criteria were deemed important: L_T/δ , σ, S_L/c_{sr}, S_L/c_{sp} , γ_r , Le, β ,d/λ . His work went further to developed an expression using constants a and b to describe relate BR, amongst other parameters, to the distance, L_D, required for the flame to reach Mach 1.

$$\frac{L_D}{R}\frac{10S_L(\sigma-1)}{C_P} \approx \alpha\left(\frac{1-BR}{1+b\cdot BR}\right)$$

PDE Operation:

The PDE used in this research has no valves in the air supply line, but uses solenoid valves to meter the fuel supply, allowing cyclic operation up to 30 Hz. Air from a facility compressor continuously flows through the 2" diameter PDE at fill velocities ranging from Mach 0.05 to 0.09. Fuel flow, controlled by a solenoid valve in the head end of the tube, is allowed to enter through a mixing element for a specified amount of time to fill a pre-defined percentage of the combustion chamber volume based on the velocity of air through the system. The fuel valve is then closed and the mixture is initiated using a spark located just downstream of the mixing element. The initial flame kernel grows as it begins to propagate down the tube. The flame speed increases as it propagates down the tube and encounters turbulence, eventually transitioning to a supersonic detonation wave. The steady-state detonation wave travels in excess of 1960 m/s (for hydrogen-air mixtures) or 1800 m/s (for ethylene-air mixtures) burning the remaining reactants and pushing the gases out of the open end of the tube, resulting in a thrust. The tube is then purged of the combustion products by the continuously flowing air and refilled with fuel to repeat the cycle (Figure 4). The quick rate of the combustion process, the linear proportionality of pulse frequency to thrust, the lack of significant moving parts, and the simplicity of the cycle all contribute to the attractiveness of this type of propulsion device and the large research effort currently being expended by academia and many major corporate research centers around the world.

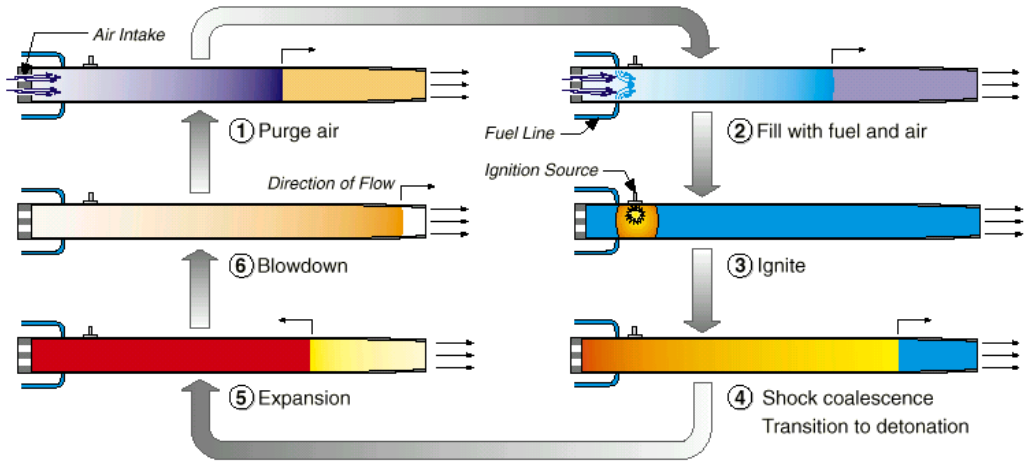

Figure 4: *Schematic of elements of a PDE cycle [Reference 10]*

The distance required for the transition to detonation to occur affects the physical length that the PDE must be. The longer the length that this transition to detonation takes to occur, the longer the detonation chamber will need to be. This extra length has a direct effect on timescales of the different steps in the PDE cycle and therefore on the maximum frequency that can be achieved. Any extra length can also add significantly to the weight of the engine, hindering its overall performance and feasibility.

One of the most common methods for shortening the DDT distance is the addition of a turbulence-enhancing device such as the Schelkin Spiral [3], placed downstream of the spark. This device, essentially a coiled spring press fit into the tube, serves to create large-scale turbulent structures that distribute the combustion front, effectively increasing its surface area, in turn accelerating the flame and creating local hotspots. In this manner, the transition to supersonic detonations can occur in significantly reduced lengths. One can imagine many other turbulence inducing devices that could be placed in the tube. The drawback to these types of obstacles is that they protrude into the main flow of the

tube, creating pressure drops and areas of constricted flow, which subtract from the overall specific impulse/performance (Figure 5). The presence of obstacles can also interfere with gas exchange processes, such as the fill cycles or purge cycles. This may require the tube to be significantly overfilled with fuel to ensure uniform distribution between obstacles in the areas of constricted flow. On the same basis, the purge time may need to be significantly lengthened in order to remove the combustion products from these same problem spots. The ideal obstacle induced DDT section would be characterized as having turbulence enhancing properties while offering small pressure drop and reduced areas of flow recirculation.

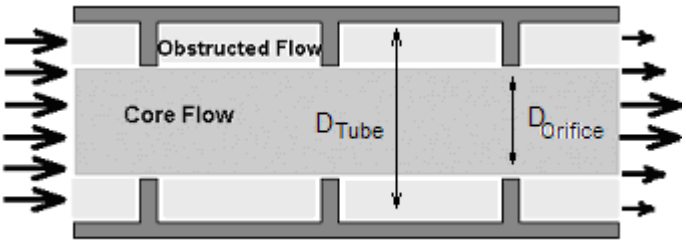

Figure 5: *Schematic defining core flow region*

The focus of this study was to identify the important factors that influence the DDT process in order to determine direction of this thesis research and find the optimal designs.

Factors Influencing DDT:

The following list of factors was deemed to be important to DDT behavior in a pulsed detonation engine. This list was based on previous research by others in the PDE community as well as personal experience and that of peers.

1. Obstacle geometry and spacing
    a. Blockage ratio
    b. Spacing
    c. Length
2. Placement of obstacle section in tube
3. Fuel/Air equivalence ratio
4. Fuel/Air mixing
5. Fuel Valve open/close time
6. Inlet air velocity
7. Initial pressure/temperature
8. Mixture characteristics listed above (L_T/δ , $\sigma = \rho_{reactant}/\rho_{product}$, S_L/c_{sr}, S_L/c_{sp} , γ_r , Le, β , d/λ) – Table 1 lists some of these values for the fuels of interest.

Table 1: *Detonation Parameters for the reactants with phi=1*

	C_2H_4 – Air	H_2 - Air
λ [mm]	25.7	15.1
γ	1.384	1.405
S_L [cm/s]	73	225
L_e	1.21	1
Z_e	6.58	6.5

The objective of this thesis is to characterize the effects of obstacle geometry and inlet air velocity on flame velocity and run-up distance/time to detonation, to prove the hypothesis that excess obstacles can inhibit detonation transition, to demonstrate a high resolution data collection/visualization technique, and to provide validation experiments for computational analysis.

CHAPTER III: METHODS

Two main experimental configurations were used to obtain results presented in this paper. The following descriptions detail each configuration starting at the upstream position and moving towards the tube exit. The basic designs of these configurations were based upon previous General Electric designs that were shown to reliably create detonations. The main modifications included the interfaces between the components in order to allow easy interchangeability of tubes and modularity of the components.

Setup:

Configuration I (Figure 6) consisted of a pipe end-cap with two ¾" Swagelok connections for the air inlets, that connected to the fuel mixer assembly contained within a 2" coupler through a 2" NPT threaded nipple. A second nipple connected aft of the mixing element led into the threaded union. The tube PDE (with instrument ports) was attached directly to the union. A 2.5" coupler was used to extend the length of the tube to one meter using another length of schedule 40 pipe. The DDT geometry (Figure 7), consisting of orifice obstacles spaced along #6 threaded rod using lengths of 1/4" tubing, with eight nuts clamping the assembly together, was held in place by clamping a larger diameter orifice obstacle in-between the two halves of the union. The velocity of the combustion wave was determined using two dynamic pressure transducers located 1" and 5" from the exit of the tube.

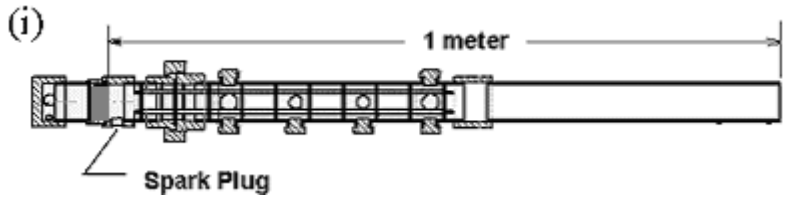

Figure 6: *Configuration I - Steel Optical diagnostic tube PDE*

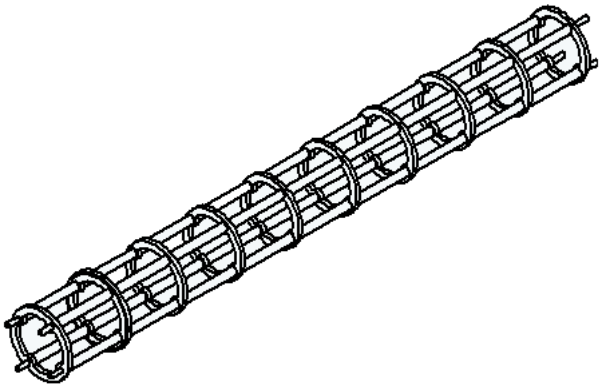

Figure 7: *2" outer diameter DDT obstacle assembly – slides into PDE*

Configuration II (Figure 8) simplified the downstream geometry by removing the need for the union. The front-end assembly consisted of the end cap and fuel mixing assembly, however, the geometry down-stream from mixing element was replaced with a length of polycarbonate hollow rod (two lengths connected by a coupler). The DDT geometry in this case was held in place by 6 staggered #8 setscrews spaced along one circumference of the tube. Three screws on each side of the upstream ring held the DDT geometry rigid inside the detonation chamber in the same location downstream as configuration I.

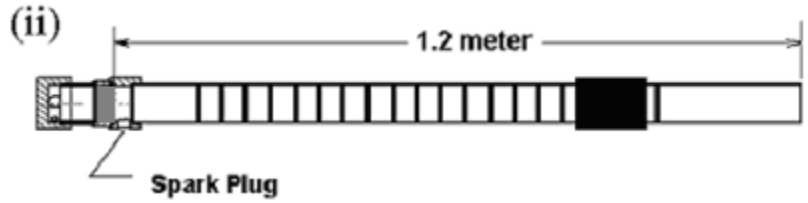

Figure 8: *Configuration II - Polycarbonate tube PDE for high speed imaging*

The clear combustion chamber (Figure 9) allowed the use of a Phantom VII high-speed digital camera, which was able to record flame position along the length of the tube as a function of time from the spark [11]. This method resulted in more continuous data. During testing a mirror was positioned so that the camera could sit in a safe area out of the range of the PDE.

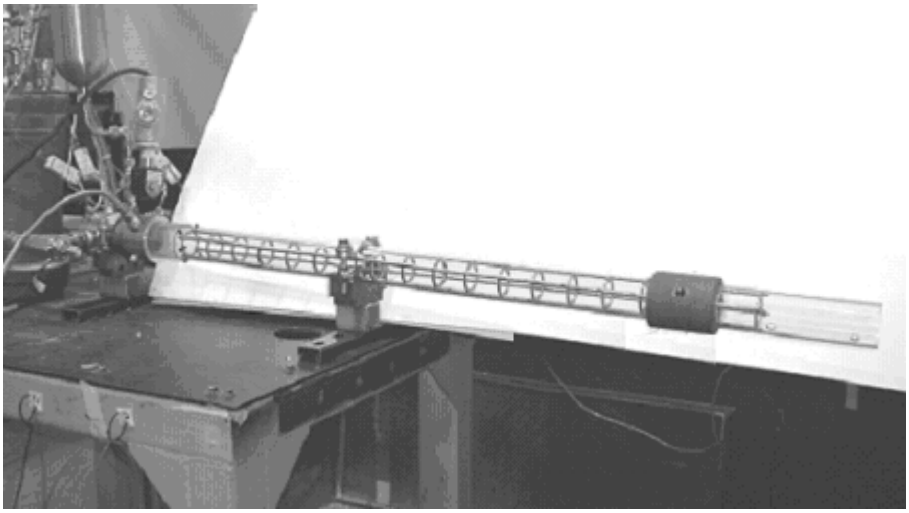

Figure 9: *Image of Configuration II PDE setup*

Facility:

During PDE operation the air was continuously flowed through the tube by way of two 3/4" NPT openings located opposite of each other around the circumference of the end cap. The air was supplied through the house compressor, and flowed through a 15'

long, 1” diameter hose that fed into an upstream volume (~500 cu in). Two ¾” hoses left the volume and terminated in the end cap openings of the PDE. The purpose of this upstream volume was to minimize effects of pressure waves resulting from the combustion events that might travel up through the air supply hoses.

The gaseous fuel was injected through a mixing element. A Solenoid valve located about 2” upstream of this element regulated the fuel injection. The spark was located 0.6” downstream of the forward geometry of the mixer.

DDT Obstacle Geometries:

During the initial DOE study into the effects of internal geometry on DDT, three factors were examined: The length of the DDT section (8” and 18”), the blockage ratio of the geometry (.43 and .55), and the spacing between the blockages (1 diameter and 2 diameters) (Table 2). The blockage ratio of an obstacle is defined as the ratio of the area that the orifice blocks to the cross sectional area of the PDE. The obstacles were cut via water jet from 1/8” 304L stainless steel sheet metal to dimension that would provide the desired blockage ratios (Figure 10). The obstacles were then assembled using four #8-32 stainless steel threaded rods with ¼” diameter stainless steel tubing separating each obstacle to the desired distance. Locking nuts were used on both ends of the assembly to keep the device rigid. Each experiment was given a label that identified the DDT geometry used. For example (0.15 lb/s, 0.43, 18”, 1D) corresponds to an experiment that was run with 0.15 lb/s of air, obstacles that had a blockage ratio of 0.43, DDT geometry length of 18”, and spacing between obstacles of one diameter (2”).

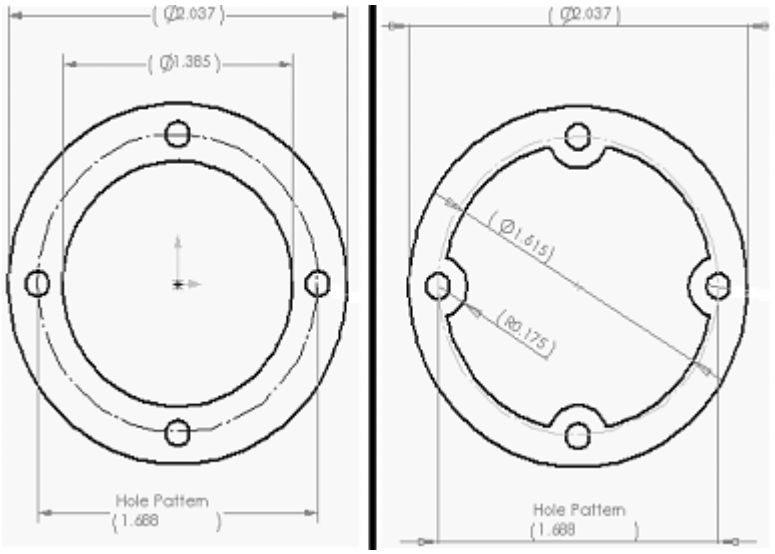

Figure 10: *Dimensions of DDT obstacles used (0.55 and 0.42 BR respectively)*

The test plan followed for the initial DOE is presented below. These parameters were determined to be important based on data from previous research as mentioned in preceding sections. The fuel used was hydrogen, with an airflow rate of 0.15 lb/sec. Replicates of the majority of the runs were made in order to extract statistical significance of each factor in the results.

Table 2: *Test plan – 3 factor, 2 level randomized order DOE*

Run Order	Blockage Ratio	Length [in]	Spacing [in]
1	.43	16	4
2	.43	8	4
3	.43	18	2
4	.55	18	2
5	.55	8	2
6	.55	8	4
7	.43	8	2
8	.55	16	4

Experimental Method:

The basic operation of the PDE consists of 4 main components: The fuel system, the spark system, the air system, and the timing of each. The air for this setup was continuously flowed at some designated mass flow rate (0.15 lbs/sec). Calculations were performed to determine the amount of fuel fill time (valve open time) required to achieve 100% fill with a 300 psi back pressure for Hydrogen studies and ~210 psi for Ethylene studies. After the tube achieved 100-150% fill, the fuel valve was closed and a 0.5 ms system delay was followed by the spark from the Unison spark system (Figure 11). A trigger box was implemented to receive the spark signal and subsequently coordinate the rest of the system timing from that.

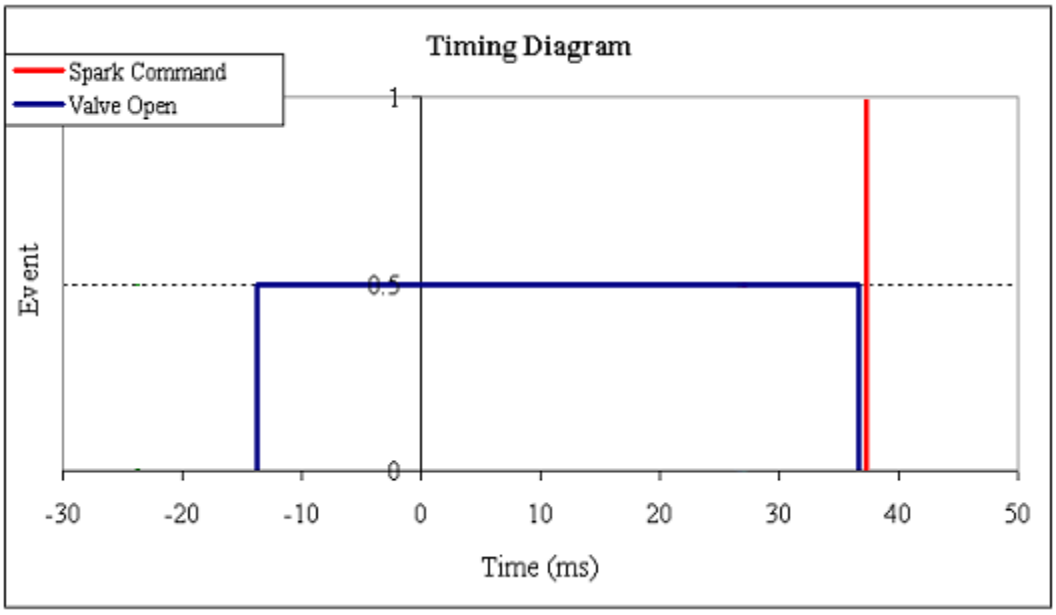

Figure 11: *PDE timing diagram based on 46" PDE and 0.15 lbs/s air*

Before each run, the pressure transducers were installed, the signal conditioner was turned on, the airflow was started, and the calculated timing was input to the trigger box. The slow and fast data acquisition systems were prepared and the camera software

was engaged (if applicable). The first spark acted as a trigger to start the fast data acquisition as well as the camera sequence. To adequately capture the peaks of the dynamic pressure signals for time-of-flight measurements, a sample data rate of 250 MHz was utilized. Based on the data acquisition rate used and an assumed error of up to 1mm during the location of the dynamic pressure transducers on the tube, an uncertainty of 11.9% was calculated to be associated with this method for calculating flame velocity. This was deemed acceptable since distinct velocity bands were expected.

After each test, the data from the high-speed data acquisition software was saved as a text file for future reduction. A Matlab script (Appendix A) was written to reduce the data, output calculated flame velocities between the two pressure transducers, and plot pressure as a function of time for the duration of the test. A series of 5 cycles was recorded for each experiment. The setup, acquisition, reduction, and conversion of the high-speed camera data were conducted following the Phantom VII camera operating procedure.

High Speed Digital Camera:

For the experiments using the high-speed video camera (configuration II), the experimental procedure followed was the same. The camera used was the Vision Research, Inc Phantom VII digital camera with capabilities of up to 100 kHz operation. The camera was triggered using the noise from the spark cable. Framing rate for the camera was varied from 50 kHz to 80 kHz depending on the size of the image that was being acquired. Typically a 35 mm lens was used with f-stop adjusted to capture the chemiluminescence with ~2μs exposure time.

Pressure Transducers:

The *PCB Piezotronics* dynamic pressure transducers used for this experimentation were the model 113A with the 402A inline amplifier and a three inch connecting cable. This transducer was determined to best suit the needs of this experiment by performing a trade off analysis taking into account rise time, resolution, sensitivity, temperature range, and cost. The transducer rig was placed in a 1/8" NPT holder, part number PCB 062 A01, and recessed from flush about 40 mils in this holder. In order to protect the head of the transducer and to reduce the thermal effects on the output signal, this recess was filled with RTV. It was required that each transducer be visually examined after each day of experimentation to verify the integrity of the RTV coating was intact. The 4-channel *PCB Piezotronics* signal conditioner was model number 482A22 (AC coupled). It was determined that although this type of conditioner was suitable for timing purposes, a DC coupled signal conditioner would be beneficial to more adequately trace pressures seen in the tube.

CHAPTER IV: RESULTS AND DISCUSSION

The Results and Discussion section is divided up into six parts. The first part will present and discuss the results for the hydrogen-air screening Design of Experiments (DOE). This will be followed by hydrogen-air results for the optically clear tube test performed with the high-speed video camera. The third section will explore the use of alternate fuels including ethylene-air. The fourth section will look at the effects of airflow and fill velocity on run-up distance and times in ethylene-air mixtures. The fifth section will present cold-flow pressure drop measurements across the tube PDE. The final section will present and discuss validation of computational analysis.

Results - Screening Doe (Configuration I):

Table 3: *Test results - Green represents successful detonations ($V_{Det}>0.88V_{CJ}$)*

Run Order	Blockage Ratio	Length [in]	Spacing [in]	**Ave Vel [m/s]**
1	.43	16	4	**2116**
2	.43	8	4	**1270**
3	.43	18	2	**1954**
4	.55	18	2	**2032**
5	.55	8	2	**1129**
6	.55	8	4	**2117**
7	.43	8	2	**1016**
8	.55	16	4	**2031**
1 *replicate*	.43	16	4	**2032**
2 *replicate*	.43	8	4	**1239**
3 *replicate*	.43	18	2	**1954**
4 *replicate*	.55	18	2	**1954**
5 *replicate*	.55	8	2	**1081**
6 *replicate*	.55	8	4	**2032**
7 *replicate*	.43	8	2	**1104**
8 *replicate*	.55	16	4	**1752**

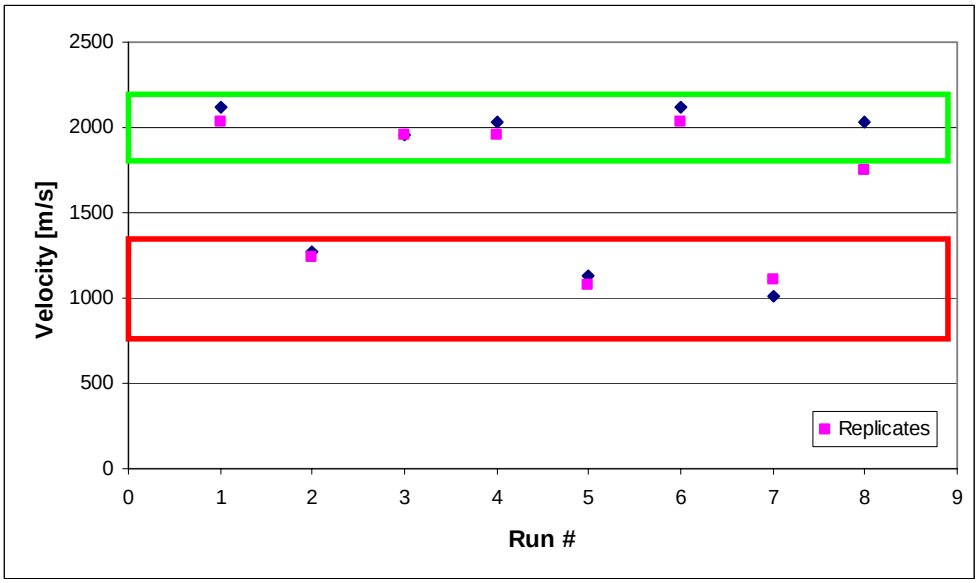

Figure 12: *Velocities measured at end of PDE tube - Two velocity bands signifying detonations and fast flames are identified*

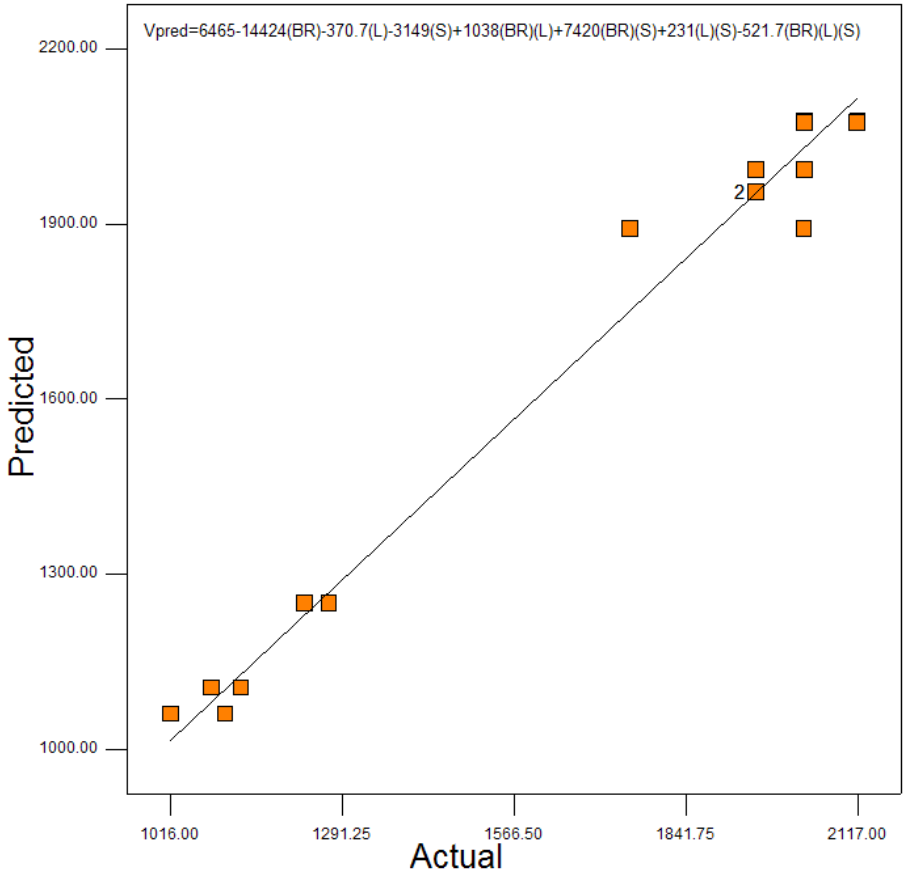

Figure 13: *Plot of predicted versus actual velocity - Validation for transfer function*

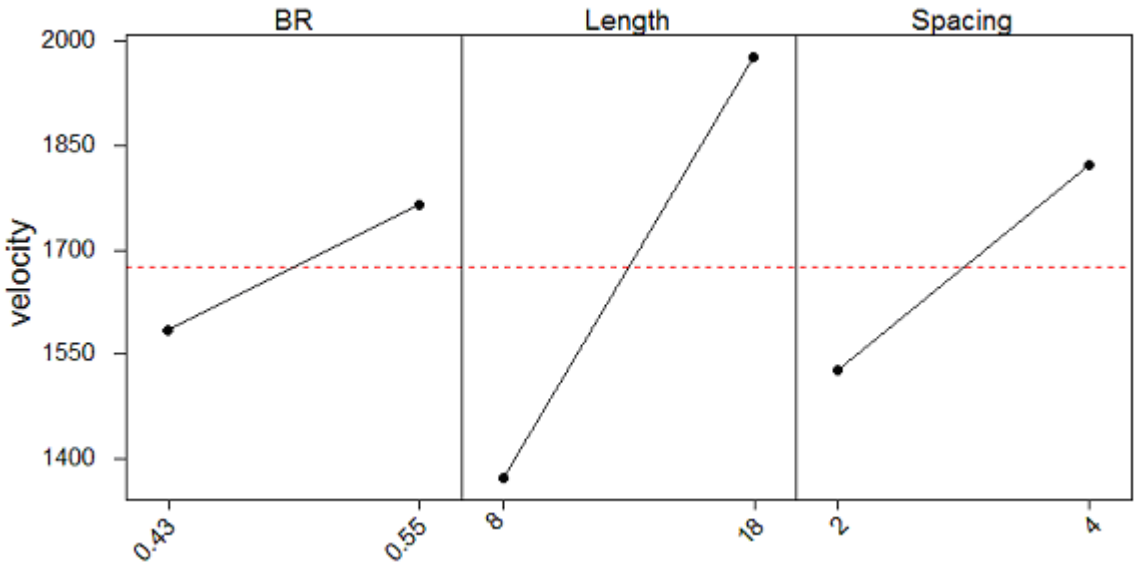

Figure 14: *Main effects plot for initial DOE*

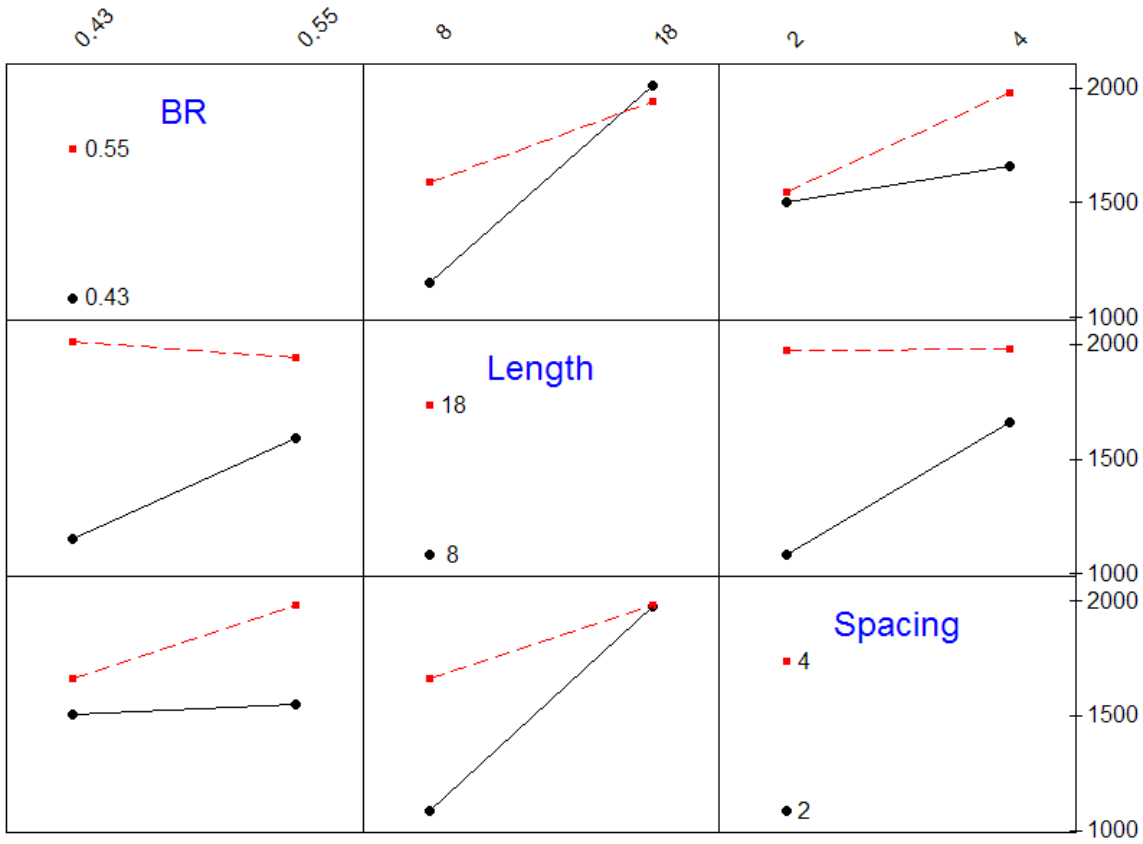

Figure 15: *Interaction plot for initial DOE*

Discussion – Initial DOE (Configuration I):

The two values used for each factor in this fundamental study (Table 2) were chosen based on literature searches and previous jugular experimental results. The fundamental study assumes a linear relationship between factors and behavior and maps out the 8 corners of the design space. DDT is not assumed to be a linear process, however the levels were chosen to be fairly close to each in order to tighten the design space. In this manner, a linear relationship could be approximated. Due to the fact that a length of 18" could not be obtained using obstacles spaced 4" apart, a length of 16" was used for two of the runs. The statistical software used for this analysis was fully able to factor this into the results seamlessly. MiniTab and Design-Experiment were the programs used for this analysis.

Results for the initial DOE study were in the form of combustion flame velocity at the exit of the tube calculated using a time of flight measurement between dynamic pressure transducers (Table 3). After examining the velocity data, two bands of velocities were seen (Figure 12). The first band, the detonation band, spanned velocities from 1752 m/s through 2117 m/s. The range of velocities that would be considered detonations was determined by the uncertainty of 11.9% associated with this measurement technique. The second band, the fast flame band, spanned velocities from 1000 m/s through 1270 m/s. These trends align with Dorofeev's results, except he saw three distinct bands (Slow Flame, Fast Flame, and Quasi Detonation), and none of his results showed characteristic Chapman-Jouguet velocity of 1960 m/s for Hydrogen detonation. According to his classification, the two ranges that are seen in this data would be considered detonations and quasi-detonations.

A Response Surface Regression was performed, resulting in plots of actual vs predicted flame velocities (Figure 13), main effects (Figure 14), and two-way interactions (Figure 15). The predicted velocities were calculated using a transfer function that the analysis created based on the statistically significant terms. The results indicate that all three factors have statistically significant effects (P-values less than 0.05) on the final flame velocity (Figure 16). The length and spacing are most significant followed by the blockage ratio. Increasing the length of the DDT section, the spacing between the obstacles, and the blockage ratio all have a positive effect on flame acceleration (Figure 14).

ANOVA for selected factorial model

Analysis of variance table [Partial sum of squares - Type III]

Source	Sum of Squares	df	Mean Square	F Value	p-value Prob > F
Model	2.856E+006	7	4.080E+005	59.47	< 0.0001
A-BR	*54438.19*	*1*	*54438.19*	*7.93*	*0.0226*
B-Length	*1.301E+006*	*1*	*1.301E+006*	*189.69*	*< 0.0001*
C-spacing	*4.344E+005*	*1*	*4.344E+005*	*63.32*	*< 0.0001*
AB	*3.118E+005*	*1*	*3.118E+005*	*45.45*	*0.0001*
AC	*22681.09*	*1*	*22681.09*	*3.31*	*0.1065*
BC	*1.879E+005*	*1*	*1.879E+005*	*27.39*	*0.0008*
ABC	*3.059E+005*	*1*	*3.059E+005*	*44.59*	*0.0002*
Pure Error	54887.50	8	6860.94		
Cor Total	2.911E+006	15			

Std. Dev.	82.83	R-Squared	0.9811
Mean	1675.31	Adj R-Squared	0.9646
C.V. %	4.94	Pred R-Squared	0.9246
PRESS	2.196E+005	Adeq Precision	17.321

Figure 16: *Results from statistical analysis of fundamental DDT study*

All of the two-way interactions, except for the interaction of blockage ratio with spacing are statistically significant. The three-way interaction of all the factors is also

significant. The replicate runs were made in order to characterize the error in the results. The resulting adjusted R-squared value of 0.9811 is in reasonable agreement with the predicted R-squared value of 0.9246. The model F-value of 59.47 implies the model is significant. The value of 17.32 for "Adeq Precision" is greater than the desired value of 4, meaning this model can be used to navigate the design space.

Although these '*Configuration I*' results yielded information on the significant main factors influencing DDT, the design space was assumed to be linear. Although this might be an acceptable approximation for a tight design space, in reality the DDT phenomenon is non-linear event. The data for this experiment is discrete and more insight could be gained into the complex behavior of DDT with better resolution measurements. To better represent and understand this data, it was decided to modify the experimental setup to Configuration II (Figure 8) in order to visualize internal combustion behavior, and track the flame front position over time.

Results – Optical DDT Tube (Configuration II):

The manner in which this configuration II was setup allowed the qualitative analysis of flame interaction with the obstacles and quantitative extrapolation of flame position over time. A series of images was obtained that represented the progression of the flame front through the PDE (Figure 17, Figure 18). Quantitative X-T diagram comparisons (Figure 19) showed the position of the combustion with respect to time for each case. This data was used to obtain velocity profiles along the length of the tube and provided better visualization of DDT run-up distance (Figure 20). Preliminary qualitative

results captured behavior from the benchmark case (.43 BR, 18” Length, 1D spacing, and .15 lbs/sec air), and the shortest DDT case achieved (.55 BR, 12” Length, 2D spacing, and 0.15 lbs/sec air).

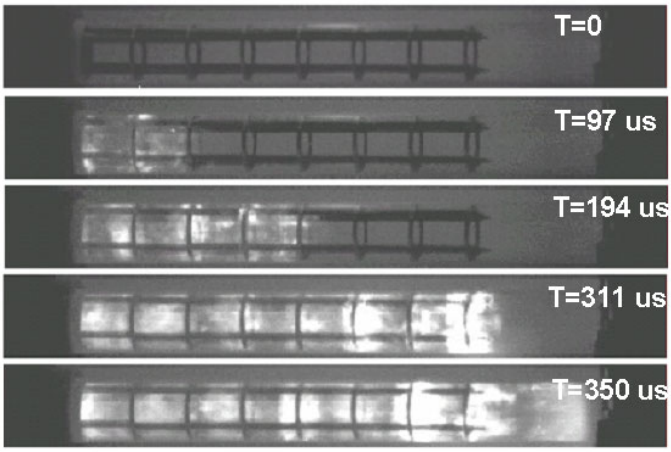

Figure 17: *Benchmark PDE showing DDT and resulting detonation in stoichiometric hydrogen-air with 0.43 BR (time started from initial appearance in the clear section)*

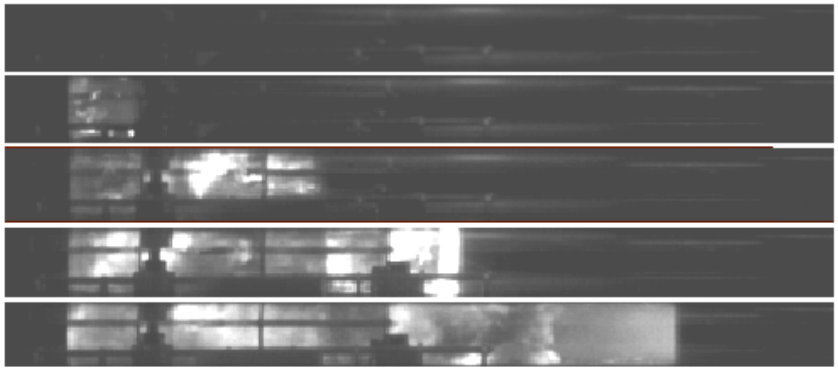

Figure 18: *DDT in Stoichiometric hydrogen-air with 0.55 BR (12" length, 2D spacing, and 0.15 lb/sec air)*

By extrapolating the position of the flame front from the high-speed images, accurate representations of position and velocity curves were obtained. This was done for both the benchmark case and the short DDT case. Position was normalized for diameter, and was taken relative to the beginning of the polycarbonate tube, which occurs

2.5-3 L/D downstream of the spark location (Figures 17 and 18). These plots yielded valuable insight into not only whether the combustion had transitioned to detonation, but also precisely where and when the transition had occurred (run-up distance and time).

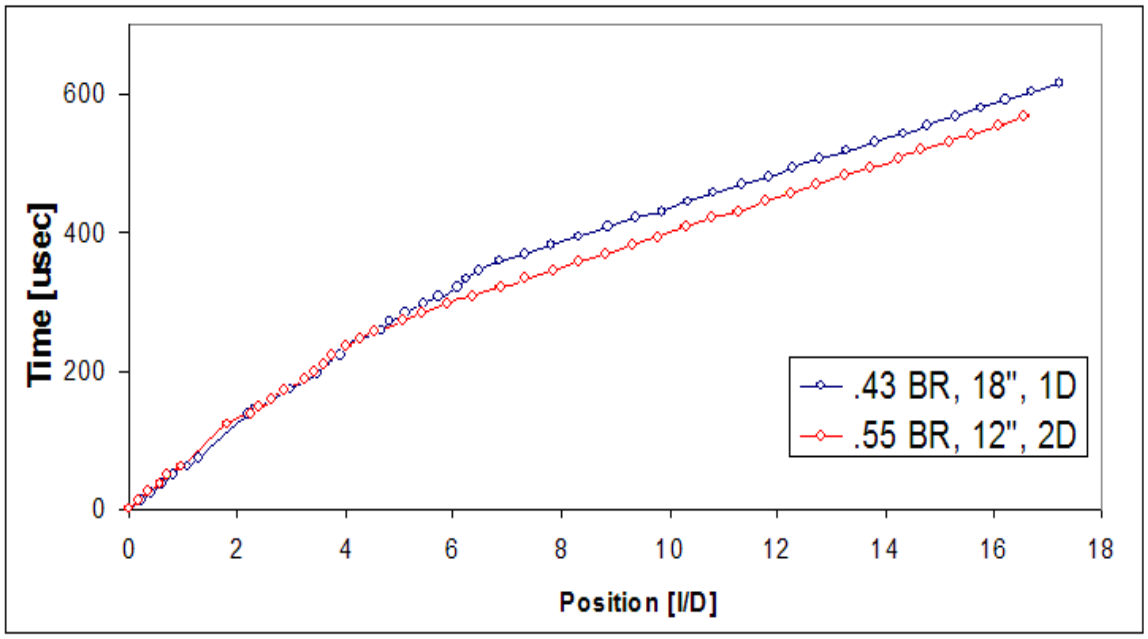

Figure 19: *Position versus time for hydrogen-air, 0.15 lbs/s air, different DDT geometries*

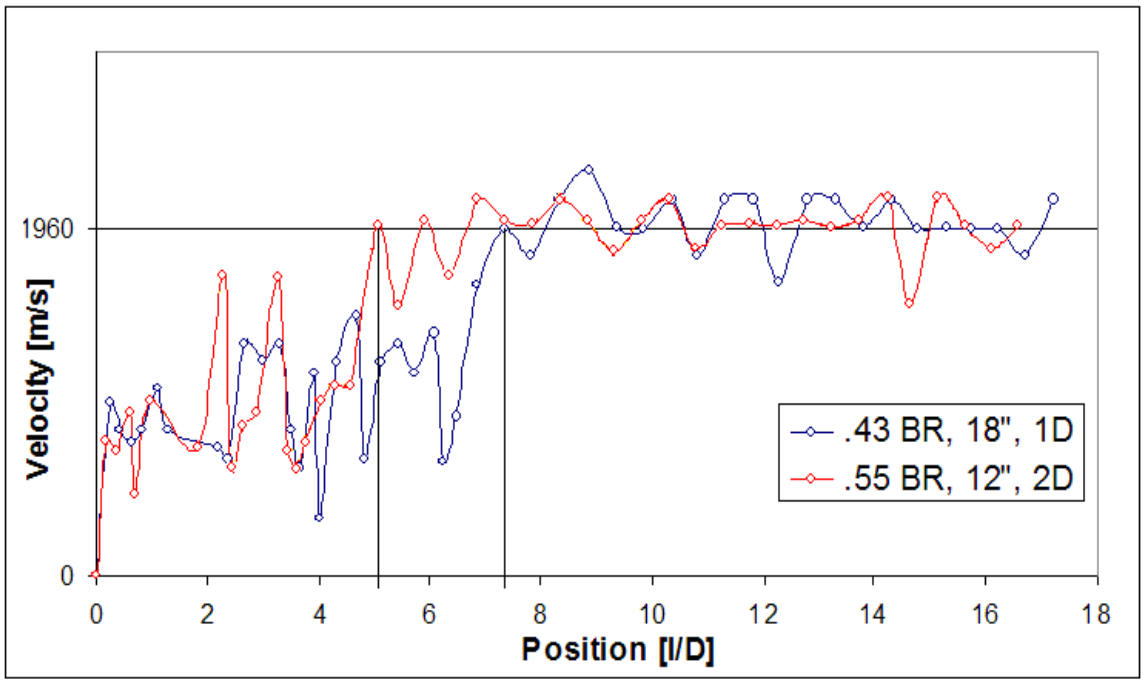

Figure 20: *Velocity profile for hydrogen-air, 0.15 lbs/s air, different DDT geometries*

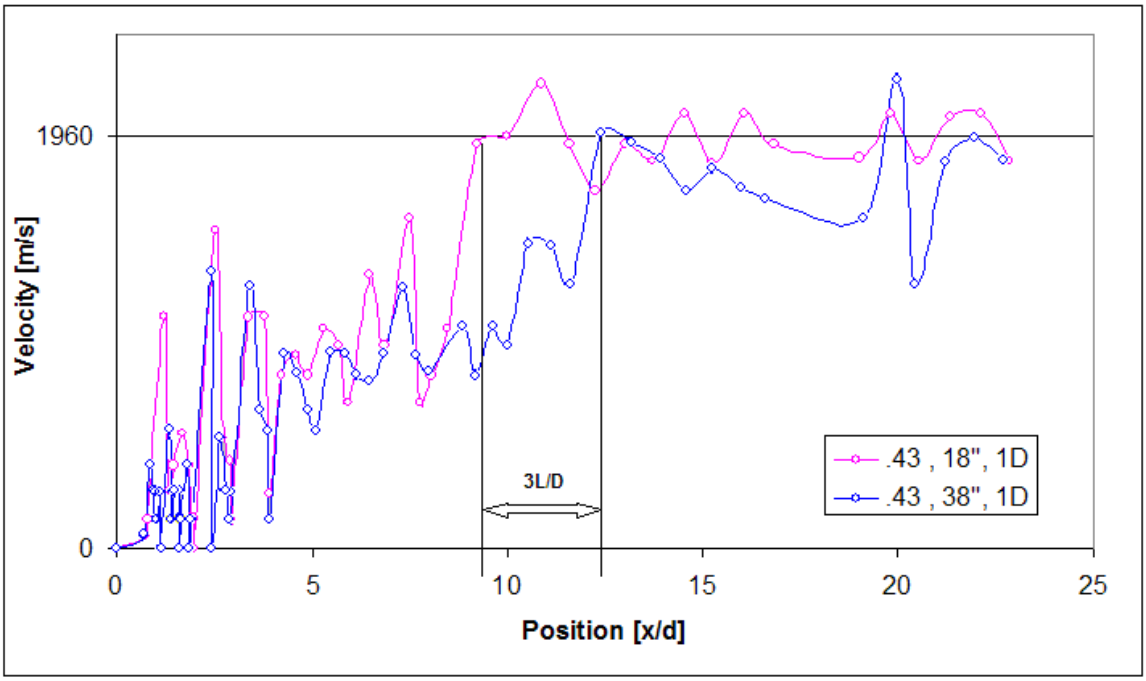

Figure 21: *Effect on DDT caused by excess of obstacles in hydrogen-air. Position and time taken from spark location and occurrence*

Discussion – Optical DDT Tube (Configuration II):

From this data, it was observed that the larger blockage ratio with larger spacing, and smaller length succeeds in detonating the fuel about 2.5 L/D's (5") before the benchmark DDT configuration. Although detonated in a shorter distance, the larger blockage ratio could lead to larger pressure drops, resulting in a decrease in engine efficiency compared to the 0.43 BR rings. This will be examined more in following sections.

Additional results showed that longer obstacle sections tended to require longer distances and longer times to transition than the optimized length DDT sections. Optimized being defined as the minimum number of obstacles in a given configuration/run-condition to detonate a mixture. This finding led to further investigation of the prohibitive effects of obstacles on detonation propagation and initiation. A test was performed that was similar to the benchmark geometry and run conditions, except the length of the obstacle section was doubled (38"). The results indicated the .43 BR obstacles inhibit the transition to detonation if there are excess than what is minimally required to transition (Figure 21). The distance to detonation was increased ~3 L/D, or 6 inches. This behavior shows that configurations used by previous PDE researchers [6], where excess obstacles were used to make sure transition to detonation occurred, might have had the opposite affect and actually prohibited transition to detonation. This was a significant find because it not only showed the need for a length optimized DDT section, but also led to the exploration of new DDT geometries that would incorporate smaller blockage ratios and minimize detonation propagation

effects. New geometries could possibly incorporate all the favorable detonation transitioning characteristics into a design that would limit the negative effects on detonation propagation/initiation. This could prove to be more crucial a task as heavier hydrocarbon gas or liquid fuels are used in PDEs.

Results – Alternate Fuels (Hydrocarbons):

The ultimate goal for a PDE is to be operated using common aviation fuels such as Jet-A or JP-10. These are both fairly non-reactive fuels when compared with the hydrogen-air mixtures that were currently being used. Therefore, the primary step was to move to heavier hydrocarbon gaseous fuels, specifically ethylene which is a suitable surrogate for vaporized aviation fuel.

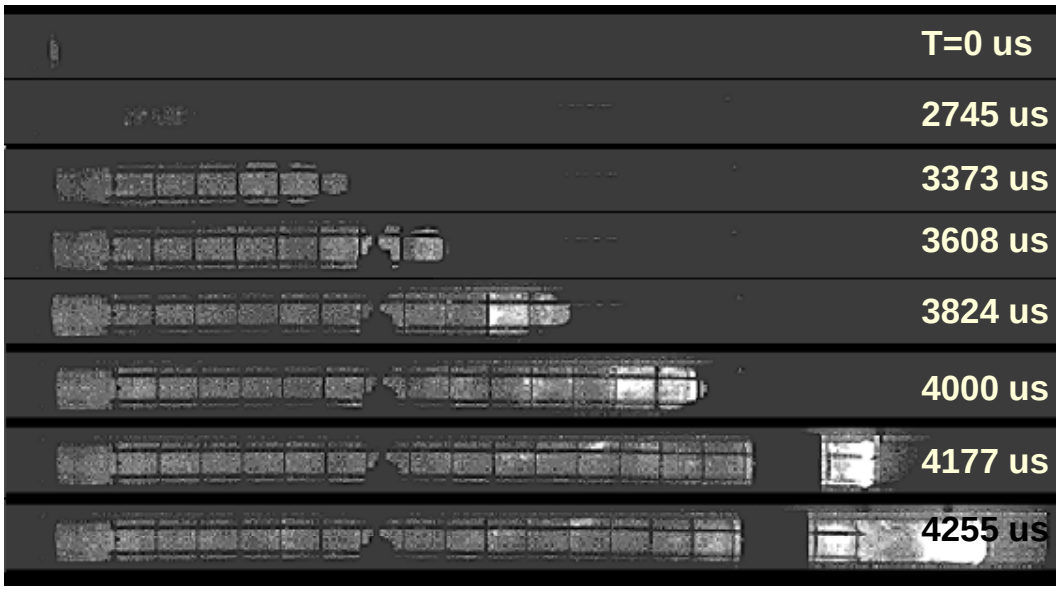

Figure 22: *Sequence of frames for ethylene air (0.15 lb/sec, 36", 1D). See appendix B for full sequence*

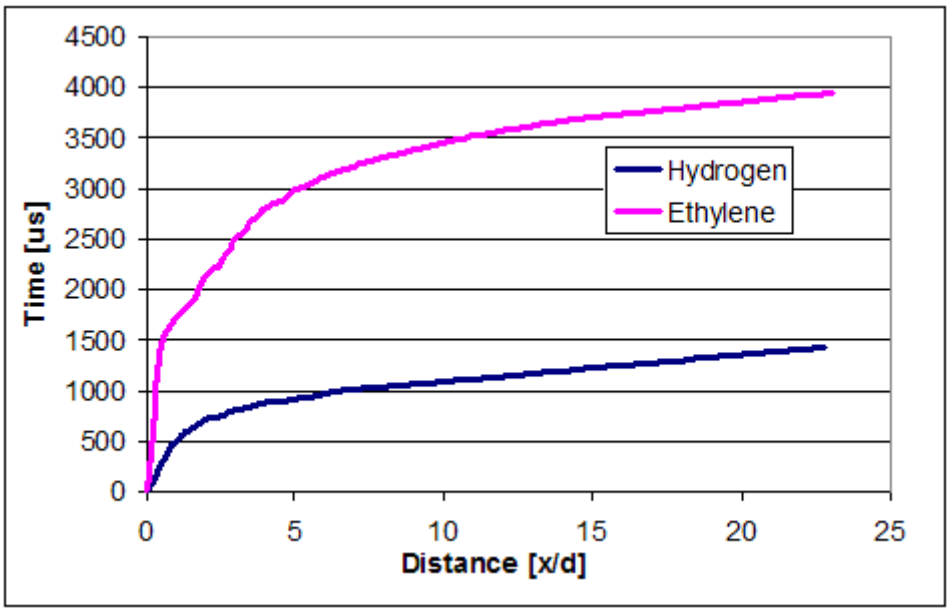

Figure 23: *Comparison of DDT run-up for ethylene-air and hydrogen-air in benchmark configurations*

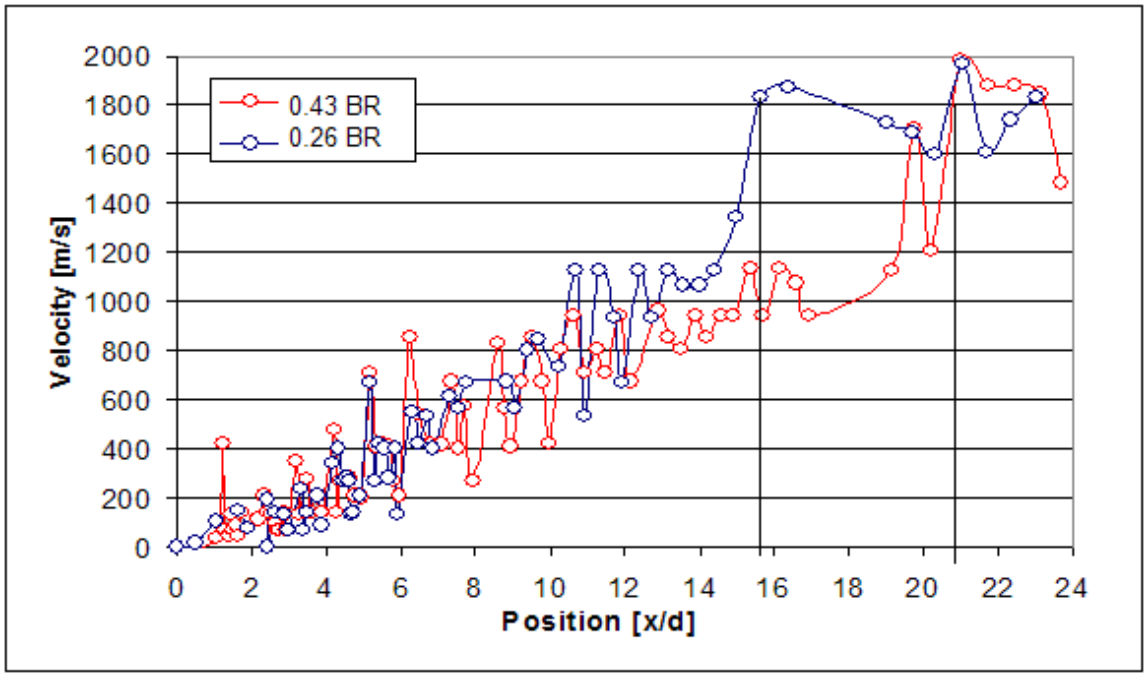

Figure 24: *Enhancement in DDT distance due to improved 0.26 BR obstacle geometry*

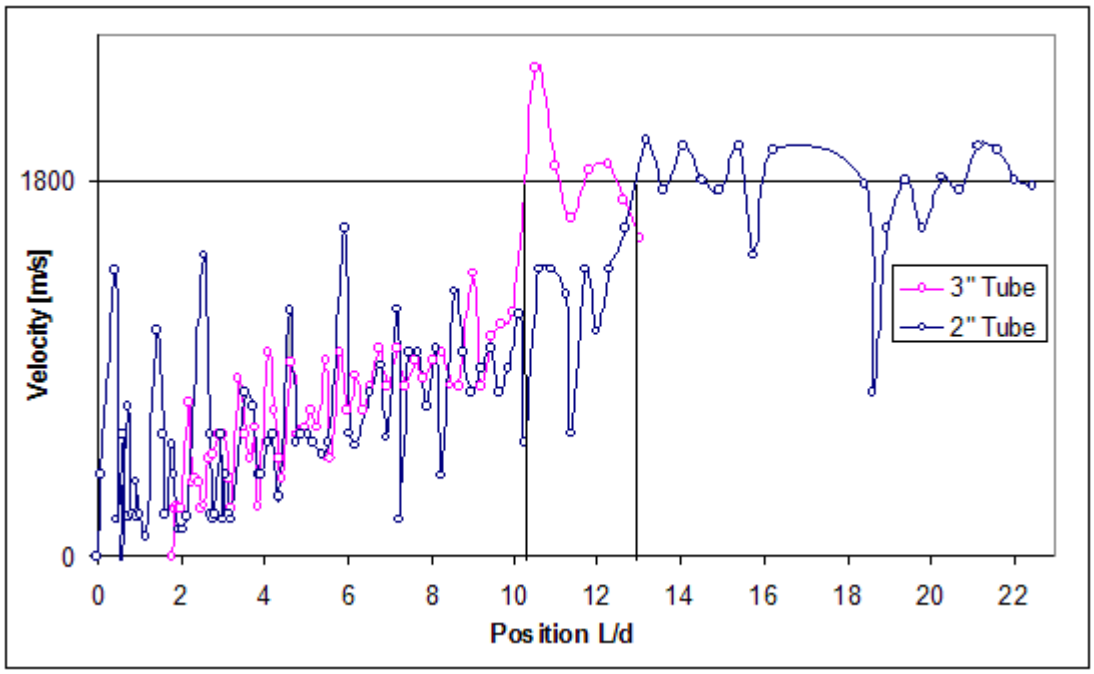

Figure 25: *Comparison of 2" and 3.25" diameter PDEs - Position normalized for diameter*

Discussion – Alternate Fuels (Hydrocarbons):

Many of the same trends that were seen in the hydrogen-air tests were also seen in the ethylene-air tests. The chemiluminescence was noticeably fainter, however, it still provided adequate light to track the combustion behavior and obtain data (Figure 22). The ignition delay time was greatly increased for the ethylene, which contributed in large part to the longer total cycle time observed for ethylene over hydrogen (Figure 23). It was clearly seen that the time taken for the detonation to exit the tube, about 4 ms, is almost a factor of 2.7 times longer than the hydrogen, only about 1.5 ms. The longer ignition time was expected, and may need to be addressed in the future as larger hydrocarbons are used. A new obstacle was introduced to the experimentation that had a blockage ratio of 26%. The design was based on data obtained during this

experimentation. The 0.26 BR obstacles had a noticeable improvement over the benchmark DDT configuration when keeping all other factors constant. Figure 24 illustrates a 24% reduction in run up distance, from ~21 L/D to 16 L/D over the 0.43 BR obstacles. This obstacle geometry was also seen to minimize detonation propagation effects seen in the previous obstacles.

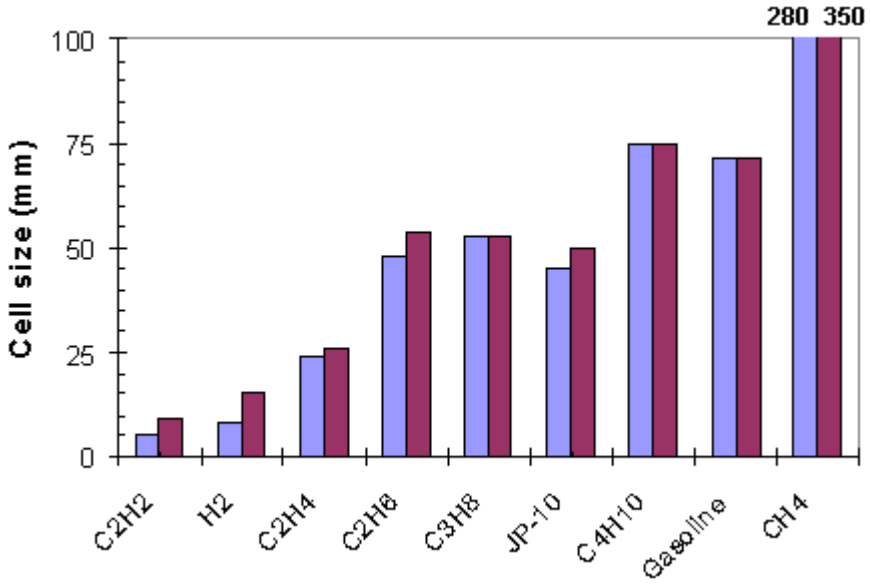

Figure 26: *Comparison of various fuel cell sizes in (1 atm, stoich)*

Due to the larger cell-size of ethylene, about 25mm compared to 15 mm for hydrogen, it was thought initially that larger diameter tubes might need to be used for atmospheric pressure testing. The cell-size (λ) of a fuel is determined by the traces left by the complex 3-D structure as it propagates through a chamber. The cell size is determined by a given fuel-oxidizer combination as well as other factors such as the size of the chamber that confines the detonation. As a rule of thumb, the larger the cell size, the less sensitive a fuel is to achieve detonations.

To determine what effects a larger cross-sectional area would have, tests with a 3.25” polycarbonate tube, connected through a reducer to the 2” nipple on the union were performed. Results indicated a longer run up distance to achieve detonation compared to the 2” tube, however, when the position was normalized to account for the larger diameter, it was seen that the DDT occurred about 2.25 L/D’s earlier than in the 2” tube with 26% BR obstacles (Figure 25). The obstacles used for the 3.25” tube were calculated to have a 22% blockage. These findings are encouraging for future testing when larger cell size hydrocarbons are used in atmospheric PDEs.

Results - Effects of Air Flow Rate on DDT:

Preliminary findings had shown an influence of airflow on DDT. Increasing the airflow from 0.1 to 0.15 lb/sec had resulted in a 2 L/D reduction in run-up distance. To further explore the effects of airflow velocity on DDT, the large in-house compressors were utilized to supply air to the PDE. Using this setup, mass flow rates from .15 through .4 lbs/sec were tested. Results showed little to no effect on the position of the combustion wave at the onset of transition to detonation in terms of distance from the spark location, however, the faster air flow rate did serve to decrease the ignition delay and time for flame kernel growth of the ethylene air mixture, thereby decreasing the overall cycle time significantly. By increasing the airflow from .15 lbs/sec to .3 lbs/sec, the time from spark until detonation transition was effectively decreased from ~3.9 ms to ~2.9 ms. This decrease of 26% in run-up time could lead to increases in attainable PDE frequency. The initial finding of minimal effect on run up distance could again be

attributed to the fact that excess obstacles might have been present for the higher airflow tests thereby inhibiting transition to detonation. More research will need to be performed in this area.

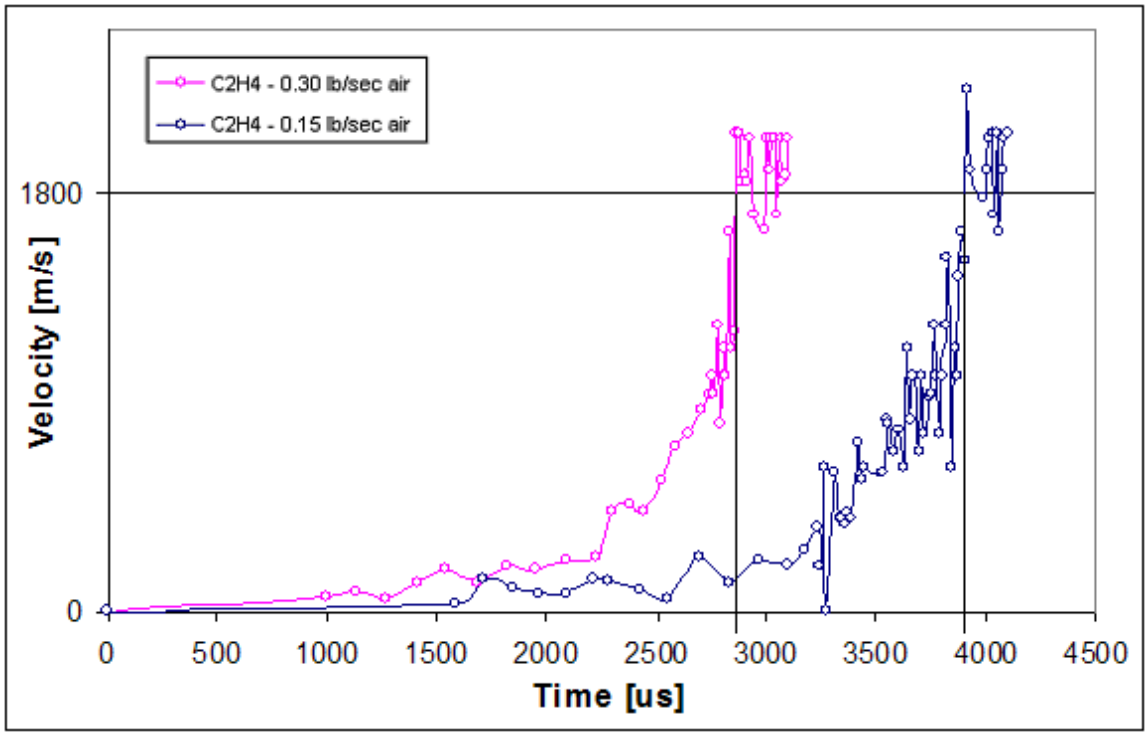

Figure 27: *Effects of airflow rate on DDT run-up time for ethylene-air*

For airflows exceeding .2 lbs/sec, it was increasingly difficult to detonate the mixture. Many of the cycles were essentially misfires, in that no deflagration occurred. However, when deflagration did occur, it transitioned to detonation consistently. Recommendations for future testing would be to move the location of the spark downstream a few inches to ensure fuel contact with the spark and consistent cycling of the PDE.

The velocity vs. time plot for the 0.4 lbs/sec case looked nearly identical to the 0.3 lbs/sec case, and therefore was omitted from Figure 27. A run condition was difficult to

find for this airflow due to the problem mentioned above, and it cannot be said that this case was optimized.

Results - Cold Flow Pressure Drop Across Obstacles:

To characterize the performance drain caused by the internal obstacles in the DDT section of the PDE, cold flow measurements were taken at varying airflow rates from 0.0 to 0.2 lbs/sec. Pressure taps were located upstream of the mixer in the end-cap, just down stream of the mixer, and at the exit of the tube (taken to be atmospheric).

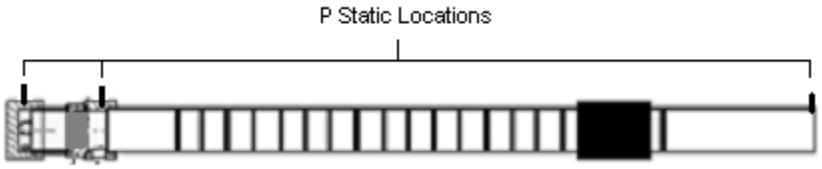

Figure 28: *Location of cold flow static pressure transducers*

The two obstacle geometries that were tested were the 0.43 BR and the 0.26 BR. Both DDT assemblies consisted of 17 obstacles spaced two inches apart. Pressure readings were taken every second at each of the upstream P static locations shown in Figure 28, while the exit pressure was assumed to be atmospheric (14.7 psi). The pressure drop across the mixer was taken as the difference between the two upstream pressure taps, while the pressure drop across the obstacle section was taken as the difference between the aft mixer tap and atmospheric pressure.

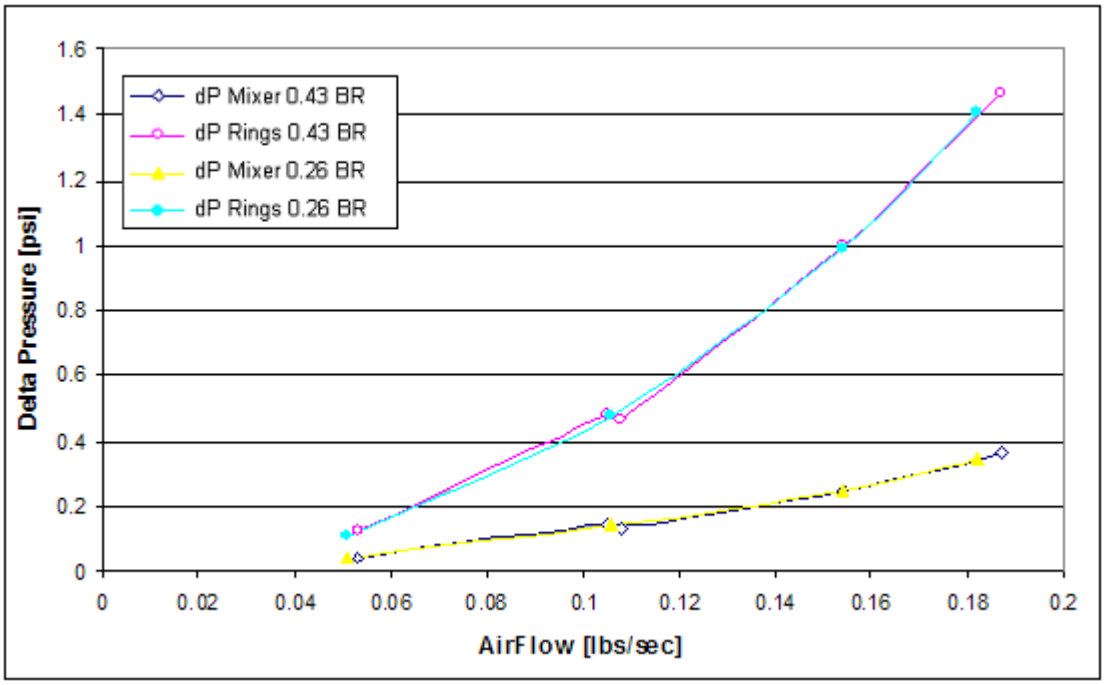

Figure 29: *Effects of airflow on cold flow pressure drop across mixing element and obstacle section*

Results show that although there is a 17% difference in blockage ratios between the obstacles tested, there is a negligible effect on pressure drop at these flow rates. This is counterintuitive to what was thought. More tests should be performed to characterize what length, spacing, blockage ratio is necessary to yield changes in pressure drop as this is an important criteria for the design of PDEs.

Results - Computational Comparisons

In order to obtain more insight into what factors contribute to DDT, two-dimensional computational studies of the PDE cycle were performed by Venkat Tangirala [12][13]. The configurations he used in these computational runs were chosen

to match the experimental configurations presented in this thesis so that validation could be provided. This numerical software is a cornerstone of the research being performed at GE GRC. It yields insight into much of the internal flow mechanisms of PDEs and demonstrates predicted behavior to allow for simpler future PDE designs. These types of comparisons are the first of its class being performed for unsteady continuous flow PDEs.

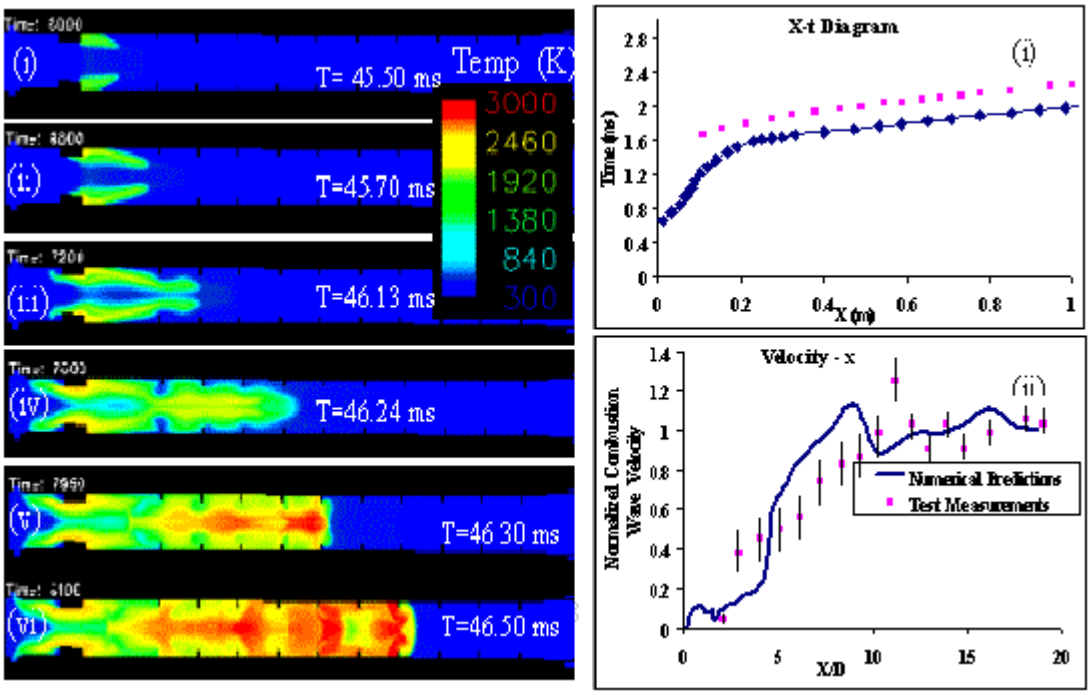

Figure 30: *Computational hydrogen-air temperature profile and run-up distance results for 0.43 BR benchmark PDE [Reference 12]*

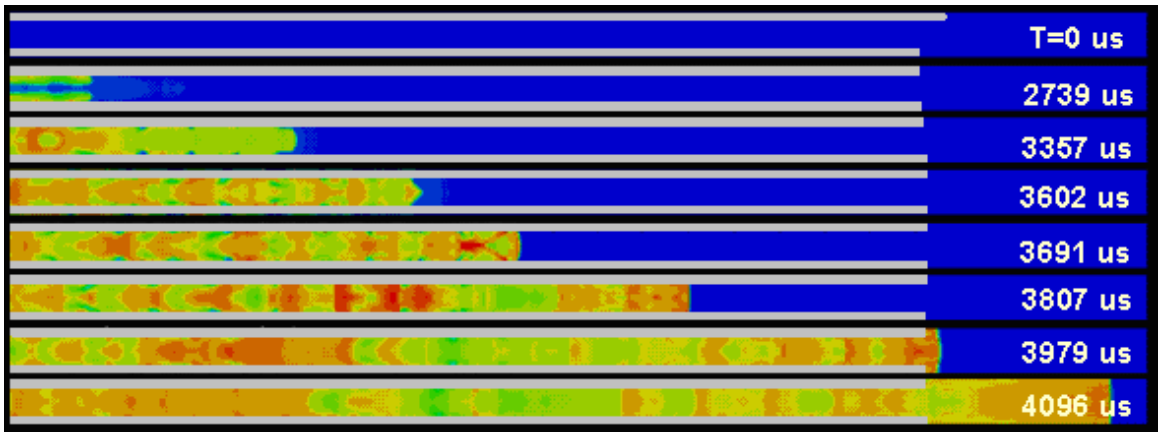

Figure 31: *Computational ethylene-air temperature profile frames for 0.26 BR DDT configuration*

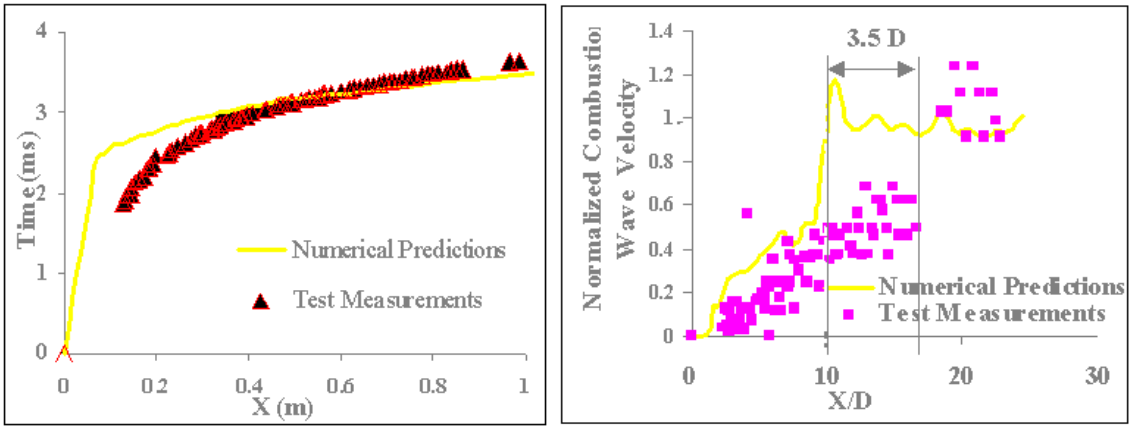

Figure 32: *Computational vs. experimental comparison of DDT run-up for ethylene-air with 0.15 lb/sec air (0.43, 18", 1D) [Reference 13]*

Discussion - Computational Comparisons

For two of the three cases presented above, good computational/experimental agreement was found. The best agreement was seen with the hydrogen benchmark test with the .43 blockage rings, and the ethylene test with the 0.26 BR obstacles. Both these numerical cases had about 20% difference between the experimental tests. The third

comparison was that of the ethylene test with the long .43 blockage DDT section. The large inherent error of about 40% was attributed to the fact that the software did not seem to account for the prohibitive nature of larger blockage ratio rings for transition to detonation that was seen in experiments.

As previously mentioned, experimentation showed that 0.43 and 0.55 obstacles had a negative effect on DDT propagation/initiation, in that deflagrations took longer to transition in the presence of excess obstacles with higher blockage ratios. The numerical model however, did not seem to represent this effect, and the detonation transitioned within in the DDT section each time.

Numerical predictions agreed with initial findings that airflow had a large influence over the distance required for DDT. These computations predicted that increasing the airflow from 0.1 lbs/sec to 0.4 lbs/sec would drastically decrease DDT run-up distance. Although this reduction in run-up distance was not verified experimentally, the large influence on run-up time was also observed.

CHAPTER V: CONCLUSION

The fundamental study performed indicates that all three factors tested, obstacle blockage ratio, number of obstacles, and spacing between obstacles are all statistically significant. DDT section length and spacing are most significant, followed by the blockage ratio. All of the two-way interactions, except for the interaction of blockage ratio with spacing, significant impact flame velocity. Increasing blockage ratio, number of obstacles, and spacing (within the design space that was examined) will all accelerate the flame faster within the bounds tested. It was shown that for a given fuel, DDT obstacle section length had the highest effect on detonation initiation behavior, followed by the spacing between the obstacles along the tube.

From the data obtained it was seen that the process of using the polycarbonate tubes with the high-speed camera is invaluable to the amount of data that can be extrapolated from each run. This data acquisition process is recommended for visualizing and obtaining data for DDT in a round cross-section tube for future single shot or low frequency low duration experiments where detonation transition location is desired.

Airflow was shown to have a large effect on the DDT run-up time at higher air velocities (> 0.2 lb/sec), reducing run up time by over 25% by increasing airflow from 0.15 lb/sec to 0.3 lb/sec. This finding has important implications for frequency performance of pulse detonation engines, especially as heavier hydrocarbons and eventually liquid fuels are examined. Ethylene gas in air was seen to require almost

double the length and triple the time to transition to detonation than hydrogen gas in air, and this trend would likely continue as heavier/less sensitive hydrocarbons are used.

Another important finding showed that excess 0.43 and 0.55 obstacles (excess defined as more than minimally required to transition the flame to detonation) served to inhibit run-up distance and detonation propagation through the tube. This finding was important in that it established a limit to the fundamental study results showing that longer DDT section are more effective for DDT. Transition to detonation was delayed by 3 L/D in a hydrogen-air mixture by placing extra 0.43 BR obstacles at the end of the existing obstacle section, showing a great need to either optimize DDT section length or design new obstacles that eliminate these prohibitive effects, and also indicating the non-linearity of the DDT phenomenon. A newly designed 0.26 BR obstacle drastically reduced the effects that excess obstacles have on DDT and was seen to transition an ethylene-air mixture over 5 L/D sooner than the benchmark 0.43 BR obstacles (an improvement of 25%).

The preliminary computational experiments presented within are a large step forward in this field, and more validation will provide an invaluable design and optimization tool for future PDE experiments. This is a complex area that has had a large effort contributed to recently at GE and elsewhere. The difference in run-up distance between the computational and experimental setups was within 20% for the benchmark 0.43 BR hydrogen-air test and the 0.26 BR ethylene-air test, and 40% for the benchmark 0.43 BR ethylene-air test.

Although larger blockage ratio obstacles should create a larger pressure drop across the combustion chamber, experimental results presented showed minimal difference between the 0.43 BR and 0.26 BR obstacles.

Experiments showed that run-up distance does not scale exactly with L/D; in fact even with a slight decrease in obstacle blockage ratio 0.22 versus 0.26, the ethylene-air mixture detonated almost 2.5 L/Ds sooner in the 3.25" rig over the 2" rig.

The final recommendations for DDT obstacle geometry are made based on all the data presented in this paper. For a two-inch detonation tube, the 26% BR geometry with 2 inch (1D) spacing between the rings and a total length of 10 L/D is recommended for hydrogen-air studies. Although the entire length of 10 L/D is not necessary for transition to detonation, studies showed that there were no negative effects of having a longer section with this obstacle design, and this extra length could be used for insurance that the DDT would occur every cycle.

For Ethylene tests, the same general recommendation is made, however with a 30" DDT overall length (16 obstacles). To achieve 3.0-sigma reliability, a tube length of 49.5" is required with a DDT section of 37" length. This recommendation is made for a 2" ID tube PDE. If a 3" tube PDE is manufactured, a smaller blockage ratio of 22% with a length of 36" was shown to be effective.

Future tests that need to be performed include additional pressure drop tests across the length of the tube to better quantify effects of obstacle blockage ratio and length on PDE performance. In conjunction with this testing, the effects of initial airflow need to be further examined after modifying the test rig by moving the spark slightly downstream to insure good fuel/air content. These tests would serve to validate results

that numerical studies and initial experimental studies have shown, where DDT length (not only time) is significantly decreased as velocity of the airflow is increased. More experiments should also be performed to examine further the effects of combustion chamber diameter on run-up distance and run-up time. These tests would create a more complete story surrounding the DDT phenomena and the factors that influence it, and could lead to better DDT designs.

APPENDIX A: Matlab Flame Velocity and Pressure Plotting Program

```
% Define User Modifiable Constants
format('long')                  ; %declare output format
clear                           ; %clear all variables
PDEFreq = 5                     ; %PDE Operation Frequency [Hz]

%Input Data File Path

FilePath='I:\testxxxx\rundirectory';

%Input Data File Name

DataFileName = 'xxxxxxxxx.txt'  ;

NumofTransDataColumns = 4       ; % Number of transducers in the input file to load
(should be 3 or 4)
PlotTransducers = [1,2]         ; %Transducers to plot
                                % the first transducer in the above list
                                % is used as the timing transducer
                                % The list should indicate the order
                                % of the transducers on the tube in
                                % the data file. (eg. if data file
                                % has data in columns P2 P3 P1, then
                                % the list should read [3,1,2]
Transducers = [1,2]             ; %Transducers to use (must be >= 2 elements in the list)
Ymin = -5                       ; %Plot Ymin value
Ymax = 20                       ; %Plot Ymax value
YThrustMin = -1                 ; %Plot Ymin value for Static Thrust [lb]
YThrustMax = 5                  ; %Plot Ymax value for Static Thrust [lb]
PressureThreshold = 9.0         ; %Pressure threshold for finding detonation pressure
rise time [atm]
Distance = .1016                ; %distance between transducers [m]
LegendText ={'P1';'P2'}         ; %Labels to use for legend

% Define Constants
[Junk, NumTrans] = size(Transducers) ; %number of pressure transducers
Colours = ['b';'r';'g';'c';'y']      ; %plotting colours
PDEPeriod = 1/PDEFreq           ; %PDE Operation Period [s]
PreTrigger = 0.1                ; %PreTrigger [fraction of PDEPeriod]


% Load Data File
if NumofTransDataColumns == 3
```

```
  [Time Spark Thrust FF SledPos P(:,1) P(:,2) P(:,3)] =
textread([FilePath,DataFileName], '%f %f %f %f %f %f %f %f', 'headerlines', 33);
end

if NumofTransDataColumns == 4
  [Time Spark Thrust FF SledPos P(:,1) P(:,2) P(:,3) P(:,4)] =
textread([FilePath,DataFileName], '%f %f %f %f %f %f %f %f %f', 'headerlines', 33);
end

% Clear unused arrays to save memory
clear Spark
clear Thrust
clear FF

% Find out the number of data points for each channel
[NumDataPts iJunk] = size(Time);

% Plot the graph
figure(1)
hold on
iIndex = 1;
for iPlotVector = P
  plot(Time,iPlotVector,Colours(iIndex));
  iIndex = iIndex+1;
end

% Make the plot look pretty
grid on
title(['Pressure Trace - ',DataFileName])
ylabel('Pressure (atm)')
xlabel('Time (s)')
legend(LegendText)
axis([Time(1) Time(NumDataPts) Ymin Ymax])

% Find the first pressure rise on the first channel
[FirstPRise] = find(P(:,1)>PressureThreshold);
[Junk Junk2] = size(FirstPRise);

% Determine the sampling period
SampPeriod = Time(2) - Time(1);

% Determine the number of data points in the period
NumPtsInPeriod = round(PDEPeriod/SampPeriod);

% Determine the number of periods
NumPeriod = round(NumDataPts/NumPtsInPeriod);
```

```
% Make the ZeroTime equal to the pretrigger datapoints before the pressure rise
ZeroTimeIndex = round(FirstPRise(PlotTransducers(1)) - PreTrigger*NumPtsInPeriod);
if ZeroTimeIndex <= 0
   ZeroTimeIndex = 1;
end

% Plot the first yellow dashed lined indicating the zero mark
plot([Time(ZeroTimeIndex),Time(ZeroTimeIndex)],[Ymin,Ymax],':y');

% Parse the data into the periods
for iIndex = 1:NumPeriod
  TempTimeIndex = ZeroTimeIndex + iIndex*NumPtsInPeriod;
  if TempTimeIndex < NumDataPts
     plot([Time(TempTimeIndex),Time(TempTimeIndex)],[Ymin,Ymax],':y');
    % Store the pressure trace for his period for each channel in a 3d
    % array
    for iIndex2 = 1:NumTrans
      % DATA FORMAT:  PParsed(Data, Period, Channel) = P(Data, Channel)
      PrevTimeIndex = TempTimeIndex-NumPtsInPeriod;
      PParsed(:,iIndex,iIndex2) = P(PrevTimeIndex:TempTimeIndex-1,iIndex2);
      StaticThrustParsed(:,iIndex) = StaticThrust(PrevTimeIndex:TempTimeIndex-1);
      TParsed(:,iIndex,iIndex2) = Time(PrevTimeIndex:TempTimeIndex-1);

      % Populate the timing array - DATA FORMAT TimingArray(Period, Channel)
      [Junk] = find(PParsed(:,iIndex,iIndex2)>PressureThreshold);

      if isempty(Junk)
        TimingArray(iIndex,iIndex2) = 0.0;
      else
        TimingArray(iIndex,iIndex2) = TParsed(Junk(1),iIndex,iIndex2);
      end
  end
  end
end
hold off

% Calculate the Velocity Array
ShiftedTimingArray = circshift(TimingArray,[0 1]);
VelocityArray = Distance./(TimingArray-ShiftedTimingArray);

% Print the Timing Array
TimingArray

% Trim the velocity array to drop the first column which is garbage
VelocityArray = VelocityArray(:,2:NumTrans)
```

```
% Print the shot to shot mean velocity
MeanVelocityArray = mean(VelocityArray)

% Plot the first period zoomed in
figure(2)
hold on
for iIndex = 1:NumTrans
  plot(TParsed(:,1,iIndex), PParsed(:,1,iIndex),Colours(iIndex));
end

% Make the plot look pretty
grid on
title(['Pressure Trace (First Pulse) - ',DataFileName])
ylabel('Pressure (atm)')
xlabel('Time (s)')
legend(LegendText)
Xmin = TParsed(1,1,1);
Xmax = TParsed(NumPtsInPeriod,1,1);
axis([Xmin Xmax Ymin Ymax])
text(Xmin+(Xmax-Xmin)*0.85, Ymin+(Ymax-Ymin)*0.67, 'Velocity (m/s):')
text(Xmin+(Xmax-Xmin)*0.85, Ymin+(Ymax-Ymin)*0.65,
num2str(transpose(VelocityArray(1,:)), '%6.1f'))
hold off
```

APPENDIX B: Sequential images of Ethylene-Air DDT
0.15 lbs/s air-flow rate (Time in µs)


2988
3531

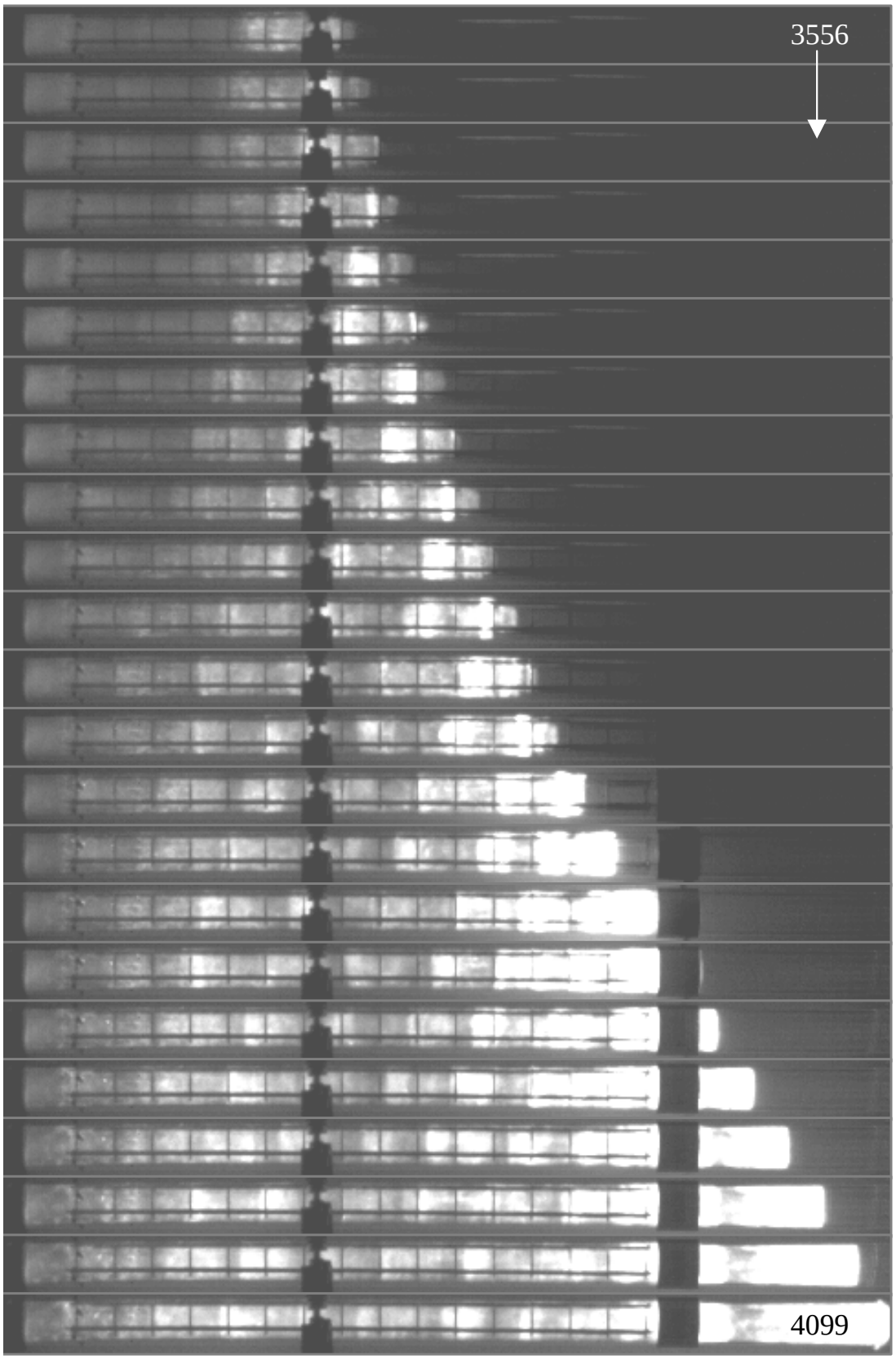
3556
4099

APPENDIX C: Co-authored 19th ICDERS paper

INVESTIGATIONS OF CYCLIC PULSED DETONATION PROCESSES: EXPERIMENTS AND CALCULATIONS

V. E. Tangirala, A. J. Dean, D. M. Chapin, P. F. Pinard and B. Varatharajan
Energy and Propulsion Technologies Laboratory
General Electric Global Research Center
One Research Circle, Niskayuna, NY 12309

Abstract
Computational and experimental investigations of performance are reported for a Pulsed Detonation Engine (PDE) operating in a cycle, using ethylene-air mixtures. Simulations are performed for two geometry configurations, namely an ideal tube PDE with a smooth wall fueled with premixed C_2H_4-O_2 and a benchmark tube PDE with internal geometry and a valveless air supply fueled with C_2H_4. A 2-step reduced chemical mechanism for C_2H_4-air is used to model chemical reactions. The computational method simulates all the processes of the PDE cycle (fill, Deflagration-to-Detonation Transition (DDT), detonation propagation, blowdown and purge). Experiments are performed to validate the simulation of the key PDE cycle processes. Experimental measurements include DDT visualizations and dynamic pressure measurements.
A 2-step reduced mechanism for a C_2H_4-O_2 mixture is validated using existing test measurements for an ideal PDE tube from the literature. The computational method successfully simulates the propagation and blow down processes of an ideal tube PDE, and the performance estimates show good agreement with the test data. Simulations of the benchmark tube PDE yield important insights into continuous cycle operation. Comparisons of experimental and computational visualizations show good agreement in cycle process time scales. The predicted decrease (up to 40%) in the fuel-specific impulse (I_{spf}) for the benchmark tube when compared to the I_{spf} of an ideal tube is attributed to nonuniformities in the mixture composition, the pressure drop resulting from internal geometry (DDT-promoting obstacles and a fuel-air mixing element) and backflow in the valveless benchmark tube due to a compression wave propagating into the upstream geometry. Increasing the bulk velocity of the flow through the benchmark tube has an adverse effect on the fuel-air profiles during the filling process. The bulk velocity, together with the percent fuel fill, impacts the performance metrics by affecting the fuel-air mixing processes in the benchmark PDE.

1.0 Introduction

Pulse detonation engines (PDE's) have recently emerged as potential new devices to better utilize the chemical energy content of reactive fuel/air mixtures [0]. One of the main advantages of PDE's is that the detonations create less entropy than conventional constant pressure processes such as those used in current gas turbines [2]. Establishing whether PDE's can achieve higher operating efficiency than conventional propulsion systems (i.e. gas turbines, ramjets, etc) is the focus of many research groups around the world.
One of the main challenges in making practical PDE's is the repeated initiation of detonations within the detonation chamber. Many implementations of pulse detonation engines rely on DDT to avoid the high energy required for direct initiation. DDT is the process whereby a deflagration is initiated using a weak energy source (typically tens of milli-Joules), and the combustion front accelerates via a series of gasdynamic processes and eventually detonates. A drawback to this approach for practical devices is the necessary length for transition (referred to as the run-up distance) to detonation, which for practical fuels such as Jet-A can be in the order of meters. One method to reduce the run-up distance is the addition of oxygen in the initiation region [3]. This can greatly reduce the length required for DDT but can add significant complexity and weight to a propulsion system and additional logistical requirements. Another method is to add obstacles inside the tube. This has also been shown to significantly reduce run-up distance with fuel-air mixtures, and there is little additional weight or complexity. For detonation initiation in fuel-air systems, DDT optimization is a trade-off between minimizing run-up distance via more obstacles or higher blockage ratio, and minimizing performance loss (pressure losses) via less obstacles or smaller blockage ratio. Numerical models could provide a powerful tool to develop new configurations. However, while numerical models have been used reliably to simulate cases of direct initiation, simulation of the DDT process remains a challenge and is a focus of this paper. For the modeling of detonation processes, there is a need for validated hydrocarbon chemical mechanisms. Considering the computational effort involved in the use of detailed/short chemical mechanisms for simulation of detonation initiation events, reduced chemical mechanisms, developed from basic elementary reactions

through a systematic process with fewer chemical reactions and fewer species, become critical for predictions of occurrence or failure of initiation and of detonation propagation. Such reduced chemical mechanisms must be validated over the range of fuel types, initial pressure, and temperature conditions of interest.

Many investigations of PDE thrust estimation [4-11] have focused on an ideal tube PDE which can be described as a constant cross-sectional tube, closed at one end and open at the other end, uniformly filled with quiescent fuel-air mixtures. Ideal tube configurations typically have a diameter of 0.051 or 0.076 m and a length of 1.0-1.5 m. These investigations include multi-level multidimensional (0D, 1D, 2D and 2D axisymmetric) computations with and without chemical kinetics. The fuel-air systems investigated include H_2-air, C_2H_4-O_2, and C_2H_4-air. Real gas effects are found to have an impact on PDE cycle performance [15]. A recent analytical model was extensively validated for various fuel-oxidizer systems, initial pressures, and equivalence ratios using single shot test measurements, and it has proven to be a valuable tool for thrust estimations within ± 15% [7].

Prediction of the propulsive performance of a pure tube PDE is of great interest in order to understand and improve the design of an engine in a parametric space comprising geometric parameters, fuel type, bulk velocity of the flow, frequency, igniter geometry, mixture uniformity and cycle process time scales. Purely computational studies of a simple tube PDE have been performed by a number of investigators. Even for the tube filled with a stoichiometric hydrogen-air mixture, there was a significant variation in the estimated values of the fuel-specific impulse (I_{spf}) over a single cycle, ranging from 3000s to 8000s. However, more recent detailed comparisons [4,5] have shown that most of this variation could be explained on the basis of initial and boundary conditions used in the various computational studies. For an ideal PDE tube completely filled with hydrogen-air mixture (at initial conditions of 1 atm., 300 K and an equivalence ratio of 1.0), a convergence of estimations for I_{spf} at a value of about 4160 s has been reported by the computational PDE research community [9-11].

There is a need for detailed multi-dimensional time unsteady computations which can predict PDE performance with realistic geometry. However, a reliable estimation of thrust, developed by a repeating PDE cycle by simulating realistic PDE cycle processes, is a complex computational problem. Therefore, the computed PDE processes must be validated with data from experiments.

Internal geometry has a significant impact on the thrust developed by the PDE. Optimization of internal geometry is necessary to ensure sufficient fuel-air mixing and successful detonation initiation while minimizing the pressure loss in the system. Nonuniformity in fuel-air mixing can lead to failure of initiation and/or detonation propagation resulting in decreased thrust.

The physical mechanisms governing deflagration-to-detonation transition are described in recent reviews [12-14]. Previous computational investigations [16] suggest that the hot spots arise from fluctuations that increase as the turbulent flame becomes more intense, and the mechanism by which a hot spot transitions to a detonation is attributed to spontaneous pressure waves that arise due to gradients of induction time. Several computational studies of DDT have been performed, and they include direct numerical simulations of combustion wave and gas dynamical wave interactions in small-scale geometric configurations [15] and state-of-the-art modeling of turbulence-chemistry-gasdynamic interactions in large-scale nuclear reactor accident scenarios [14]. The latter study provides comprehensive descriptions of various turbulent combustion and gas dynamical models necessary for simulation of flame acceleration and DDT. However, there exists little information on application of these detailed DDT process simulations to a PDE cycle operation.

The blowdown process determines the thrust generated by the PDE cycle. Simulating the blowdown of the supersonic combustion products from the detonation chamber requires the use of realistic boundary conditions involving multidimensional computations.

The objectives of the present investigation of the cyclic detonation processes are: (i) to develop computational methods to model key PDE cycle processes including fuel-air mixing, DDT initiation, and blowdown for a stoichiometric mixture of C_2H_4 and air; (ii) to validate the computational method by applying a 2-step reduced mechanism for a C_2H_4-O_2 mixture in an ideal PDE tube and by comparing results with existing test measurements in the literature; (iii) to apply the computational method for performance estimation during a repeating PDE cycle operation, and (iv) to investigate the effect of bulk velocity on the thrust produced by a PDE during cyclic operation.

In order to achieve the objective of understanding thrust generation during each PDE process, a benchmark tube having a 0.051 m diameter, a 1.27 m length, with a specified mass flowrate, filled with a stochiometric C_2H_4-air mixture at initial conditions of 1.0 atm. and 298 K, is used.

The outline of the remainder of the paper is as follows. First, the numerical method and the experimental setup are described. The results of a realistic simulation of a PDE cycle operation are presented. A summary of the effect of bulk velocity on the flow through the PDE on cycle performance is discussed. Finally, the conclusions of the ongoing PDE investigations and future plans are summarized.

2.0 Computational Method

A commercially available numerical solver [17] was used to obtain time-resolved predictions of the PDE cycle processes presented in this paper. The following solver-specific features were invoked in this study: (i) unstructured grid treatment enabling the use of complex geometries, (ii) second-order accuracy in space with total variation diminishing interpolation together with a HLLC Reimann solver to avoid spurious numerical oscillations in the computed flow field, (iii) a multidimensional second order total variation diminishing (TVD) interpolation that more accurately represents the local behavior of flow dependent variables with a 'MinMod' slope limiter, (iv) second order time accuracy, (v) coupled solver, (vi) implicit relaxation approach, to avoid time-step restrictions, for both flow and scalar variables, (vii) a nonlinear Reimann solver for estimation of fluxes at the cell interfaces, (viii) implicit boundary condition treatment, (ix) dual time stepping for convergence acceleration, (x) use of algebraic grid approach for convergence acceleration, (xi) point-wise implicit relaxation methodology to enable parallel processing capability, (xii) Navier-Stokes solver with perfect gas assumption with variable thermal and transport properties for air, and (xiii) a realizable k-□ model for modeling turbulence processes. For all the simulations reported here, viscous terms are included. Such terms are considered important for the PDE cycle processes, including fuel fill, initiation and purging.

Geometries and Grids

Ideal Tube

The ideal PDE tube configuration used in the present study is a two-dimensional axisymmetric geometry, 1.43 m in length and 0.038 m in diameter. This geometry is the same as the idealized PDE geometry considered in a previous experimental study [19] in which performance measurements were reported.

The unstructured grid that was used for the ideal tube without obstacles is the same as reported earlier [11]. The computational domain extends to a length of 1.62 m (5 diameters in the axial direction at the exit of the tube) and the maximum radial coordinate of the domain outside the tube is 0.19 m (5 diameters in the radial direction at the exit of the tube). The grid spacing is □x = 0.75 mm and □y = 0.75 mm inside the tube, and the total mesh size is 75000 elements. A dual time-stepping method in which the global CFL number (defined as (u+c)*dt/dx where u is the local convective speed, c is the speed of sound, dx is the spatial grid spacing and dt is the global time step) of 0.1-1.0, was specified for all the simulations reported here.

Benchmark Tube

The benchmark PDE tube configuration used in the present study is a two-dimensional axi-symmetric geometry, 1.27 m in length and 0.051 m in diameter. Figure 2.1(i) shows the geometry of the benchmark PDE tube with obstacles. Care was taken to model the upstream geometry with local 3D features in the context of a 2D axisymmetric assumption, while preserving upstream volume and surface-to-volume ratio in the geometric model. For the benchmark tube geometry with internal obstacles (Fig. 2.1(i)), the blockage ratio, defined as the ratio of obstacle area to the total tube cross-sectional area, is 0.43. The obstacle spacing is one diameter, and there are a total of 20 obstacles evenly distributed downstream of the fuel injector.

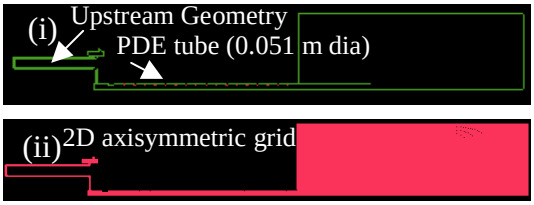

Fig. 2.1: 2D-axisymmetric (i) geometry and (ii) grid of size 90000 cells of the benchmark tube used for simulation of Cases 4, 5, 6 and 7 (shown in Table 1).

The unstructured grid that was used for the benchmark tube with obstacles is shown in Fig. 2.1(ii). The computational domain considered extends to a length of 1.63 m (7 diameters are considered in the axial direction at the exit of the tube) and the maximum radial coordinate of the domain outside the tube is 0.27 m (7 diameters in the radial direction at the exit of the tube). The grid spacing is □x = 0.75 mm and □y = 0.75 mm inside the tube, and the total mesh size is 90000 quadrilateral elements.

Computational Model

The computational model considers an unsteady Reynold's averaged Navier Stokes (RANS) simulation with a variable property formulation including real gas effects. A realizable k-□ model was used for turbulence, and a 2-step reduced chemical mechanism [18] was used for simulating C_2H_4-O_2 and C_2H_4-air chemical reactions. Initial conditions of 1.0 atm., 298 K and a stoichiometric C_2H_4-O_2 mixture, are specified for the ideal tube PDE simulations. For the benchmark tube, a steady state solution for a specified inlet air flowrate at an inlet temperature of 298 K serves as the initial condition. The boundary conditions for the domain outside the tube are: the back pressure condition of 1 atm., for the right (downstream) boundary condition in the axial direction and far stream boundary conditions for all other external boundaries. In addition, fuel (C_2H_4) is brought in separately using either a timing valve model (to simulate

a fuel valve) at a specified boundary surface or a volumetric source term in a range of interior elements.

For the case of the ideal tube, a shock-induced detonation initiation model is used. This model was described in detail in an earlier investigation of detonation intiation [11]. In the case of the benchmark tube, the simulation of weak/DDT initiation is achieved by adding energy as a volumetric source to a range of tagged ignition cells. The amount of energy provided for initiation is similar to the spark energy required in the experiment.

Summary of Variation of Parameters

Case #	Inlet Air Flowrate (kg/s)	C_2H4_+ Oxidizer	Fuel Fill Time (ms)
1	0	O_2	N/A
2	0	O_2	N/A
3	0	Air	N/A
4	0.0682	Air	50
5	0.0682	Air	42
6	0.125	Air	24
7	0.182	Air	17

Ideal tube

Benchmark tube

Table 1: Summary of tube PDE run conditions, including those chosen to study the effect of bulk velocity of the inlet air flow on PDE cycle operation.

Table 1 shows a summary of the ranges of parameters varied in order to understand the effect of bulk velocity on both fuel-air mixing and the performance parameters, namely thrust (T), impulse per unit volume (I_v) and fuel-specific impulse (I_{spf}). The bulk velocity of the flow through the benchmark PDE is varied by changing the air mass flowrate. A range of 0.0682 – 0.182 kg/s in mass flowrate results in a variation of 30-80 m/s in the bulk velocity. The fuel fill time for 100% fill is determined using the tube length divided by bulk velocity, resulting in a range of 42-17 ms for 100% fill.

3.0 Experimental setup

Figure 3(i) shows a photograph of the PDE tube setup, and Fig. 3(ii) shows a schematic of the PDE tube geometry. The benchmark PDE tube used in the present experiments is a 51 mm diameter tube (2" diameter polycarbonate pipe). Air flows continuously into the tube through two opposing holes in the end cap, and ethylene fuel is pulsed via a solenoid valve. Fuel-air mixing occurs directly in the tube using a mixing element. The tube length (1.27 m) is measured from the mixing element aft face to the tube exit. A spark plug igniter is mounted within one diameter downstream of the fuel injection. Seventeen orifice plates with a blockage ratio of 0.43 were installed at 51 mm intervals starting 150 mm from the aft face of the mixing element. The PDE tube was run with 100% fill of nominally stoichiometric ethylene-air mixture at 10 Hz and an airflow rate of 0.068 kg/s. The upstream geometry consists of 1 meter long hoses connected to a tank (150 mm diameter, 200 mm long). The purpose of this tank is to maintain a nearly constant supply pressure to the PDE tube. This tank is supplied with air via a 25.4 mm flexible hose that runs approximately 6.1 m to an air control valve.

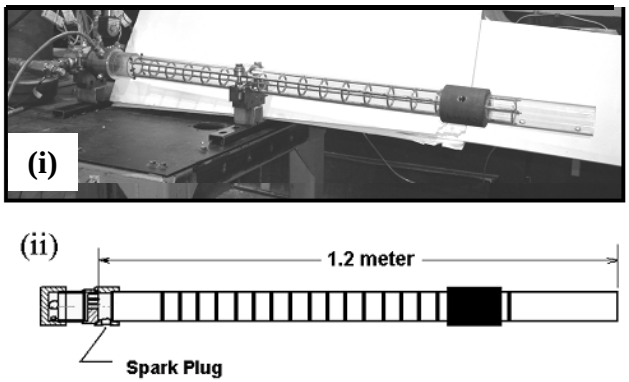

Fig. 3.1: Photo of the PDE facility showing (i) transparent DDT section, and (ii) cross-section of 50 mm diameter benchmark PDE tube.

Pressure traces were obtained using three PCB transducers (Model Number 113A/402A) located at the end cap, 127 mm and 25.4 mm from the end of the tube. The last two transducers were used to calculate the time of flight of the pressure wave to verify detonation. Typical measured time-of-flight velocity was 2030 ± 100 m/s which is comparable to the Chapman-Jouguet detonation velocity for H2-Air of 1980 m/s.

A high-speed imaging system was used to visualize the DDT process within the PDE tube. The primary component is a high framing rate digital video camera (Vision Research Phantom 7) with a framing rate between 56500 and 81000 frames per second, and a 1 □s exposure time.

4.0 Validation of the Computations for an ideal TUBE PDE

Simulations of an ideal tube PDE fueled with a stoichiometric mixture of C_2H_4-O_2 are used to both validate the computational method and the ability of the 2-step reduced chemical mechanism to model detonation propagation and to obtain performance estimates. A

shock-induced ignition of the mixture is simulated by introducing a high temperature and high pressure region (2000 K and 10.0 atm, respectively) 5 mm thick at the closed end of the tube. The C_2H_4-O_2 mixture is initially at 1 atm., and 298 K (T_0), and at an equivalence ratio (ϕ_0) of 1.0. Autoignition occurs after an induction delay, which is a strong function of local temperature, in a region between the leading shock wave and the contact surface [9]. Hence, the initial temperature has a strong impact on the occurrence/ non-occurrence of detonation initiation. Subsequent heat release results in pressure waves which couple with the leading shock wave to form a detonation. For lower initiation-region temperatures (Ts < 1000 K), no detonation was initiated. The initiation-region pressure has only a secondary effect through the shock compression of the fresh reactants, which raises the temperature of the fresh mixture and thus influences the initiation of detonation. Figure 4.1 shows the predicted variation of detonation velocity along the length of the ideal PDE tube. The detonation velocity is calculated from time-of-arrival of pressure peaks at various locations along the length of the tube. During the initial part of the transient (time < 50 μs or x < 0.1 m), the flow near the spark region was found to be unsteady, which is reflected in the predicted time evolution of detonation velocity. For x > 0.1 m, the predicted detonation velocity is independent of axial distance (x) or transient time and is in close agreement with the Chapman-Jouguet velocity, V_{CJ} of 2370 m/s for this mixture. The total time for the detonation to traverse the length of the tube (1.43 m) is 430 μs.

Figure 4.2 compares the predicted pressure-time traces adjacent to the closed end of an idealized PDE tube with test measurements of the Stanford single shot ideal PDE tube [19]. Overall comparison shows good agreement between predicted and measured pressure–time traces. Two noteworthy differences are noted as follows. At the beginning of the transient (t ~ 0.0), the deviation of the predicted pressure from the measured value is attributed to the shock-induced intiation model which was used in the simulations as opposed to spark-induced initiation in the experiments. In addition, the fluctuations in the predicted pressure time trace is not as pronounced when compared to the fluctuations in the measured pressure-time trace. The predicted 'plateau' pressure of 11.5 bar is in close agreement with the test measurements and with the value reported by Kailasnath et al. [8].

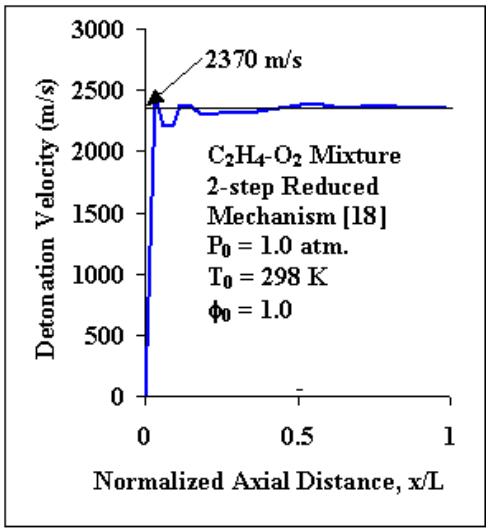

Fig. 4.1: Predicted detonation velocity as a function of normalized axial distance for an ideal PDE tube during the detonation propagation.

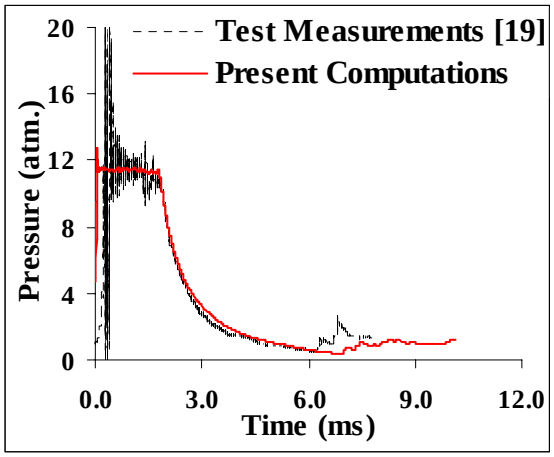

Fig. 4.2: Comparison of predicted pressure at the closed end of the tube as a function of time with Stanford ideal tube PDE test measurements [19].

The performance metrics of the ideal PDE tube for the case of stoichiometric C_2H_4-O_2 mixture obtained using the 2-step reduced mechanism are given below. Figure 4.3 shows the cumulative net impulse during the blowdown process. The predicted net impulse during the blowdown of a single shot PDE cycle is estimated to be 3.2 N.s. The predicted impulse per unit volume (I_v) is 2082 N-s/m3, the predicted mixture-based specific impulse (I_{sp}) is 167s and the fuel-based specific impulse (I_{spf}) is 741 s. Table 2 shows the comparison of the predicted performance parameters with existing data in the literature [8,19,20]. The performance parameters are in close agreement with the performance predictions reported by Kailasanath et al. [8], Cooper et al. [20] and Hinckley et al [19].

In summary, the computational method using a 2-step reduced chemical mechanism for C_2H_4-O_2 mixture successfully simulates the propagation and blowdown processes of an ideal tube PDE. The performance estimates show good agreement with existing data in the literature.

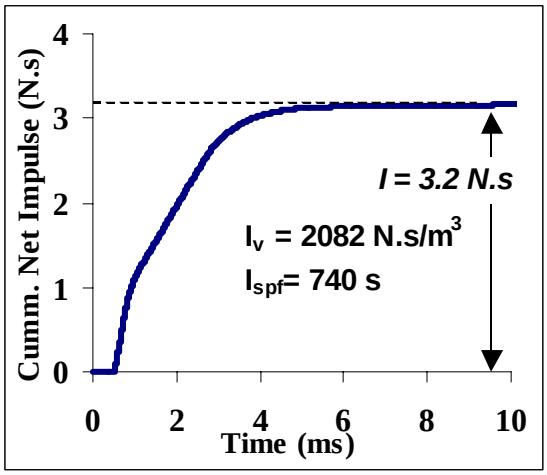

Fig. 4.3: Variation of cumulative impulse as a function of time for an ideal PDE tube using a stoichiometric mixture of C_2H_4 and O_2 during the blowdown.

5.0 simulation of Benchmark tube PDE cycle and comparison with experiment

The main processes of the PDE cycle are summarized in Table 3. For both the experiments and calculations in this report, the initial conditions in the PDE tube are stoichiometric ethylene-air at the mixing element during fill, 101.3 kPa outlet pressure, 300 K inlet temperature, 0.068 kg/s average mass flow and an operating frequency of 10 Hz. For these conditions, the approximate duration of each part of the cycle is shown in Table 3.

Steady Flow

Steady flow calculations reveal the basic features of the flow through the PDE tube. For an average mass flow through the PDE tube of 0.068 kg/s, Figure 5.1 shows the axial velocity and pressure through the tube. Due to the pressure drop across each orifice, the velocity increases through the DDT section. For these conditions and a blockage ratio of 0.43, the pressure drop in the DDT section is about 5%. The pressure drop downstream of the DDT section is negligible. This value is in good agreement with the pressure drop measured in the rig at the same conditions.

	P_3 (atm)	I_V (N.s/m^3)	I_{spf} (s)
Stanford Test Measurements,	11.5	2089	720
Caltech Test Measurements		2136	758
Caltech Analytical Predictions, Case 1 Wintenberger et al.	11.0	1843	668
NRL Computations, Kailasanath et al. [88]	12.0	2100	732
GE-GRC, Present Computations	11.5	2082	740

Table 2: Comparison of impulse per unit volume and fuel specific impulse of the ideal tube PDE (Case 2) with results from previous studies.

At the upstream mixing element, fuel is added to the air resulting in an initially uniform mixture. As this mixture flows through the DDT section, there is a core flow convecting fresh charge at ~80 m/s (see Figure 5.1(ii)). This core flow is moving much faster than the bulk velocity of 30 m/s that would occur with no obstacles. If the duration of the fill cycle is timed to achieve one volume change in the tube, then a lean fuel-air mixture will exit the tube before the fill cycle is complete. As a consequence, the fill time would need to be reduced to avoid sending fuel out the end of the tube, resulting in pockets of leaner mixture near the wall between obstacles. The resulting axial and radial profiles of fuel concentration deviate from the goal of achieving a uniform, 100% charge of fresh detonable mixture (Figure 5.2(iv)).

PDE cycle process	Duration Cycle Time (ms)
Fuel fill	0 - 50.0
Ignition Transition Propagation	50 - 52 52 - 53.2 53.2 - 53.6
Blowdown	53.6 - 58.0
Purge	58.0 - 100.0

Table 3: PDE Cycle Timing for Case 4.

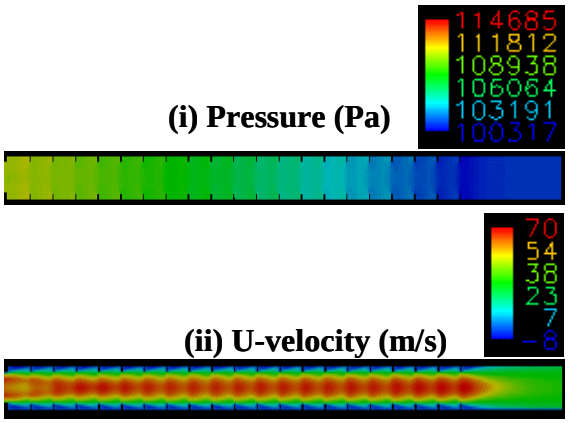

Fig. 5.1: Predicted steady state contours of (i) pressure contours (Pa) and (ii) axial velocity (m/s) through the PDE tube at steady state flow conditions of P_{in} = 1.15 bar, T_{in}=300K, mair = 0.068 kg/s (Case4).

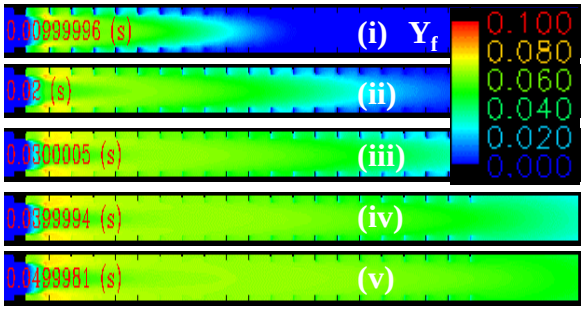

Fig. 5.2: Predicted fuel mass fraction contours at various times during the fuel fill process (Case 4).

Detonation Initiation and Propagation

In the benchmark experiments, the combustion process is initiated via a weak spark (~30 mJ) timed to closely coincide with the end of the fill cycle. The spark plug is located near the head end of the PDE tube. A set of seventeen orifice plates (blockage ratio = 0.43) is used to reduce the run-up distance to detonation.

Detonation initiation was visualized by imaging chemi-luminescence through a transparent polycarbonate tube and using a high-speed video camera. For the imaging runs, the PDE was fired in short bursts with the valve and spark timing consistent with 10Hz operation. All other parameters (mass flow, inlet T&P, etc) were kept the same as for Case 4.

Figure 5.3 shows a series of images of a DDT event where time zero is taken when the spark flash is detected at the head end. The dark sections between obstacles 8 – 9 and beyond obstacle 16 correspond to metal support features outside the tube. The spark is initiated at the end of the fill cycle when the tube is filled with a combustible mixture (Fig. 4.3(i)). After 2.6 ms, a turbulent flame appears from the left and propagates to the right (Fig. 5.3(ii)). The flame continues to accelerate, and more intense chemiluminescence is observed at obstacle 12 (Fig. 5.3 (iv)). The frame of Fig. 5.3(vi) shows a nearly planar detonation emerging from the DDT section, while there is still considerable chemiluminescence from the turbulent combustion region.

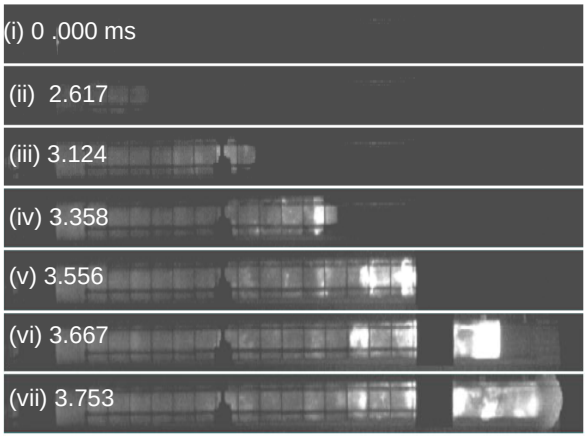

Fig. 5.3: High speed imaging of ethylene-air DDT in PDE tube at various times of the PDE cycle (Case 4).

The predictions of flame propagation and transition to detonation are shown in Figure 5.4. In the numerical simulation, the combustion process is initiated by depositing energy in the same axial location as the spark plug in the PDE experiments. Energy deposition for initiation corresponds to the end of the fuel fill cycle. Figures 5.4(i) through 5.4(iv) show a turbulent flame propagating through the obstacles. Transition to detonation is observed in Fig. 5.4(viii), which shows the formation of a planar shock front, and the wave velocity approaches Chapman-Jouguet (C-J) velocity. The detonation achieves characteristics of a steady-state detonation as it propagates toward the exit of the tube (Fig. 5.5). The predicted time of flight (the time interval between the spark initiation and the exit of the detonation wave from the tube) of 3.6 ms agrees very closely with the experimentally measured value of 3.8 ms.

A key qualitative difference between the measurements and calculations is that the transition occurs within the DDT section in the calculations. Transition was not observed until the turbulent flame front reached the last 2-3 obstacles in the experiments, and it appeared that the obstacles hindered final transition to detonation. A more detailed comparison between the measurement and calculation of DDT is shown on the X-t diagram in Fig. 5.6(i). This diagram shows that the leading wave travels faster in the calculation (approx. 35%) than in the experiment in the DDT section of the tube and reaches a steady value that agrees well with calculated CJ velocity. Figure 5.6(ii) shows a more detailed comparison of

propagation velocity (normalized with the CJ velocity of 1850 m/s for stoichiometric C_2H_4-air mixture) along the tube. The numerical predictions reveal rapid flame acceleration leading to over-driven detonation and finally relaxing to C-J velocity. This behavior agrees well with behavior reported by Cooper et al [18].

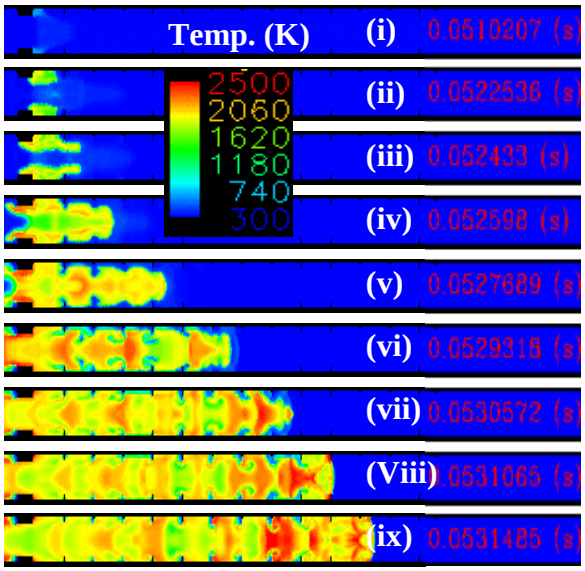

Fig. 5.4: Predicted temperature contours at various times during the detonation initiation process (Case 4).

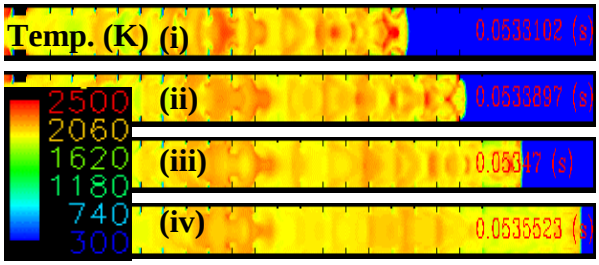

Fig. 5.5: Predicted temperature contours during the detonation propagation process (Case 4).

Blowdown

The blowdown process is responsible for most of the thrust production. There are three phases of blowdown: emergence of the blast wave, supersonic blowdown, and subsonic blowdown. A comparison of measured and numerical prediction of the initial phase of blowdown is shown in Figure 5.7. The numerical predictions are presented as numerical schlieren images produced by post-processing the results. As the detonation emerges from the tube, the reaction front separates from the leading shock wave. The shock wave wraps around the tube and travels both upstream and downstream. The hot combustion products follow the leading shock, but the reaction zone quickly de-couples from the leading shock wave.

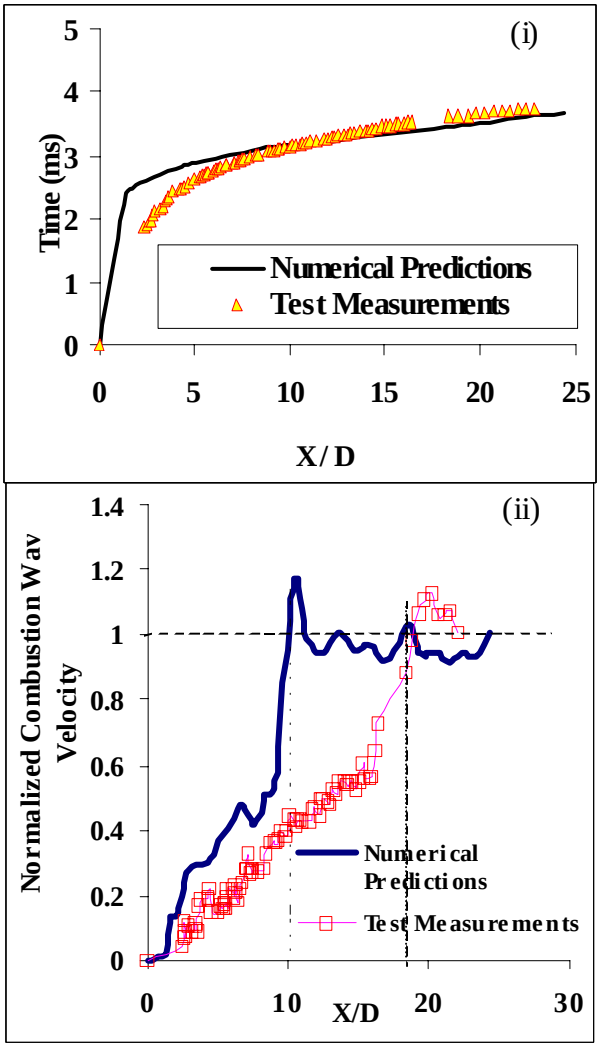

Fig. 5.6: Comparison of numerical prediction and measurement of (i) X-t diagram and (ii) velocity-position

Purging

Figure 5.8 shows predicted time evolution of oxygen concentration contours during the purging process. At the end of detonation and blowdown processes, oxygen is completely consumed. As the blowdown is completed, the pressure in the end cap plenum decreases, and the purge flow enters the tube. Figure 5.8(i) shows the oxygen mass fraction at the end of the blowdown process, and Fig. 5.8(iv) shows the oxygen mass fraction contours at the end of purge process. The purging process is completed approx. 30 ms after the completion of the blowdown process.

Predicted and Measured Pressure-time Traces

Figure 5.9 shows comparisons of predicted and measured pressure-time traces in the end cap cavity.

Overall, there is good agreement in the shape between the calculation and the experiment. The predicted plateau pressure of 5.3 atm is less than the measured value of over 8 atm. The source of the difference is under investigation and may be due to either instrumentation calibration or a higher initial head pressure in the experiment than in the calculation.

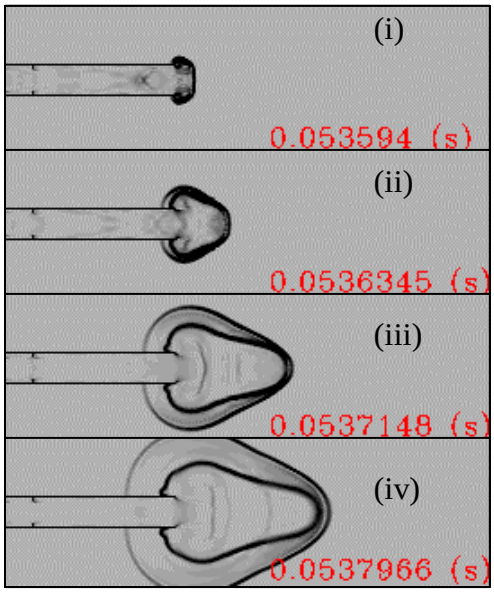

Fig. 5.7: Predicted schlieren contours at various times of the blowdown process (Case4).

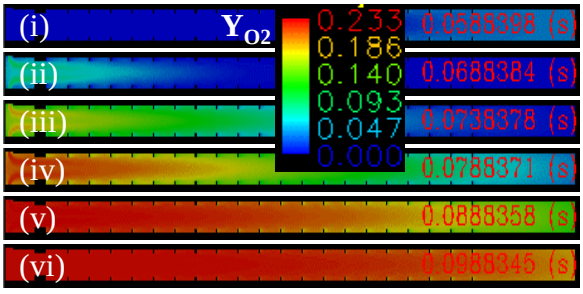

Fig. 5.8: Predicted oxygen mass fraction contours during blowdown and purging processes (Case 4).

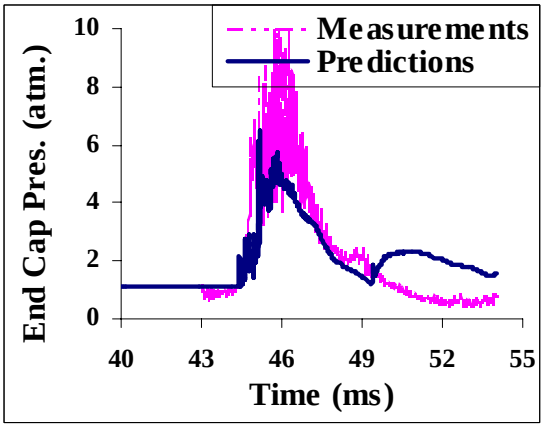

Fig. 5.9: Comparison of predicted and measured pressure-time traces in the end-cap cavity (Case 5).

Influence of bulk velocity on thrust and Fuel air mixing
The benchmark tube study includes all the processes of a multi-cycle PDE with realistic geometry. This results in differences in performance between the benchmark tube and the ideal PDE tube. One important parameter in the benchmark PDE study is the bulk velocity of purge flow and fresh fuel-air mixture during the cycle. This velocity influences gas exchange during purge, fuel-air mixing, DDT and overall thrust production. In this section, the effect of bulk velocity of flow through the benchmark tube on fuel-air mixing and thrust is studied, while keeping all other parameters fixed.

Thrust Estimations

The key parameters for determining the net impulse over a PDE cycle are momentum flux and pressure forces acting in the axial direction at the tube exit. Here, the thrust calculation is illustrated by using a control volume, as shown in Figure 6.1. Alternatively, a control volume which follows the walls of the tube can be used, and the key parameters are then pressure forces and shear stresses on internal surfaces.

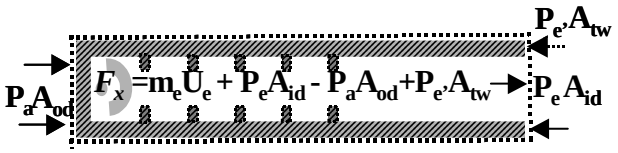

Fig. 6.1: Control volume 1 as applied to Cases 4, 5, 6 and 7a for thrust estimations.

A force balance for control volume 1 can be written as follows:

$$F_x = \dot{m}_e u_e + P_e A_{id} - P_a A_{od} + P_{e'} A_{tw} \rightarrow (1)$$

Where

$F_{x,}$ Instantaneous thrust developed by the PDE,

m_e: mass flow rate at the exit of the tube,

u_e: x-velocity component at the exit of the tube

P_e tube exit pressure, A_{id} is the corresponding area,

$P_{e'}$ exit pressure adjacent to tube walls, A_{tw} is the corresponding area, and

P_a ambient pressure, A_{od} is the corresponding area.

To estimate the thrust using Eq. 1, knowledge of mass flow rate, velocity and pressure at the exit as a function of time is needed. This information is easily extracted from unstructured CFD results at the tube exit plane. Thrust estimations using control volume 1 and Eq. 1 are obtained for the benchmark cases 4, 5, 6 and 7. A specific correction is applied to the thrust estimated by Eq. 1. This correction applies to the benchmark tube cases and is equal to the thrust generated by the tube operating under steady flow conditions with no chemical reactions. This correction is directly proportional to the mass flow rate of the mixture flowing through the tube. The thrust generated by a PDE is the sum of the supersonic blowdown and the subsonic blowdown. The exit Mach number for Case 5 during the blowdown is plotted in Fig. 6.2 and shows the relative duration of each part of the blowdown. Initially, there is choked supersonic flow for a period of 2 ms (20% of the total blowdown time of 10 ms). The remainder of the blowdown (80%) is a subsonic blowdown. Figure 6.2 shows that the exit Mach number drops to a minimum after approximately 5 ms into the blowdown process and then increases again. This is caused by variation in depressurization of the tube due to obstacles.

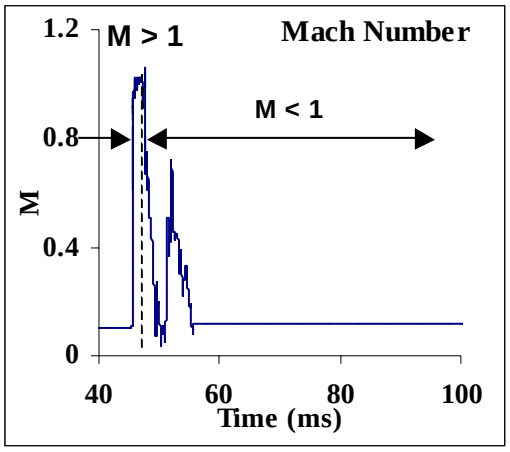

Fig. 6.2: Time variation of the tube exit Mach number during the blowdown (Case 5).

The cumulative net impulse generated by the benchmark tube (Case 5) is shown in Fig. 6.3. It attains a constant value of 1.7 N.s in approximately 15 ms from the start of the blowdown process. This includes a correction of 0.2 N.s for the thrust developed during steady state initial conditions with no reactions. This net impulse translates into a value of 17 N for thrust generated by the benchmark tube operating at 10 Hz and a mass flow rate of 0.068 kg/s, a value of 733 N.s/m3 for impulse per unit volume (I_v) and a value of 1109 s for fuel-specific impulse (I_{spf}).

Ideal Tube vs. Benchmark Tube

The operation and thrust estimations of an ideal tube PDE are well documented in the literature. The key differences between the simulation of an ideal tube and the simulation of the benchmark tube for obtaining thrust estimates can be summarized as follows: in an ideal tube PDE, the fuel is initially premixed with air, and the fuel-air mixture is well characterized by the initial condition specification. In addition, the ideal tube PDE does not have any internal geometry features which can cause a pressure drop in the system. For thrust estimation of an ideal tube PDE, it is sufficient to simulate detonation initiation, detonation propagation and blowdown processes.

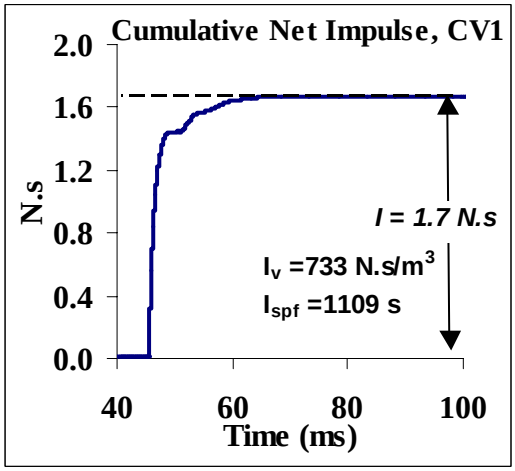

Fig. 6.3: Time variation cumulative net impulse for the PDE cycle operation of the benchmark tube (Case 5).

The benchmark tube can be distinguished from the ideal tube in the following ways.

The fuel and air are brought in separately (overall equivalence ratio is 1.0, air flowrate is 0.068-0.18 kg/s) in the mixing segment of the tube, and this results in mixture nonuniformities and leads to local equivalence ratios which are less than or greater than the overall equivalence ratio. For an overall equivalence ratio of 1.0 of the fuel-air mixture, the variation in local equivalence

ratios can only lower the impulse produced by the benchmark tube.

The upstream section of the tube is not closed, and air flows through the system continuously except for the time interval during which high-pressure conditions exist in the tube. A strong compression pulse (retonation) is formed during the initiation process and then travels upstream causing back flow in the upstream section of the tube, resulting in a reduction of the net impulse. The benchmark tube has internal geometry features such as the DDT-promoting obstacles and a mixing element, which result in a pressure drop through the tube. These internal flow resistances can cause substantial reductions in the thrust developed by the benchmark tube.

The performance parameters, namely impulse per unit volume (I_v) and fuel specific impulse (I_{spf}) for the ideal case fueled with C_2H_4-air mixtures (Case 3), obtained using the analytical method [7], are 1328 (N.s/m3) and 1839 s respectively. The corresponding metrics for the benchmark tube are 733 (N.s/m3) and 1109 s respectively. The predicted decrease of 40% in I_{spf} of the benchmark tube (Case 5) when compared to the I_{spf} of an ideal tube (Case 2) can be attributed to (i) the pressure drop in the benchmark tube resulting from a realistic simulation of benchmark tube internal geometry (DDT obstacles), (ii) nonuniformities in the mixture composition for the benchmark case as opposed to assumed uniform mixture composition for the case of an ideal tube and (iii) backflows in the inlet section of the benchmark tube due to a compression wave propagating into the upstream geometry.

Effect of Bulk Velocity on Fuel Air Mixing

In order to understand the effect of bulk velocity on the fuel air mixing in the benchmark tube, the bulk velocity of the air flow is systematically varied from 33 m/s for Case 5 to 85 m/s for Case 7. For all the cases considered, the fuel fill fraction (defined as the amount of fuel injected into the tube divided by the amount of fuel in the tube corresponding to a stoichiometric mixture) is maintained as close to unity as possible by varying the fuel fill time. This resulted in decreasing the fuel fill time from 42 ms (Case 5) to 17 ms (Case 7). Figure 6.4 shows the axial variation of the centerline fuel mass fraction, at the end of fuel fill process for varying bulk velocities (33, 59, and 85 m/s). Near the mixing element where the fuel is injected into the air flow, ($x < 0.2$), the predicted fuel mass fraction is higher than the stoichiometric value (0.063). For $x\ 0.2 < x < 1.2$, the predicted fuel mass fraction is lower than the stoichiometric value.

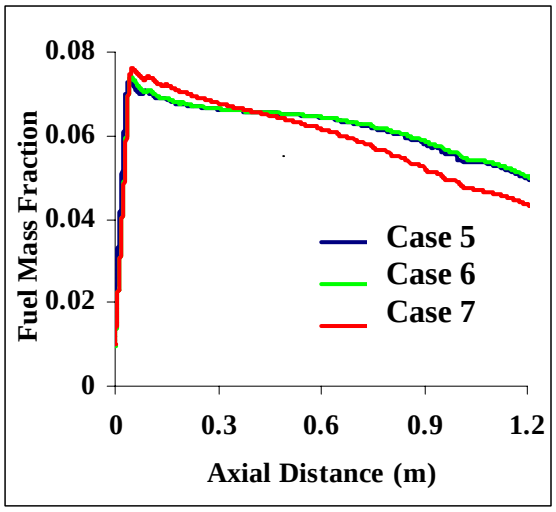

Fig. 6.4: Predicted axial variation of fuel mass fraction at the end of fuel fill process for varying bulk velocities (33, 59, and 85 m/s) of the flow through the benchmark tube.

Figure 6.4 also shows a more pronounced effect of bulk velocity on fuel air mixing for Case 7 (85 m/s) than for Cases 5 and 6 (33 and 58 m/s respectively). The centerline fuel mass fraction decreases more rapidly for Case 7 due to higher core flow velocities. This results in a mixture equivalence ratio of 0.75 near the end of the tube for higher bulk velocity. This nonuniformity in fuel air mixing in the axial direction results in the DDT process occurring upstream in a rich/stoichiometric mixture and the detonation propagation occurring downstream in a leaner mixture.

Figure 6.5 shows the axial variation of the predicted centerline fuel mass fraction at three distinct radial locations (r/D_t = 0.0, 0.39 and 0.78). The first two curves denoted by 1 and 2 are located in the core flow, one at the centerline and another off-centerline. The third curve denoted by 3 is radially located inside the obstacle region (as seen by the broken segments of the curve, caused by the presence of obstacles). Figure 6.5 shows that the radial variation in both the igniter section and the obstacle region of the benchmark tube is very significant as shown by the large radial gradients of the predicted fuel mass fraction in regions outside the core flow. The effect of these nonuniformities of mixture composition in the radial direction are expected to impact the flame acceleration and the detonation initiation processes.

Effect of Bulk Velocity on Thrust

Figure 6.6 shows the effect of varying the bulk velocity on the net impulse generated by the benchmark tube PDE for Cases 5, 6, and 7. For all cases considered, the transient time over which the performance metrics are estimated is set to 10 ms despite the variations in the

bulk velocity and the fuel fill time. For all the performance metrics reported in this subsection, an effort was made to maintain the percent fuel fill at 100%, by an *a priori* estimation of the fuel fill time ($t_{fill} = L/V_b$, where L is the tube length and V_b is the bulk velocity). However, the detailed CFD computations show this results in slightly higher than 100% fuel fill as shown in Table 4. The combined effect of the percent fuel fill and the fuel air mixing nonuniformities (which decreases the average mass fraction of the fuel at high bulk flow velocities) result in a small increase (13%) in the predicted fuel-specific impulse.

In summary, the bulk velocity together with the percent fuel fill are predicted to have an effect on the performance metrics by affecting the fuel-air mixing processes in the benchmark PDE.

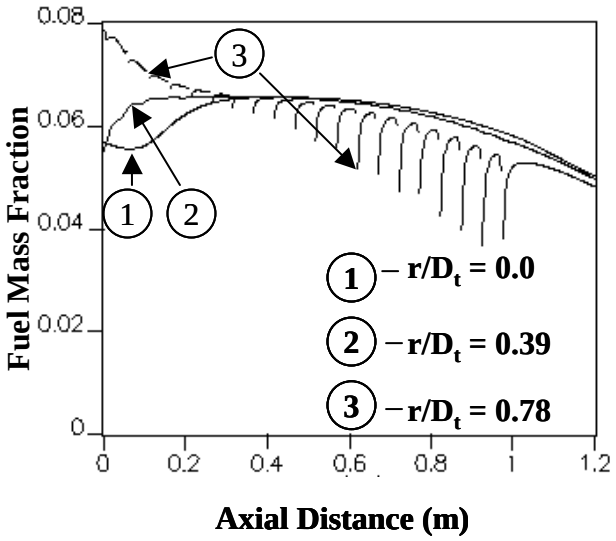

Fig 6.5: Predicted axial variation of the fuel mass fraction at the end of the fuel fill process at various radial locations for Case 7 (bulk velocity = 80 m/s and D_t = 5.09 cm).

	Thrust* (N)	I_V (N.s/m^3)	I_{spf} (s)
Case 5	16	626	820
Case 6	18	715	893
Case 7	19	764	925

Table 4: Summary of performance estimates as a function of bulk flow rate through the benchmark PDE tube fueled with C_2H_4-air mixture.

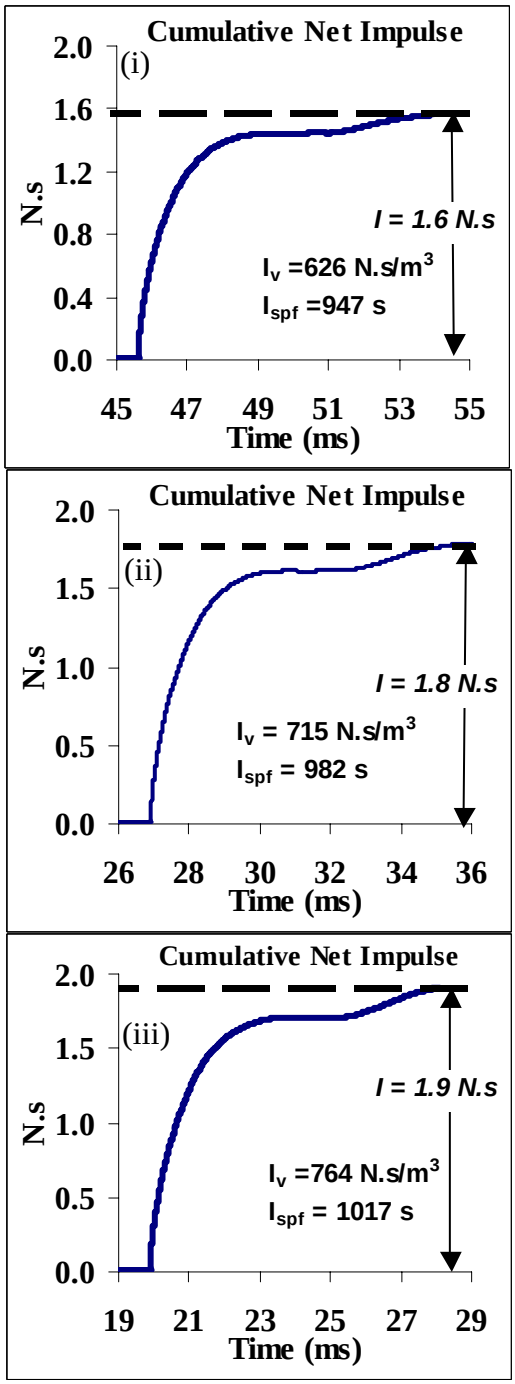

Fig. 6.6: Effect of bulk velocity on predicted fuel-specific impulse (I_{spf}) for (i) Case 5, (ii) Case 6 and (iii) Case 7.

7.0 Conclusions

Computational and experimental investigations of performance are reported for a Pulsed Detonation Engine (PDE) operating in a cycle, using ethylene-air mixtures. Simulations are performed for two geometry configurations, namely an ideal tube PDE with a smooth wall fueled with a premixed C_2H_4-O_2 charge, and a benchmark tube PDE with internal geometry and a

valve-less air supply fueled with a C_2H_4-air mixture. A 2-step reduced chemical mechanism for C_2H_4-air is used to model chemical reactions. The computational method simulates all the processes of the PDE cycle (fill, Deflagration to Detonation Transition (DDT), detonation propagation, blowdown and purge). Experiments are performed to validate the simulation of the key PDE cycle processes. Experimental measurements include DDT visualizations and dynamic pressure measurements.

A 2-step reduced mechanism for the C_2H_4-O_2 mixture is validated using existing test measurements for an ideal PDE tube from the literature. The computational method successfully simulates the propagation and blowdown processes of an ideal tube PDE. The performance estimates show good agreement with existing data in the literature.

Simulations of the benchmark tube PDE yield important insights into continuous cycle operation. Comparison of experimental and computational visualizations shows good agreement in cycle process time scales. The predicted decrease (~ 40%) in the fuel-specific impulse (I_{spf}) for the benchmark tube when compared to the I_{spf} of an ideal tube is attributed to nonuniformities in the mixture composition, pressure drop resulting from internal geometry (DDT-promoting obstacles), and backflows in the valveless benchmark tube due to a compression wave propagating into the upstream geometry. Increasing the bulk velocity of the flow through the benchmark tube has an adverse effect on the fuel/air mixing processes. The bulk velocity impacts the performance metrics by affecting the fuel fill processes in the benchmark PDE.

ACKNOWLEDGEMENTS

Authors wish to acknowledge the technical discussions with Dr. J. Shepherd of California Institute of Technology, Dr. K. Kailasnath of Naval Research Laboratories. Ideal tube data, provided by K. Hinckley of Stanford University is sincerely acknowledged. Authors acknowledge the technical help with experimental setup provided by Dr. A. Rasheed and E. Cornell of General Electric Global Research. Computational support provided by Dr. S. Palaniswamy of Metacomp Technologies, Inc., is sincerely appreciated.

References

Eidelman, S., and Grossmann, W., "Pulse Detonation Engine: Experimental and Theoretical review", *AIAA paper 92-3168*, July 1992

Glassman, I., *Combustion*, 2nd Edition, McGraw Hill, New York, 2000

Brophy, C.M., Netzer, D., Forster, D., "Detonation Studies of JP-10 with Oxygen and Air for PDE Development", *34th Joint Propulsion Conference*, Cleveland: AIAA (1998)

K. Kailasnath, "Recent Developments in the Research of Pulse Detonation Engines," *AIAA 2002-0470, 40th AIAA Aerospace Sciences Meeting & Exhibit*, January 2002, Reno, NV

Kailasnath, K., Li, C., and Patnaik, G., "Multilevel Computational Studies of Pulse Detonation Engines," ISOABE-2001-1172, September, 2001, Bangalore, India

Mohanraj, R., Merkle, C. L., and Ebrahimi, H. B., "Modeling of Pulse Detonation Engine Operation," AIAA 2001-0475, *39th Aerospace Sciences Meeting & Exhibit*, January 2001, Reno, NV

Wintenberger, E., Austin, J .M., Cooper, M., Jackson, *S.*, and Shepherd, J.E., "An Analytical Model for the Impulse of a Single-cycle Pulse Detonation Engine," *AIAA 2001-3811*, July 2001

K. Kailasanath, G. Patnaik and C. Li, "The Flowfield and Performance of Pulse Detonation Engines," *Twenty-ninth (International) Symposium on Combustion*, The Combustion Institute, PA, Vol. 29, 2002

Y. Wu and V. Yang, "Numerical Simulation of Detonation with Detailed Chemical Kinetics Using the Space Time Method," *AIAA 2000-0317, 38th Aerospace Sciences Meeting & Exhibit*, January 2000, Reno, NV

Povinelli, L. A., and Youngster, S., "Real Gas Effects on the Performance of Hydrocarbon-fueled Pulse Detonation Engines," *AIAA 2003-0712, 41st Aerospace Sciences Meeting & Exhibit*, January 2003, Reno, NV

Tangirala, V., B. Varatharajan, B., and Dean, A. J., "Numerical Simulations of Detonation Initiation," *AIAA-2003-0716, 41st Aerospace Sciences Meeting & Exhibit*, January 2003, Reno, NV

Shepherd, J. E., and Lee, J. H. S., "On Transition from Deflagration to Detonation," Major Research Topics in Combustion, Springer Verlag, Hampton, VA, 1992

Lee, J. H. S., "Detonation Waves in Gaseous Explosives," Hand Book of Shock Waves, Volume 3, Academic Press, 2001

Kline, R. Chapter 4: Detailed modeling of FA and DDT, "Flame Acceleration and Deflagration to Detonation Transition in Nuclear Safety," a State-of- the-Art Report by a Group of Experts, OECD Nuclear Energy Agency NEA/CSNI/ R (2000), 7 August 2000

Khoklov, A. M., Oran, E. S., and Thomas, G. O., 1999b "Numerical Simulation of Deflagration to Detonation Transition: the Role of Shock-flame Interactions in Turbulent Flames", Combust. Flame 117, 323-339

Oran, E. S., and Khokhlov, A. M. "Deflagrations, hot spots and the transition to Detonation," Phil. Trans. R. Soc. Lond. A (1999) 357, 3539-3551

Chakravarthy, S., Goldberg, U., Batten, P., Palaniswamy, S., and Peroomian, O., 2001, "Some Recent progress in Practical Computational Fluid Dynamics," *AIAA-2001-0136, 39th AIAA Aerospace Sciences Meeting and Exhibit*, January 2001, Reno, NV

B. Varatharajan and F. A. Williams, "Ethylene Ignition and Detonation Chemistry, Part 2: Ignition Histories and Reduced Mechanisms", *Journal of Propulsion and Power*, Vol. 18, No. 2, pp. 352-362, 2002.

Hinckley, K., "Stanford Tube PDE Experimental Data", personal communication, Mechanical Engineering Department, Stanford University, CA, 2003.

Cooper, M., Jackson, S., Austin, J.M., Wintenberger, E., and Shepherd, J.E., "Direct Experimental Impulse Measurements for Detonations and Deflagrations," *AIAA 2001-3812*, July 2001

APPENDIX D: Co-Authored 2003 ISABE Paper

PERFORMANCE ESTIMATES OF A PULSE DETONATION ENGINE

V. E. Tangirala, A. J. Dean, A. Rasheed and D. M. Chapin
Energy and Propulsion Technologies Laboratory
General Electric Global Research Center
One Research Circle, Niskayuna, NY 12309

Abstract

Computational and experimental investigations of performance are reported for a Pulsed Detonation Engine (PDE) under cyclic operation using hydrogen-air mixtures. Simulations are performed for two geometry configurations to study how internal geometry influences performance of a PDE. The computational method simulates all the processes of the PDE cycle (fill, Deflagration to Detonation Initiation (DDT), propagation, blowdown and purge). Experiments are performed to validate simulation of the PDE cycle processes. Experimental measurements include DDT and blowdown visualizations, and dynamic pressure measurements.

The results yield important insights into performance estimations of a PDE tube operating in a continuous cycle. Comparison of experimental and computational flow and scalar field visualizations show good agreement in cycle process time scales. Overall, there is good agreement between the numerical predictions and available experimental data on thrust generated by an ideal tube PDE. The predicted decrease of ~30% in the fuel-specific impulse (I_{spf}) for the benchmark tube when compared to the I_{spf} of an ideal tube is attributed to nonuniformities in the mixture composition, pressure drop resulting from internal geometry (DDT obstacles and a fuel-air mixing element), and backflows in the valveless benchmark tube due to a compression wave propagating into the upstream geometry. The effect of DDT-promoting obstacles on the fuel-specific impulse (I_{spf}) is estimated to be 16% for the H_2-air benchmark tube with ten, 0.43 blockage ratio obstacles.

1.0 Introduction

Pulse detonation engines (PDE's) have recently emerged as potential new devices to better utilize the chemical energy content of reactive fuel/air mixtures [0]. One of the main advantages of PDE's is that the detonations create less entropy when they combust a fuel/air mixture than conventional constant pressure processes such as those used in current gas turbines [2]. Establishing whether PDE's can achieve higher operating efficiency than conventional propulsion systems (i.e. gas turbines, ramjets, etc) is the focus of many research groups around the world.

One of the main challenges to make practical PDE's is the repeated initiation of detonations within the detonation chamber. Many implementations of pulse detonation engines rely on DDT to avoid the high energy required for direct initiation. DDT is the process whereby a deflagration is initiated using a weak energy source (typically tens of milli-Joules), and the combustion front accelerates via a series of gasdynamic processes and eventually detonates. A drawback of this approach for practical devices is the necessary length for transition (referred to as the run-up distance) to detonation, which for practical fuels such as Jet-A can be of the order of a meter. One method to reduce the run-up distance is the addition of oxygen in the initiation region [3]. This can greatly reduce the length required for DDT but can add significant complexity and weight to a propulsion system and additional logistical requirements. Another method is to add obstacles inside the tube. This has also been shown to significantly reduce run-up distance with fuel-air mixtures and there is little additional weight or complexity. For detonation initiation in fuel-air systems, DDT optimization is a trade-off between minimizing run-up distance via more obstacles or higher blockage ratio, and minimizing performance loss (pressure losses) via less obstacles or smaller blockage ratio.

The objectives of the present investigation of detonations are: (i) to develop computational methods to model key PDE cycle processes including fuel-air mixing, DDT initiation, and blowdown, (ii) to validate the computational methods used for performance estimation during a repeating PDE cycle operation, (iii) to predict the thrust produced by PDE during cycle operation, including the effect of DDT-promoting obstacles.

The outline of this paper is given as follows. First, the status of thrust estimation in the literature is discussed. Then the numerical method and the experimental setup are described. Results of a realistic simulation of PDE cycle operation are presented. A summary of the effect of obstacle geometry on PDE cycle performance is given. Finally, the conclusions of the ongoing PDE performance studies and the future plans are summarized.

PDE PROCESSES AND THRUST ESTIMATION

Many investigations of PDE thrust estimation [4-11] have focused on an ideal tube PDE which can be described as a constant cross-sectional tube, closed at one end and open at the other end, uniformly filled with quiscent fuel-air mixtures. The ideal tube typically has a diameter of 0.051 or 0.076 m and its length ranges from 1.0-1.5 m. These investigations include multi-level, multidimensional (zero, 1D, 2D and 2D axisymmetric) computations with and without chemical kinetics. The fuel-air systems investigated include H_2-air, C_2H_4-O_2 and C_2H_4-air. Real gas effects are found to have an impact on PDE cycle performance [15]. A recent analytical model was extensively validated for various fuel-oxidizer syatems, initial pressures, equivalence ratios using single pulse test measurements and has proven to be a valuable tool for thrust estimations within ± 15% [7].

Prediction of the propulsive performance of a pure tube PDE is of great interest in order to understand and improve the design of an engine in a parametric space comprising of geometric parameters, fuel type, degree of mixing, and detonation initiation method. Purely computational studies of a simple tube PDE were performed by a number of investigators. Even for the tube filled with a stoichiometric hydrogen-air mixture, there was a significant variation in the estimated values of the fuel-specific impulse (I_{spf}) over a single cycle, ranging from 3000s to 8000s. However, more recent detailed comparisons [4,5] have shown that most of this variation could be explained on the basis of the initial conditions and boundary conditions used in the various computational studies. For an ideal PDE tube completely filled with hydrogen-air mixture (at initial conditions of a pressure of 1 atm., a temperature of 300 K and an equivalence ratio of 1.0) convergence of estimations for I_{spf} at a value of 4160 s has been reported by the computational PDE research community [9-11].

Estimation of reliable thrust developed by a repeating PDE cycle by simulating realistic PDE cycle processes is a complex computational problem. However, there is a need for a validated computational appraoch to estimate performance indices (such as thrust and fuel-specific impulse) for the entire PDE cycle with realistic internal geometry. This need arises from the issues associated with assessing and optimizing the performance as a function of design variables including mass throughput rates, fuel type, frequency, ignitor geometry, mixture uniformity, cycle process time scales etc.

Internal geometry has a significant impact on the thrust developed by the PDE. Optimization of internal geometry is necessary to ensure sufficient fuel-air mixing and successful detonation initiation while minimizing the pressure loss in the system. Nonuniformity in the fuel-air mixing can lead to failure of initiation and/or detonation propagation resulting in decreased thrust.

The physical mechanisms governing deflagration-to-detonation transition are well described in recent reviews [12-14]. Several computational studies of DDT have investigated combustion wave and gas dynamical wave interactions in small-scale geometric configurations [15] to large-scale nuclear reactor accident scenarios [14]. The latter study provides comprehensive descriptions of various turbulent combustion and gas dynamical models necessary for simulation of flame acceleration and DDT. However, there exists little information on application of these detailed DDT process simulations to PDE cycle operation.

The computational requirements of such extensive simulation of initiation, starting with a laminar kernel to a detonation regime, can be daunting. However, as the flow entering the ignitor section of the PDE is a highly turbulent flow, the ignition of the deflagration wave can be initiated in a very similar way as the ignition is simulated in a constant pressure deflagration wave (such as the flames in gas turbine combustors). Previous computational investigations [16] suggest that the hot spots arise from fluctuations that increase as the turbulence flame becomes more intense, and the mechanism by which a hot spot creates detonation is by creating spontaneous waves that arise due to gradients of induction time.

The blowdown process of the PDE cycle determines the thrust generated by the PDE cycle. Simulating the blowdown of the supersonic combustion products from the detonation chamber requires the use of realistic boundary conditions involving multidimensional computations.

To acheive the objective of understanding the effect of all PDE processes on thrust generated during the cycle operation, a benchmark tube (defined as a 0.051 m in diameter and 1.0 m in length, with a specified mass flowrate, filled with H2-air mixture at initial conditions of a pressure of 1.0 atm., a temperature of 298 K and an equivalence ratio of 1.0) is used for obtaining numerical simulations and test measurements. The focus of the remainder of this report is to describe the ongoing efforts to obtain reliable thrust estimates for a repeating PDE cycle operating with hydrogen-air mixture, by performing realistic simulations and test measurements of the cycle processes.

2.0 Computational Method

A commercially available numerical solver [17] was used to obtain time-resolved predictions of the PDE cycle processes presented in this paper. The following solver-specific features were invoked in this study: (i) unstructured grid treatment enabling the use of complex geometries, (ii) second-order accuracy in space with total variation diminishing interpolation together with a HLLC Reimann solver to avoid spurious numerical

oscillations in the computed flow field, (iii) a multidimensional second order total variation diminishing (TVD) interpolation that more accurately represents the local behavior of flow dependent variables with a 'MinMod' slope limiter, (iv) second order time accuracy, (v) coupled solver, (vi) implicit relaxation approach, to avoid time-step restrictions, for both flow and scalar variables, (vii) a nonlinear Reimann solver for estimation of fluxes at the cell interfaces, (viii) implicit boundary condition treatment, (ix) dual time stepping for convergence acceleration, (x) use of algebraic grid approach for convergence acceleration, (xi) point-wise implicit relaxation methodology to enable parallel processing capability, (xii) Navier-Stokes solver with perfect gas assumption with variable thermal and transport properties for air, and (xiii) a realizable k-□ model for modeling turbulence processes. For all the simulations reported here, viscous terms are considered. Such terms are considered important for the PDE cycle processes including fuel fill, initiation and purging processes.

Geometries and Grids

Ideal Tube

The ideal PDE tube configuration used in the present study is a two-dimensional axisymmetric geometry, 1 m in length and 0.0762 m in diameter. This geometry is the same as the idealized PDE geometry considered in a previous experimental study [18] in which performance measurements were reported. Figures 1(i) and 1(ii) show the geometries for the cases of an ideal PDE tube with no obstacles and with obstacles respectively. For the ideal tube geometry with internal obstacles (Fig. 1(ii)), the blockage ratio is 0.43, obstacle spacing is two diameters and there are a total of 10 obstacles distributed from the closed end thru the middle of the tube.

The unstructured grid that was used for the ideal tube without obstacles is the same as reported earlier [11]. The computational domain extends to a length of 1.4 m (5 diameters in the axial direction at the exit of the tube) and the maximum radial coordinate of the domain out side the tube is 0.27 m (3.5 diameters in the radial direction at the exit of the tube). The grid spacing is □x = 0.75 mm and □y = 0.75 mm inside the tube, and the total mesh size is 75000 elements. A dual time-stepping method in which the global CFL number (defined as (u+c)*dt/dx where u is the local convective speed, c is the speed of sound, dx is the spatial grid spacing and dt is the global time step) of 0.1-1.0 was specified for all simulations reported here.

Benchmark Tube

The benchmark PDE tube configuration used in the present study is a two-dimensional axisymmetric geometry, 1 m in length and 0.051 m in diameter. Figures 1(iii) and 1(iv) show the geometries for the cases of benchmark PDE tube with and without obstacles respectively. Care was taken to model the upstream geometry with local 3D features in the context of a 2D axisymmetric assumption, while preserving upstream volume and surface to volume ratio in the geometric model. For the benchmark tube geometry with internal obstacles (Fig. 1(iv)), the blockage ratio is 0.43, obstacle spacing is two diameters and there are a total of 10 obstacles evenly distributed downstream from the fuel injector.

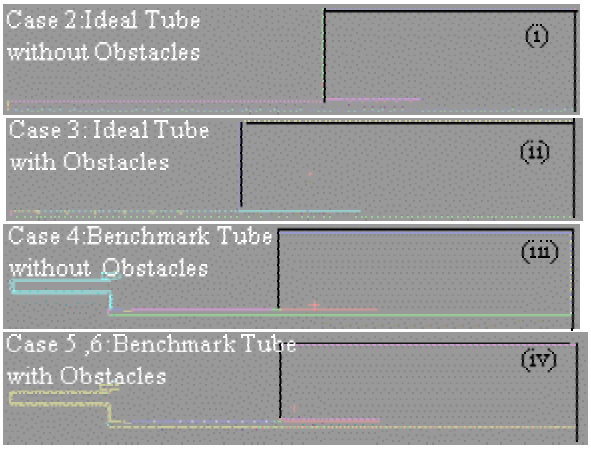

Fig. 1: Geometries of tube PDE, together with computational domain outside the tube

Fig. 2: Computational grid (size: 90000 cells) used for discretization of geometry shown in Fig. 1(iv).

The unstructured grid that was used for the benchmark tube with obstacles is shown in Fig. 2. The computational domain considered extends to a length of 1.5 m (7 diameters are considered in the axial direction at the exit of the tube) and the maximum radial coordinate of the domain outside the tube is 0.27 m (7 diameters in the radial direction at the exit of the tube). The grid spacing is □x = 0.75 mm and □y = 0.75 mm inside the tube, and the total mesh size is 90000 quadrilateral elements.

Computational Model

The computational model considers an unsteady RANS simulation with variable property formulation including the real gas effects. A realizable k-□ model was used for turbulence and a overall one-step chemical kinetic model [19] was used for simulating chemical reactions. Initial conditions of 1.0 atm., 298 K and a stoichiometric fuel-air mixture are specified for the ideal tube PDE simulations. For the benchmark tube, a steady state solution for a specified inlet air flowrate at an inlet

temperature of 298 K serves as the initial condition. The boundary conditions for the domain outside the tube are: the back pressure condition of 1 atm., for the right (downstream) boundary condition in the axial direction and far stream boundary conditions for all other external boundaries. In addition, fuel is brought in separately using a timed volumetric source model (to simulate a fuel valve) at a specified boundary surface or a range of interior elements respectively.

For the case of the ideal tube, a shock-induced detonation initiation model is used. This model was described in detail in an earlier investigation on detonation intiation [11] and will not be reproduced here. For the case of benchmark tube, the simulation of weak/DDT initiation is achieved by adding energy as a volumetric source to a range of tagged ignition cells. The amount of energy provided for initiation is similar to the spark energy required in the experiment.

Summary of Analyses

Table 1 shows a compilation of the thrust estimation analyses performed to understand the trends as a function of mass flowrate (range: 0.068-0.182 kg/s), frequency (10-40 Hz), obstacle geometry (blockage ratio: 0 and 0.43), ignition model (shock-induced vs weak/DDT initiation), nonuniformities of fuel concentration (completely premixed vs fuel injection) in the mixture and method of thrust estimation (analytical vs. numerical). Thrust estimates for Case 1 use an analytical method [7] for an ideal tube with smooth walls. For the remaining cases, thrust is estimated via post-processing of the numerical simulations. For the ideal tube simulations (Cases 2 and 3), shock-induced initiation model was used. For the benchmark tube simulations, shock-induced initiation model (Case 4) and weak/DDT initiation (Cases 5 and 6) models were used.

3.0 Experimental setup

A brief description of the experimental setup with benchmark tube is given as follows. Figure 3(i) shows a photograph of the PDE tube setup, and Fig. 3(ii) shows a schematic of the PDE tube geometry. The benchmark PDE tube used in the present experiments was a 52.5 mm diameter tube (2" diameter schedule 40 stainless steel pipe). Air flows continuously into the tube through two opposing holes in the end cap, and the hydrogen fuel is pulsed via a solenoid valve. Fuel-air mixing occurs directly in the tube using a mixing element. The tube length of 1.0 meter is measured from the mixing element aft face to the tube exit. A spark plug and ignition system is mounted within one diameter downstream of the fuel injection. Ten orifice plates with a blockage ratio of 0.43 were installed at 50 mm intervals immediately downstream of the spark. The PDE tube was run with 100% fill of nominally stoichiometric hydrogen-air mixture at 10 Hz and an airflow rate of 0.068 kg/s. The upstream geometry consists of 25.4 mm diameter tubing that runs approximately 6.1 m to an air control valve.

Case#	Tube Dia (m)	BR	Method	Freq. (Hz)	Cycle Processes Modeled	Initiation Model
1	0.076	0	Analytical [7]	NA	Propagation, blowdown	NA
2	0.076	0	Numerical	NA	Propagation, blowdown	Shock induced
3	0.076	0.43	Numerical	NA	Propagation, blowdown	Shock induced
4	0.051	0	Numerical	40	All cycle processes	Shock Induced
5	0.051	0.43	Numerical	40	All cycle processes	Weak / DDT
6	0.051	0.43	Numerical	10	All cycle processes	Weak / DDT

Table 1: A summary of all the cases considered for thrust estimations.

Pressure traces were obtained using PCB transducers (Model Number 102M250) located at the end cap, 127 mm and 25.4 mm from the end of the tube. The last two transducers were used to calculated time of flight of the wave to verify detonation. Measured time-of-flight velocity was 2030 ± 100 m/s which is comparable to the Chapman-Jouguet detonation velocity for H2-Air of 1980 m/s.

A high-speed shadowgraph imaging system was used to visualize the blowdown process at the exit of the PDE tube. The system consisted of a continuous light source (Oriel 200W xenon-mercury arc lamp), 304.8 mm spherical mirrors (focal length 1905 mm) and a high framing rate camera (Vision Research Phantom 7) arranged in a modified Z configuration. The framing rate was 56500 frames per second with each frame being exposed for 1 □s.

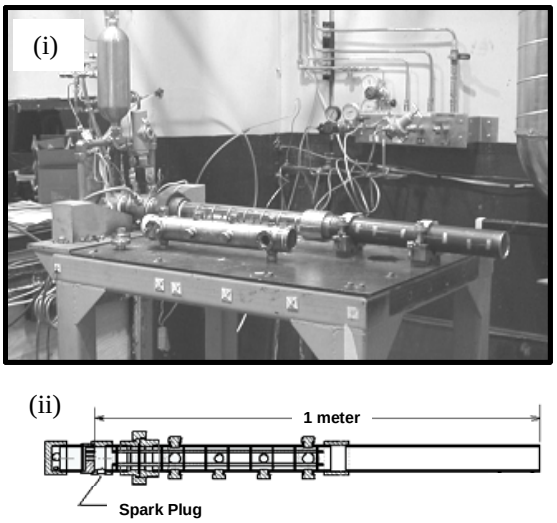

Fig. 3: Photo of the PDE facility showing (i) transparent DDT section, and (ii) a cross-section of 50 mm diameter benchmark PDE tube.

4.0 simulation of Benchmark tube PDE cycle and comparison with experiment

The main processes of the PDE cycle are summarized in Table 2. For both the experiments and calculations in this report, the initial conditions in the PDE tube are stoichiometric hydrogen-air at mixing element during fill; 106 kPa inlet pressure, 101.3 kPa outlet pressure, 300 K inlet temperature, 0.068 kg/s average mass flow and an operating frequency of 10 Hz. For these conditions, the approximate duration of each part of the cycle is shown in Table 2.

PDE Process	Approx. Duration (ms)	% of Cycle
Fill	45	45.0%
Detonation Initiation	1.6	1.6%
Detonation Propagation	0.4	0.4%
Blowdown	3.3	3.3%
Purge	49.8	50%
Total	100	100%

Table 2: PDE Cycle Processes

Steady Flow

Steady flow calculations reveal the basic features of the flow through the PDE tube. For an average mass flow through the PDE tube of 0.068 kg/s, Figure 4.1 shows the axial velocity and pressure through the tube. Due to the pressure drop across each orifice, the pressure decreases and the velocity increases through the DDT section. For these conditions and a blockage ratio of 0.43, the pressure drop in the DDT section is about 5%. The pressure drop downstream of the DDT section is negligible. This value is in good agreement with the pressure drop measured in the rig at the same conditions.

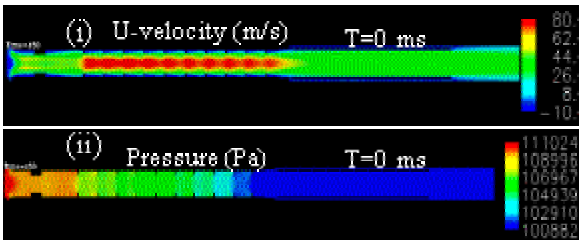

Fig. 4.1: Predicted steady state contours of (i) axial velocity (m/s) and (ii) pressure contours (Pa) through the PDE tube at steady state flow conditions of P_{in} = 1.06 bar, T_{in}=300K, mair = 0.068 kg/s (Case 6).

Fuel-Air Fill

Detonation limits of fuel-air mixtures are narrower than flammability limits, so it is important to achieve a uniform fuel-air mixture during the fill portion of the cycle. For a bulk flow velocity in the tube of 30 m/s, the time for 100% fill is about 30.0 ms. However, obstacles accelerate a core flow and interfere with exchange of gases during the fill process because there are cavities behind each orifice. Slow fluid exchange in the recirculation zones can be seen in predictions of the fuel-air fill process shown in Figure 4.2.

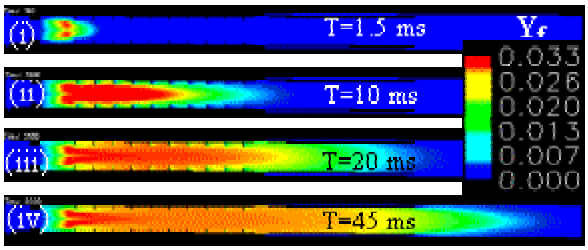

Fig. 4.2: Predicted fuel mass fraction contours at various times during the fuel fill process (Case 6).

At the upstream mixing element, fuel is added to the air resulting in an initially uniform mixture. As this mixture flows through the DDT section, there is a core flow convecting fresh charge at ~80 m/s (see Figure 4.1(i)). This core flow is moving much faster than the bulk velocity of 35 m/s that would occur with no obstacles. If the duration of the fill cycle is timed to achieve one volume change in the tube, then a lean fuel-air mixture will exit the tube before the fill cycle is complete. As a consequence, the fill time must be reduced to avoid sending fuel out the end of the tube, and there are pockets of leaner mixture. The resulting axial and radial profiles of fuel concentration deviate from the goal of achieving a uniform, 100% charge of fresh detonable mixture (Figure 4.2(iv)).

Detonation Initiation and Propagation

In this cyclic PDE study, the combustion process is initiated via a weak spark (~30 mJ) timed to correspond to the end of the fill cycle. The spark plug is located near the head end of the PDE tube. A set of ten orifice plates (blockage ratio = 0.43) is used to reduce the run-up distance to detonation.

In the experimental portion of the study, detonation initiation was visualized by imaging chemi-luminescence through a transparent polycarbonate tube and onto a high-speed video camera. For the imaging runs, the PDE was fired at 10Hz with all other parameters (mass flow, inlet T&P, etc) kept the same as for Case 6.

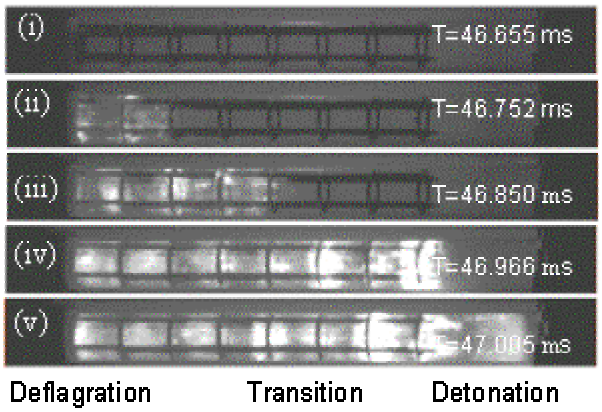

Figure 4.3: High speed imaging of hydrogen-air DDT in PDE tube (first two obstacles are not shown in the visualization) at various times of the PDE cycle (Case 6).

Figure 4.3 shows a series of images of a DDT event where the aft eight obstacles of a set of ten obstacles, are in the field of view. The spark is initiated at the end of the fill cycle when the tube is filled with a combustible mixture (Fig. 4.3(i)). The spark is outside the field of view. Within 100 □s, a turbulent flame appears from the left and propagates to the right (Fig. 4.3(ii)). The flame continues to accelerate, and much brighter chemiluminescence is observed at the final obstacle (Fig. 4.3 (iv)). The final frame (Fig. 4.3(v)) shows a planar detonation emerging from the DDT section, while there is still considerable chemiluminescence from the turbulent combustion region.

The prediction of flame propagation and transition to detonation are shown in Figure 4.4 and shows remarkable agreement with the measurements. In the numerical simulation, the combustion process is initiated by depositing energy in the same axial location as the spark plug in the PDE experiments. Energy deposition for initiation corresponds to the end of the fuel fill cycle. Figures 4.4(i) thru 4.4(iv) show a turbulent flame propagating through the obstacles. Transition to detonation is observed in Fig. 4.4(v), which shows the formation of a planar shock front, and the wave velocity approaches Chapman-Jouguet (C-J) velocity. The detonation achieves characteristics of a steady-state detonation as it propagates toward the exit of the tube (Fig. 4.5).

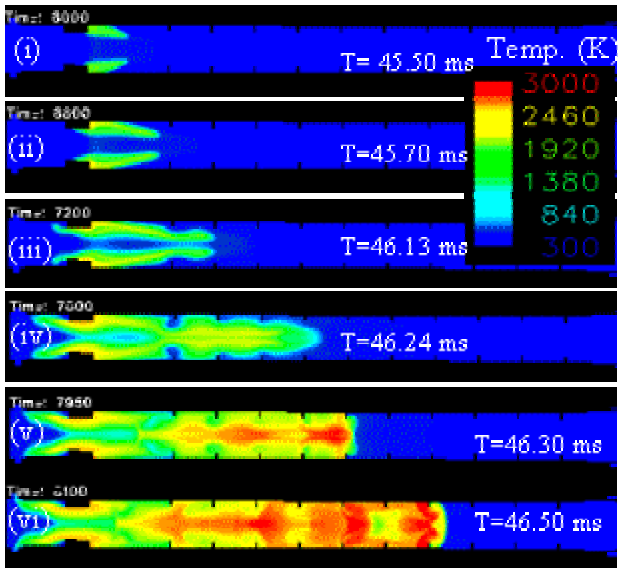

Fig. 4.4: Predicted temperature contours at various times during the detonation initiation process (Case 6).

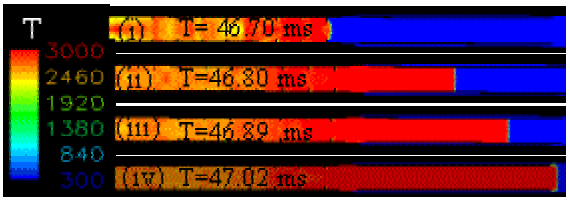

Fig. 4.5: Predicted temperature contours during detonation propagation process (Case 6).

A key qualitative difference between the measurements and calculations is that the transition occurs within the DDT section in the calculations. Transition was not observed within the DDT section in the experiments, and it appeared that the obstacles hindered final transition to detonation. It is also noted that when the total number of obstacles was reduced to eight, transition occurred after the last obstacle in the experiment. A more detailed comparison between the measurement and calculation of DDT is shown on the X-t diagram in Fig. 4.6(i). This diagram shows that DDT occurs a little earlier in the calculation (10% shorter time of flight in the DDT section) than in the experiment and the slope (indicating propagation velocity) reaches a steady value that agrees well with calculated CJ velocity. Figure 4.6(ii) shows a more detailed comparison of propagation velocity along the tube. The numerical predictions reveal rapid flame acceleration leading to over-driven detonation and

finally relaxing to C-J velocity. This behavior agrees well with behavior reported by Cooper et al [18].

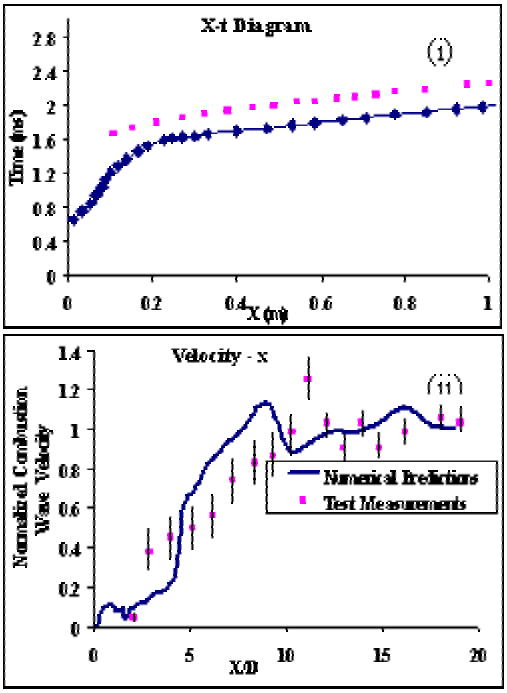

Fig. 4.6: Comparison of numerical prediction and measurement of (i) X-t diagram and (ii) velocity-position

Blowdown

The blowdown process is responsible for most of the thrust production. There are three phases of blowdown: emergence of the blast wave, supersonic blowdown, and subsonic blowdown. A comparison of measured and numerical prediction of the initial phase of blowdown is shown in Figure 4.7. The measurements are shadowgraph images of the blast wave decay obtained with a high-speed video camera. The numerical predictions are presented as numerical schlieren images produced by post-processing the results. As the detonation emerges from the tube, the reaction front separates from the leading shock wave. The shock wave wraps around the tube and travels both upstream and downstream. The hot combustion products follow the leading shock but the reaction zone quickly increases from the leading shock wave.

.

Purging

Figure 4.8 shows predicted time evolution of oxygen concentration contours during the purging process. At the end of detonation and blow down processes, oxygen is completely consumed as the initial overall equivalence ration oxygen levels are completely depleted. As the blowdown is completed, the pressure in the end cap plenum decreases, and the flow of fresh reactant enters the tube. Figure 4.8(i) shows the oxygen mass fraction at the beginning of the blowdown process, and Fig. 4.8(ii) shows the oxygen mass fraction contours at the end of blowdown process. The purging process is completed in approx. 30 ms (Fig. 4.8(iii)) from the completion of the blowdown process.

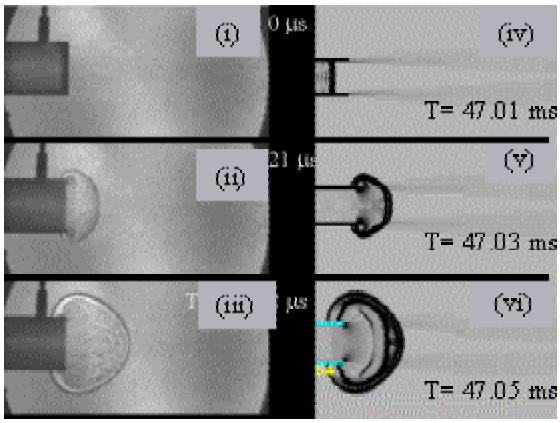

Fig. 4.7: Comparison of high speed shadowgraph visualizations of the blowdown (i, ii and iii) with numerical schlieren contours (iv, v and vi) at various times of the PDE cycle for Case 6.

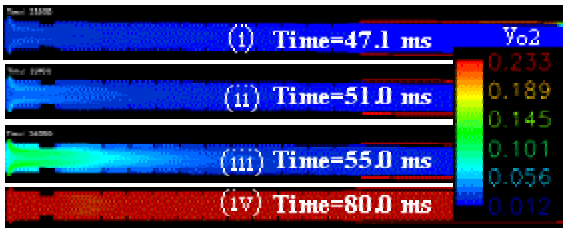

Fig. 4.8: Predicted oxygen mass fraction contours during blowdown and purging processes (Case 6).

Predicted and Measured Pressure-time Traces

Figures 4.9 (i) and (ii) show comparisons of predicted and measured pressure-time traces at two locations in the tube, (a) at a distance of 0.13 m from the exit of the tube and (b) in the end cap cavity adjacent to and at the center of cavity wall. Overall, there is good agreement between the calculation and the experiment. At the end of the tube, the pressure variation with time shows that, as the detonation wave propagates thru the tube, the pressure at the probe location experiences a spike and behind the wave, the pressure decays rapidly as the expansion waves from the open end reduces the pressure inside the tube rapidly. However, the predicted time variation of pressure in the end plenum shows a plateau pressure of 5.0 atm.

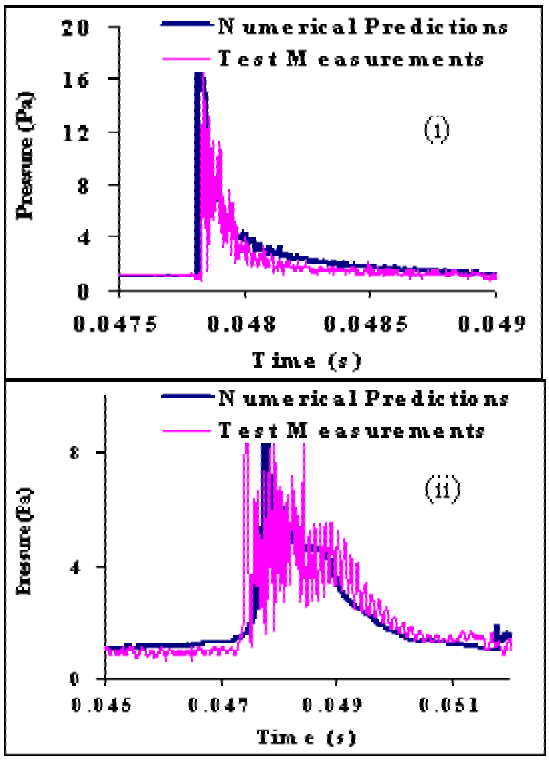

Fig. 4.9: Comparison predicted and measured pressure - time traces at (i) the tube exit and (ii) in the end-cap cavity (Case 6).

5.0 Thrust estimation methodology

In determining the net impulse over a PDE cycle, key parameters are momentum flux at the tube exit, pressure forces and shear stresses on all internal surfaces, which contribute to x-component of the net forces acting on the control volume. Here, the thrust calculation is illustrated by using two control volumes, as shown in Figures 5.1 and 5.2.

Fig. 5.1 Control volume 1 applied to Cases 2 and 3 for thrust estimations.

A force balance for the control volume 1 can be written as follows.

$$F_{x1} = (P_a A_{od} - P_t A_{id} - P_{e'} A_{tw}) + \underbrace{\sum_{obstacles} \int Pn.xdA_s + \int \tau dS}_{X'_{forces}} \rightarrow (1)$$

Where

$F_{x,1}$ thrust developed by the pde,

P_a ambient pressure, A_{od} is the corresponding area,

Pt pressure in the tube adjacent to closed end and A_{id} is the corresponding area,

$P_{e'}$ pressure adjacent to tube walls at the exit and A_{tw} is the corresponding area,

□ shear stress on all internal surfaces in x-direction,

S surface areas of all internal surfaces,

n unit vector normal to an internal surface, and

X'_{forces} (pressure +viscous) forces acting on all internal surfaces in x-direction.

Equation 1 can be rewritten as follows:

$$F_{x1} = X'_{forces} + P_a A_{od} - P_t A_{id} - P_{e'} A_{tw} \rightarrow (2)$$

To estimate the thrust using Eq. 2, integration of the last two terms of Eq. 1 is needed. They include pressure forces and viscous forces acting on all internal surfaces. The numerical computations provide this required information. A different control volume (rocket engine control volume) is also considered to ensure verification of the computed results of thrust developed by PDE. This control volume 2 is shown in Fig. 5.2.

Fig. 5.2 Control volume 2 as applied to Cases 2,3,4,5 and 6 for thrust estimations.

A force balance for the control volume 2 can be written as follows.

$$F_{x,2} = \dot{m}_e u_e - P_e A_{id} + P_a A_{od} - P_{e'} A_{tw} \rightarrow (3)$$

Where

$F_{x,2}$ thrust developed by the pde,

m_e: mass flow rate at the exit of the tube,

P_e tube exit pressure, A_e is the corresponding area,

u_e: x-velocity component at the exit of the tube

To estimate the thrust using Eq. 3, knowledge of mass flow rate, velocity, pressure at the exit as a function of time, is needed. The numerical computations provide this required information. The use of Eq. 3 for thrust estimations is rather straight forward when compared to thrust estimation method using Eq. 1, as the information required by Eq. 1 is easily extracted form

unstructured CFD results at one plane, as opposed to the tedious extraction of all forces acting on all internal surfaces. Firstly, it was demonstrated for the case of an ideal tube that Equations 1 and 3 yield exactly the same cumulative net impulse [$|\int F_{x,1}.dt| = |\int F_{x,2}.dt|$] over the cycle time. The thrust estimations using control volume 2 and Eq. 3 are then performed for the benchmark cases 4, 5 and 6.

Two specific corrections are applied to thrust estimated by Eq. 1 or Eq. 3. One pertains to shock-induced ignition which can cause net impulse even in inert flows of ideal tube as well as benchmark tube (Cases 2, 3 and 4). This ignition correction is quantified using thrust estimation with shock-induced ignition, but with reactions suppressed. This correction is estimated to be 4% for the ideal tube with no obstacles (Case 2) and 9% for the benchmark tube with no obstacles (Case 4). A second correction applies to the benchmark tube only, and is equal to the thrust generated by the tube operating in a cycle with no reactions. This correction is directly proportional to mass flowrate of the mixture flowing thru the tube. The fuel mass addition is less than 3%, hence this correction is quantified using the thrust estimated for the benchmark tube during the initial steady state flow conditions.

To estimate the thrust generated during the supersonic blowdown as opposed to the thrust generated during the subsonic blowdown, the exit Mach number variation with time (Case 6) is plotted in Fig. 5.3. Figure 5.3 shows the results of Case 6 for a fill time (30 ms) which differs from 45 ms used for simulation of Case 6 (the results for which are discussed earlier in Section 4). A value of 30 ms for fuel fill gives 100% fill (correcting for the overfill of the calculation described in Section 4). Figure 5.3 shows an initial peak in the exit Mach number caused by the blast wave exiting the tube and after this initial peak, it attains a constant value of unity for a period of 1.1 ms (15% of the total blowdown time of 7 ms). The remainder of the blowdown (85%) is essentially a subsonic blowdown. Figure 5.3 also shows that the exit Mach number has a minimum of zero after approximately 5 ms into the blowdown process, and this is caused by the complete depressurization of the aft 50% of the tube without obstacles. At this time, depressurization of the upstream 50% of the tube with obstacles continues, and the Mach number attains a second peak. This transient behavior is similar to depressurization of two plenums connected in series, with the rate-limiting resistance located between the plenums.

The cumulative net impulse generated by the benchmark tube (Case 6) is shown in Fig. 5.4. The cumulative net impulse attains a constant value of 1.6 N.s in approximately 6 ms from the start of the blowdown process. This includes a correction of 0.2 N.s for the thrust developed during steady state initial conditions with no reactions. This net impuse translates to a value of 16 N for thrust generated by the benchmark tube operating at 10 Hz and a mass flow rate of 0.068 kg/s, a value of 790 N.s/m3 for impulse per unit volume (I_v) and a value of 2795 for fuel-specific impulse (I_{spf}).

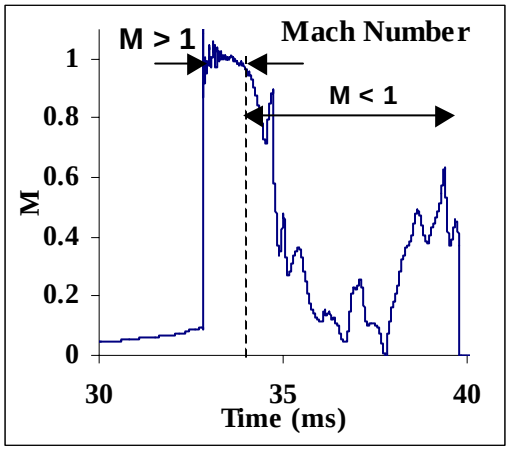

Fig. 5.3: Time variation of the tube exit Mach number during the blowdown for case 6 (benchmark tube with obstacles operating at 10 Hz).

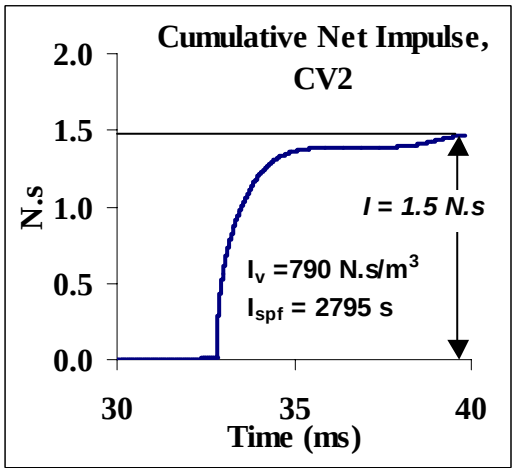

Fig. 5.4: Cumulative net impulse during the blowdown for case 6 (benchmark tube with obstacles operating at 10 Hz).

Influence of realistic initiation, blockage, and mass throughput on thrust Predictions

A summary of the influence of realistic simulation of all PDE cycle processes on thrust predictions is given. A brief discussion of the effect of varying mass flowrates, frequency of operation and blockage ratio of the obstacles on thrust predictions is provided. These analyses are performed as a set of pre-test predictions of the benchmark tube performance. Table 3 shows a summary of results of all the analyses (Cases 1-6). The

predicted qualitative trends are summarized in the remainder of this section.

Case# ----->	1	2	3	4	5	6
Air Flowrate (kg/s)	NA	NA	NA	0.182	0.182	0.068
Frequency (Hz)	NA	NA	NA	40	40	10
Ignition Corr. %	0.0	9.0	9.0	9	0.0	0.0
Net Impulse (N.s)	4.6	4.3	4.3	1.7	1.4	1.6
Thrust (N)				68	57	16
I_u (N.s/m^3)	1014	992	940	821	689	790
I_{spf}(s)	4346	4014	3804	3371	2822	2795

Table 3: A summary of tube PDE (ideal tube and benchmark tube) thrust estimations.

Ideal tube vs. Benchmark tube

The PDE operation of an ideal tube and thrust estimation of the same are well documented in the literature. The key differences between the simulation of an ideal tube and the simulation of a benchmark tube for obtaining thrust estimates can be summarized as follows. In an ideal tube PDE, the fuel is initially premixed with air, and the fuel-air mixture is well characterized by the initial condition specification. In addition, the walls of the tube are smooth and do not have any additional internal geometry features, which can cause pressure drop in the system. For thrust estimation, it is sufficient to simulate detonation initiation, detonation propagation and blowdown processes of an ideal tube.
The benchmark tube can be distinguished from the ideal tube as follows. (i) The fuel and air are brought in separately (overall equivalence ratio is 1.0, air flowrate is 0.068 kg/s) and mixed in the mixing segment of the tube, and this results in mixture nonuniformities and leads to local equivalence ratios which are less than or greater than the overall equivalence ratio. For an overall equivalence ratio of 1.0 of the fuel-air mixture, the variation in local equivalence ratios can only lower the impulse produced by the benchmark tube. (ii) The upstream section of the tube is not closed, and air flows thru the system continuously except for the time interval, during which high pressure conditions exist in the tube. A strong compression pulse (retonation) which is formed during the initiation process, travels upstream causing back flows in the upstream section of the tube, resulting in a reduction of the net impulse. (iii) The benchmark tube has internal geometry features such as the DDT-promoting obstacles and a mixing element, which result in a pressure drop through the tube. These internal flow resistances can cause substantial reductions in the thrust developed by the benchmark tube.

Figure 6.1 shows the variation of (i) instantaneous tube exit mass flow rate, (ii) instantaneous pressure at the tube close end, (iii) convective plus pressure forces in the x-direction at the tube exit, and the pressure forces plus the viscous forces acting on all internal surfaces, and (iv) the cumulative net impulse estimated using control volumes 1 and 2, for the ideal tube PDE (Case 2). The instantaneous mass flow rate at the tube exit attains a constant value after the initial peak for a major fraction (60%) of the transient. The instantaneous pressure at the closed end shows a plateau pressure of 6.0 bar. Selected instantaneous forces ($X_{forces} = X'_{forces} - P_tA_{id)}$ acting on the control volume 1 and ($m_eU_e + P_e.A_e$) on control volume 2 are plotted in Fig. 6.1(iii). The contribution of viscous forces towards net impulse is less than –1% for ideal tube without obstacles (Case 2). The cumulative net impulse (after the ignition correction is applied) is estimated to be 4.5 Ns. This value for net impulse translates to a value of 992 N.s/m3 for impulse per unit volume (I_v) and a value of 4014 s for fuel-specific impulse (I_{spf}). Figure 6.1 (iv) shows that the estimations of the cumulative net impulse, obtained using Eq. 1 and Eq. 3 are in agreement within 1%. The estimated value of 4014 s for I_{spf} is in agreement with an experimentally measured value of 4000 s reported in an earlier experimental study [20].
Figure 6.2 shows the variation of (i) instantaneous mass flow rate at the tube exit and the back flowrate at the inlet of the end cap, (ii) instantaneous pressure in the end cap volume, (iii) convective plus pressure forces in the x-direction at the tube exit, and the pressure forces plus the viscous forces acting on all internal surfaces, and (iv) the cumulative net impulse estimated using control volume 2, generated by the benchmark tube PDE (Case 6). The instantaneous Mach number variation with time at the exit of the tube is shown in Fig. 5.3. The exit mass flow rate (Fig. 6.2(i)) decays continuously after the initial peak value. The back flow rate (Fig. 6.2(i)) also shows a peak and decays as the depressurization continues. The peak in the instantaneous back flowrate is less than 5% of the peak in the exit mass flowrate. Figure 6.2(ii) shows the pressure at the tube exit. The effect of obstacles causing

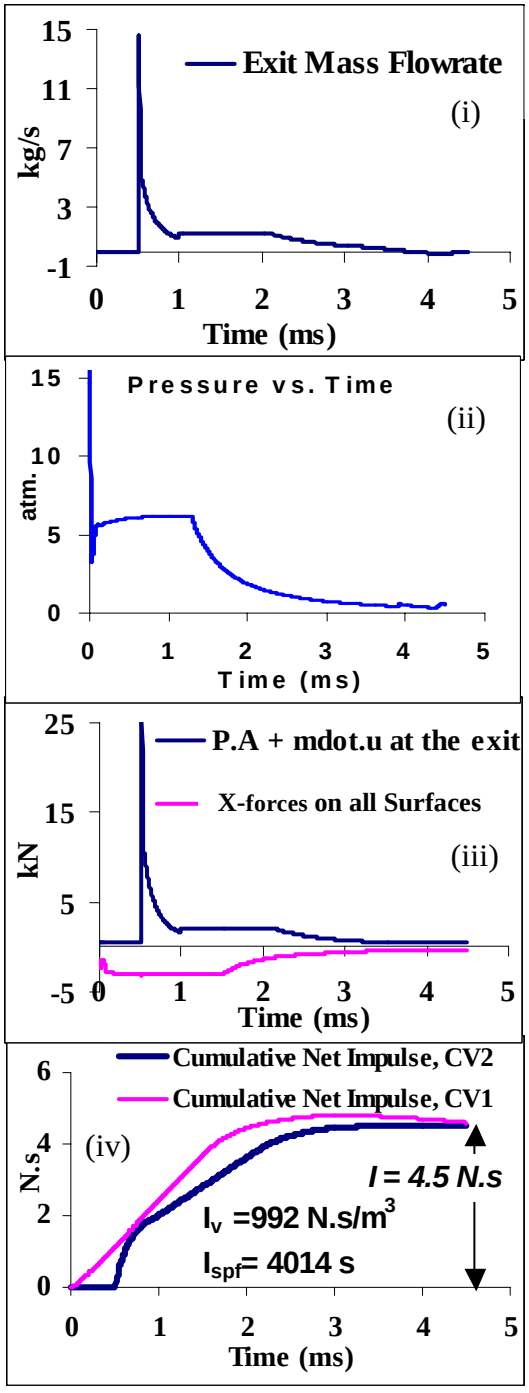

Fig. 6.1: Predicted time variation of (i) exit mass flow rate, (ii) pressure at the closed end, (iii) forces on control volume, and (iv) cumulative net impulse for Case 2 (ideal tube without obstacles).

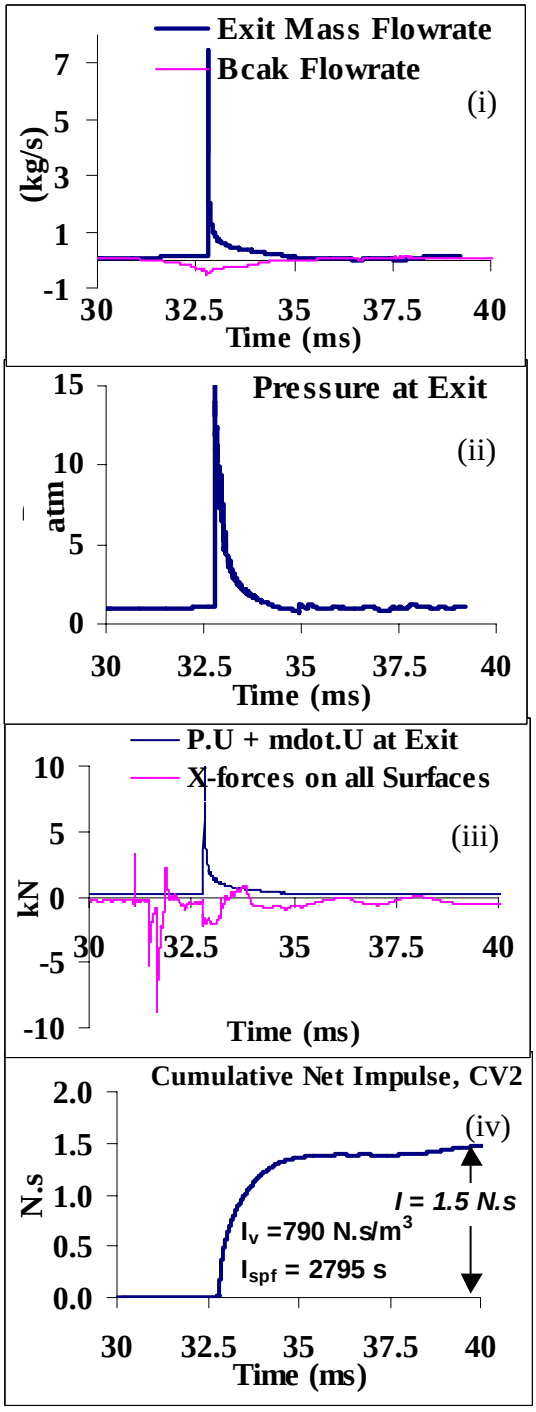

Fig. 6.2: Predicted time variation of (i) exit mass flow rate, (ii) exit pressure (iii) forces on control volume and (iv) cumulative net impulse for Case 6 (benchmark tube with obstacles operating at 10 Hz)

oscillatory behavior on the instantaneous pressure forces + viscous forces can be seen in Fig. 6.2(iii). The cumulative net impulse (after the ignition correction is applied) is estimated to be 1.6 Ns for Case 4. Figure 6.2 (iv) shows estimations of the cumulative net impulse, obtained using Eq. 3. This predicted value for the cumulative net impulse translates to a value of 790 Ns/m^3 for impulse per unit volume (I_v) and a value of 2795 s for fuel-specific impulse (I_{spf}).
The predicted decrease of 30% in the fuel-specific impulse (I_{spf}) for the benchmark tube (Case 5) when compared to the I_{spf} of an ideal tube (Case 2) can be attributed to (i) the pressure drop in the benchmark tube resulting from a realistic simulation of benchmark tube internal geometry such as obstacles and mixing element, (ii) nonuniformities in the mixture composition for the benchmark case as opposed to assumed uniform mixture composition for the case of an ideal tube and (iii) backflows in the inlet section of the benchmark tube due to a compression wave propagating into the upstream geometry.

Effect of Obstacles on Thrust Estimation

In order to assess the effect of obstacles on the net impulse generated by an ideal tube, a simulation of an an ideal tube with obstacles (Case 3) is performed. Figures 6.1(iv) and 6.3 show the net impulse generated by Case 2 and Case 3 respectively. A reduction of 5% in the fuel-specific impulse (I_{spf}) generated by an ideal tube is predicted for the case of an ideal tube with obstacles (Case 3) when compared to the I_{spf} generated by an ideal tube without obstacles. The reduction in I_{spf} is attributed to a increased pressure drop in an ideal tube with obstacles during the blowdown process (due to increased pressure forces and visous forces acting in –x direction of the on control volume 1).
To assess the effect of obstacles on the net impulse generated by a benchmark tube, two simulations of benchmark tube without and with obstacles, Case 4 and Case 5 respectively, are performed. An air flow rate of 0.182 kg/s was specified for the PDE cycle operating at 40 Hz for both simulations. Figures 6.4 and 6.5 show the net impulse generated by Case 4 and Case 5 respectively. The shock-induced initiation was used for Case 4 and the corresponding ignition was computed to be 9%. DDT is the initiation model for Case 5 (benchmark tube with obstacles) and hence no ignition correction was applied. A reduction of 16% in the fuel-specific impulse (I_{spf}) generated by the benchmark tube is predicted for the case of a benchmark tube with obstacles (Case 5) when compared to the I_{spf} generated by an ideal tube without obstacles. The reduction in I_{spf} can be attributed to increased pressure drop in the benchmark tube with obstacles during the blowdown process. The nonuniformities in fuel-air mixture are severe for the Case 5 (with obstacles) compared to Case 4 (without obstacles) which also cause a reduction of I_{spf}.

In summary, the effect of DDT-promoting obstacles on the fuel-specific impulse (I_{spf}) is estimated to be 5% for the ideal tube PDE and 16% for the benchmark tube, using H_2-air mixture . The presence of obstacles adversely affects fuel-air mixing and increases the pressure drop in the tube, thus leading to a reduction in the performance of tube PDE.

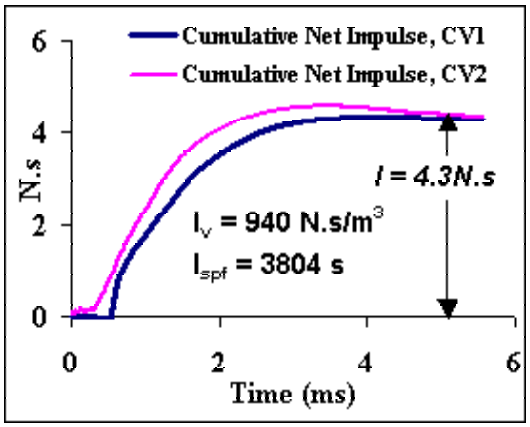

Fig. 6.3: Predicted cumulative net impulse for an ideal tube with obstacles (Case 3).

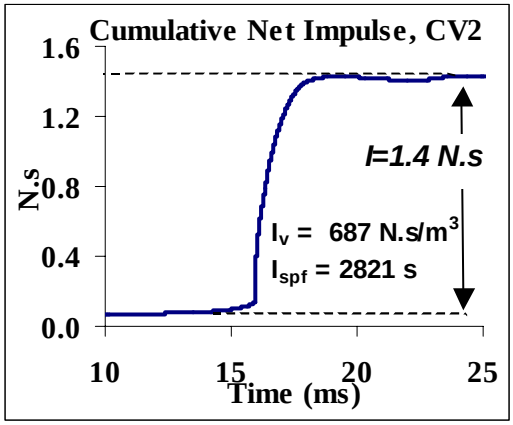

Fig. 6.4: Predicted cumulative net impulse for a benchmark tube without obstacles operating at 40 Hz.

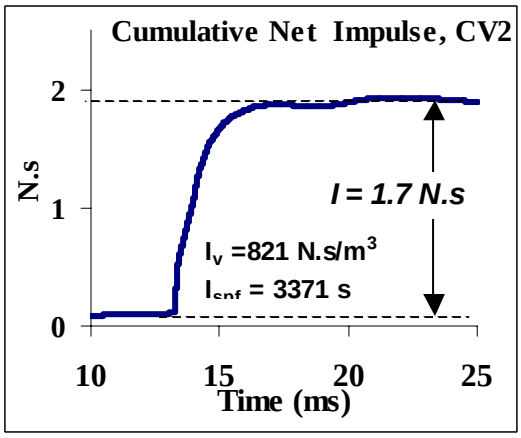

Fig.6.5: Predicted cumulative net impulse for a benchmark tube without obstacles operating at 40 Hz.

7.0 Conclusions

To understand the trends in performance estimations of a tube PDE, simulations are performed for two configurations, a 0.0762 m tube (ideal PDE tube) and a 0.051 m tube (benchmark PDE tube). The computational method simulates all the processes of the PDE cycle (fill, deflagration to detonation Initiation, propagation, blowdown and purge). A set of experiments is performed to obtain performance estimates for the benchmark PDE tube. Experimental measurements include high-speed chemiluminiscence and shadowgraph visualizations, and dynamic pressure measurements.

The results yield insights into performance estimations of a PDE tube operating in a continuous cycle. Overall, there is good agreement between the numerical predictions and available experimental data on thrust generated by an ideal tube PDE. The predicted decrease of 30% in the I_{spf} for the benchmark tube compared to the I_{spf} of an ideal tube is attributed to nonuniformities in the mixture composition, pressure drop in the benchmark tube with internal geometry such as obstacles and mixing element, and backflows in the benchmark tube due to a compression wave propagating into the upstream geometry.

The effect of DDT-promoting obstacles on the fuel-specific impulse (I_{spf}) is estimated to be 5% for the ideal tube PDE and 16% for the benchmark tube, using H_2-air mixtures. The presence of obstacles increases the pressure drop in the tube and adversely affects fuel-air mixing, thus leading to a reduction in the performance of a tube PDE.

ACKNOWLEDGMENT

Authors wish to acknowledge the technical discussions with Dr. J. Shepherd of California Institute of Technology and Dr. K. Kailasnath of Naval Research Laboratories. Authors acknowledge the technical help with experimental setup provided by P. Pinard and E. Cornell of General Electric Global Research. Computational support provided by Dr. S. Palaniswamy of Metacomp Technologies, Inc., is sincerely appreciated.

References

Eidelman, S., and Grossmann, W., "Pulse Detonation Engine: Experimental and Theoretical review", *AIAA paper 92-3168*, July 1992

Glassman, I., *Combustion*, 2nd Edition, McGraw Hill, New York, 2000

Brophy, C.M., Netzer, D., Forster, D., "Detonation Studies of JP-10 with Oxygen and Air for PDE Development", *34th Joint Propulsion Conference*, Cleveland: AIAA (1998)

K. Kailasnath, "Recent Developments in the Research of Pulse Detonation Engines," *AIAA 2002-0470, 40th AIAA Aerospace Sciences Meeting & Exhibit*, January 2002, Reno, NV

Kailasnath, K., Li, C., and Patnaik, G., "Multilevel Computational Studies of Pulse Detonation Engines," ISOABE-2001-1172, September, 2001, Bangalore, India

Mohanraj, R., Merkle, C. L., and Ebrahimi, H. B., "Modeling of Pulse Detonation Engine Operation," AIAA 2001-0475, *39th Aerospace Sciences Meeting & Exhibit*, January 2001, Reno, NV

Wintenberger, E., Austin, J .M., Cooper, M., Jackson, *S.*, and Shepherd, J.E., "An Analytical Model for the Impulse of a Single-cycle Pulse Detonation Engine," *AIAA 2001-3811*, July 2001

K. Kailasnath, G. Patnaik and C. Li, "The Flowfield and Performance of Pulse Detonation Engines," *Twenty-ninth (International) Symposium on Combustion*, The Combustion Institute, PA, Vol. 29, 2002

Y. Wu and V. Yang, "Numerical Simulation of Detonation with Detailed Chemical Kinetics Using the Space Time Method," *AIAA 2000-0317, 38th Aerospace Sciences Meeting & Exhibit*, January 2000, Reno, NV

Povinelli, L. A., and Youngster, S., "Real Gas Effects on the Performance of Hydrocarbon-fueled Pulse Detonation Engines," *AIAA 2003-0712, 41st Aerospace Sciences Meeting & Exhibit*, January 2003, Reno, NV

Tangirala, V., B. Varatharajan, B., and Dean, A. J., "Numerical Simulations of Detonation Initiation," *AIAA-2003-0716, 41st Aerospace Sciences Meeting & Exhibit*, January 2003, Reno, NV

Shepherd, J. E., and Lee, J. H. S., "On Transition from Deflagration to Detonation," Major Research Topics in Combustion, Springer Verlag, Hampton, VA, 1992

Lee, J. H. S., "Detonation Waves in Gaseous Explosives," Hand Book of Shock Waves, Volume 3, Academic Press, 2001

Kline, R. Chapter4: Detailed modeling of FA and DDT, "Flame Acceleration and Deflagration to Detonation Transition in Nuclear Safety," a State-of- the-Art Report by a Group of Experts OECD Nuclear Energy Agency NEA/CSNI/ R (2000), 7 August 2000

Khoklov, A. M., Oran, E. S., and Thomas, G. O., 1999b "Numerical Simulation of Deflagration to Detonation Transition: the Role of Shock-flame Interactions in Turbulent Flames", Combust. Flame 117, 323-339

Oran, E. S., and Khokhlov, A. M. "Deflagrations, hot spots and the transition to Detonation," Phil. Trans. R. Soc. Lond. A (1999) 357, 3539-3551

Chakravarthy, S., Goldberg, U., Batten, P., Palaniswamy, S., and Peroomian, O., 2001, "Some Recent progress in Practical Computational Fluid Dynamics," *AIAA-2001-0136, 39th AIAA Aerospace Sciences Meeting and Exhibit*, January 2001, Reno, NV

Cooper, M., Jackson, S., Austin, J.M., Wintenberger, E., and Shepherd, J.E., "Direct Experimental Impulse Measurements for Detonations and Deflagrations," *AIAA 2001-3812*, July 2001

D. R. White and G. E. Moore, "Structure of Gaseous Detonation, Induction Zone Studies in H_2-O_2 and CO-O_2 Mixtures," *Proceedings of 10th Symposium (International) on Combustion*, 785, 1965

Schauer, F., Stutrud, J., and Bradley, R., "Detonation Initiation Studies and Performance Results for Pulse Detonation Engines," 39th AIAA Aerospace Sciences Meeting and Exhibit, January 8-11, 2001, Reno, NV, AIAA, 2001-1129

APPENDIX E: Co-authored Combustion Science Journal Article

PULSED DETONATION ENGINE PROCESSES: EXPERIMENTS AND SIMULATIONS

V. E. Tangirala, A. J. Dean, D. M. Chapin, P. F. Pinard and B. Varatharajan
Energy and Propulsion Technologies Laboratory
General Electric Global Research Center
One Research Circle, Niskayuna, NY 12309

Abstract
Computational and experimental investigations of a pulsed detonation engine (PDE) operating in a cycle using ethylene-air mixtures are reported. Simulations are performed for two geometry configurations, namely, an ideal tube PDE with a smooth wall fueled with premixed C_2H_4-O_2 and a benchmark tube PDE with internal geometry and a valveless air supply fueled with C_2H_4. Performance estimates of fuel-specific impulse (I_{spf}) of an idealtube PDE, obtained using a 2-step reduced mechanism for a C_2H_4-O_2 mixture, are in good agreement with existing test measurements from the literature. Realistic simulations of all processes of the PDE cycle (fill, deflagration-to-detonation transition (DDT), detonation propagation, blowdown and purge) of a benchmark tube PDE yielded important insights into continuous cycle operation. Experimental measurements include DDT visualizations and dynamic pressure measurements. Comparisons of experimental and computational visualizations show good agreement in cycle process time scales. However, run-up distance is underpredicted, indicating a need to improve the flame propagation mechanism. The predicted decrease in the fuel-specific impulse (I_{spf}) for the benchmark tube when compared to the I_{spf} of an ideal tube may be attributed to nonuniformities in the mixture composition, the pressure drop resulting from internal geometry, and backflow in the benchmark tube due to a compression wave propagating into the upstream geometry.

Introduction
Pulse detonation engines have recently emerged as potential new devices to better utilize the chemical energy content of reactive fuel/air mixtures (Eidelman et al., 1992). One of the main advantages of PDE is that the detonations create less entropy than conventional constant pressure processes such as those used in current gas turbines (Glassman, 2000). Establishing whether a PDE can achieve higher operating efficiency than a conventional propulsion system (i.e. gas turbine, ramjet, etc) is the focus of many research groups around the world.

One of the main challenges in making a practical PDE is the repeated initiation of detonations within the detonation chamber. Many implementations of pulse detonation engines rely on DDT to avoid the high energy required for direct initiation. DDT is the process whereby a deflagration is initiated using a weak energy source (typically tens of milli-Joules), the combustion front accelerates via a series of gasdynamic processes and eventually detonates. A drawback to this approach for practical devices is the necessary length for transition (referred to as the run-up distance) to detonation, which for practical fuels such as Jet-A can be in the order of meters. One method to reduce the run-up distance is the addition of oxygen in the initiation region (Brophy et al., 1998). This can greatly reduce the length required for DDT but can add significant complexity and weight to a propulsion system and additional logistical requirements. Another method is to add obstacles inside the tube. This has also been shown to significantly reduce run-up distance with fuel-air mixtures, and there is little additional weight or complexity. For detonation initiation in fuel-air systems, DDT optimization is a trade-off between minimizing run-up distance via more obstacles or higher blockage ratio, and minimizing performance loss (pressure losses) via less obstacles or smaller blockage ratio. Numerical models could provide a powerful tool to develop new configurations. However, while numerical models have been used reliably to simulate cases of direct initiation, simulation of the DDT process remains a challenge and is a focus of this paper.

For the modeling of detonation processes, there is a need for validated hydrocarbon chemical mechanisms. Considering the computational effort involved in the use of detailed/short chemical mechanisms for simulation of detonation initiation events, reduced chemical mechanisms, developed from basic elementary reactions through a systematic process with fewer chemical reactions and fewer species, have become critical for predictions of occurrence or failure of initiation and of detonation propagation. Such reduced chemical mechanisms must be validated over the range of fuel types, initial pressure, and temperature conditions of interest.

Many investigations of PDE thrust estimation (Kailasanath, 2002; Kailasanath et al., 2001; Mohanraj et al., 2002; Wintenbeger et al., 2001; Kailasanath et al., 2002, Wu and Yang, 2000; Povinelli et al., 2003; Tangirala et al., 2003) have focused on an ideal tube PDE which can be described as a constant cross-sectional tube, closed at one end and open at the

other end, uniformly filled with quiescent fuel-air mixtures. Ideal tube configurations typically have a diameter of 0.051 or 0.076 m and a length of 1.0-1.5 m. These investigations include multi-level multidimensional (0D, 1D, 2D and 2D axisymmetric) computations with and without chemical kinetics. The fuel-air systems investigated include H_2-air, C_2H_4-O_2, and C_2H_4-air. Real gas effects are found to have an impact on PDE cycle performance (Povinelli et al., 2003). A recent analytical model was extensively validated for various fuel-oxidizer systems, initial pressures, and equivalence ratios using single shot test measurements, and it has proven to be a valuable tool for thrust estimations within ± 15% (Wintenberger et al. 2001).

Prediction of the propulsive performance of a pure tube PDE is of interest in order to understand and improve the design of an engine in a parametric space comprising geometric parameters, fuel type, bulk velocity of the flow, frequency, igniter geometry, mixture uniformity and cycle process time scales. Purely computational studies of a simple tube PDE have been performed by a number of investigators. Even for the tube filled with a stoichiometric hydrogen-air mixture, there was a significant variation in the estimated values of the fuel-specific impulse (I_{spf}) over a single cycle, ranging from 3000s to 8000s. However, more recent detailed comparisons (Kailasanath, 2002; Kailasanath et al., 2001) have shown that most of this variation could be explained on the basis of initial and boundary conditions used in the various computational studies. For an ideal PDE tube completely filled with hydrogen-air mixture (at initial conditions of 1 atm., 300 K and an equivalence ratio of 1.0), a convergence of estimations for I_{spf} at a value of about 4160 s has been reported by the computational PDE research community (Wu and Yang, 2000; Povinelli et al., 2003, Tangirala, at al. 2003).

The physical mechanisms governing deflagration-to-detonation transition are described in recent reviews (Shephard and Lee, 1992; Lee, 2001; Kline, 2000). Shepherd and Lee, 1992 note that the accurate prediction of a complete flame acceleration and transition to detonation event is made complex due to the practical limitations on spatial and temporal resolution in multidimensional computations. Previous computational investigations (Khokhlov et al., 1999; Oran and Khokhlov, 1999) suggest that the hot spots arise from fluctuations that increase as the turbulent flame becomes more intense, and the mechanism by which a hot spot transitions to a detonation is attributed to spontaneous pressure waves that arise due to gradients of induction time. Several computational studies of DDT have been performed, and they include direct numerical simulations of combustion wave and gas dynamical wave interactions in small-scale geometric configurations (Khoklov et al., 1999) and the modeling of turbulence-chemistry-gasdynamic interactions in large-scale nuclear reactor accident scenarios (Kline, 2000).

There is a need for detailed multi-dimensional, unsteady computations which can predict PDE performance with realistic geometry. However, a reliable estimation of thrust, developed by a repeating PDE cycle by simulating realistic PDE cycle processes, is a complex computational problem. Internal geometry has a significant impact on the thrust developed by the PDE. Optimization of internal geometry is necessary to ensure sufficient fuel-air mixing and successful detonation initiation while minimizing the pressure loss in the system. Nonuniformity in fuel-air mixing can lead to failure of initiation and/or detonation propagation resulting in decreased thrust. The blowdown process determines the thrust generated by the PDE cycle. Simulating the blowdown of the supersonic combustion products from the detonation chamber requires the use of realistic boundary conditions involving multidimensional computations.

The objectives of the present investigation of the cyclic detonation processes are: (i) to develop computational methods to model key PDE cycle processes including fuel-air mixing, DDT initiation, and blowdown for a stoichiometric mixture of C_2H_4 and air; (ii) to validate the computational method by applying a 2-step reduced mechanism for a C_2H_4-O_2 mixture in an ideal PDE tube and by comparing results with existing test measurements in the literature; (iii) to apply the computational method for performance estimation during a repeating PDE cycle operation, and (iv) to investigate the effect of bulk velocity on the thrust produced by a PDE during cyclic operation. The outline of the remainder of the paper is as follows: first, the numerical method and the experimental setup are described, then the results of a realistic simulation of a PDE cycle operation are presented. A summary of the effect of bulk velocity on the flow through the PDE on cycle performance is discussed. Finally, the conclusions of the ongoing PDE investigations and future plans are summarized.

Experimental setup

Figure 1(i) shows a photograph of the PDE tube setup, and Fig. 1(ii) shows a schematic of the PDE tube geometry. The benchmark PDE tube used in the present experiments is a 51 mm diameter tube (2" diameter polycarbonate pipe). Air flows continuously into the tube through two opposing holes in the end cap, and ethylene fuel is pulsed via a solenoid valve. Fuel-air mixing occurs directly in the tube using a mixing element. The tube length (1.27 m) is measured from the mixing element aft face to the tube exit. A spark plug igniter is mounted within one diameter downstream of the fuel injection. Seventeen orifice plates with a blockage ratio of 0.43 were installed at 51 mm intervals starting 150 mm from the aft face of the mixing element. The PDE tube was run with 100% fill of nominally stoichiometric ethylene-air mixture at

10 Hz and an airflow rate of 0.068 kg/s. The upstream geometry consists of 1 meter long hoses connected to a tank (150 mm diameter, 200 mm long). The purpose of this tank is to maintain a nearly constant supply pressure to the PDE tube. This tank is supplied with air via a 25.4 mm flexible hose that runs approximately 6.1 m to an air control valve.

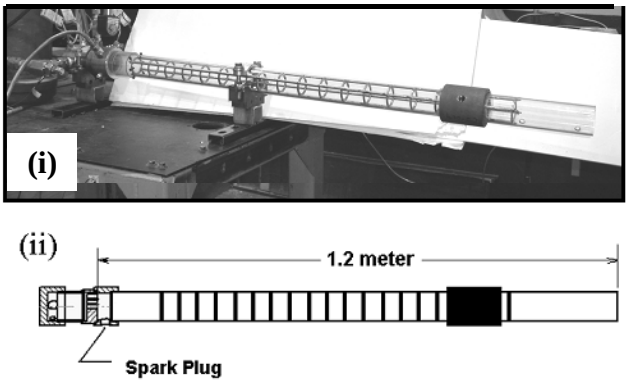

Figure 1: Photo of the PDE facility showing (i) transparent DDT section, and (ii) cross-section of 50 mm diameter benchmark PDE tube.

Pressure traces were obtained using three PCB transducers (Model Number 113A/402A) located at the end cap, 127 mm and 25.4 mm from the end of the tube. The last two transducers were used to calculate the time of flight of the pressure wave to verify detonation. Typical measured time-of-flight velocity was 2030 ± 100 m/s which is comparable to the Chapman-Jouguet detonation velocity for H2-Air of 1980 m/s. A high-speed imaging system was used to visualize the DDT process within the PDE tube. The primary component is a high framing rate digital video camera (Vision Research Phantom 7) with a framing rate between 56500 and 81000 frames per second, and a 1 □s exposure time.

Computational Method

The unsteady Reynolds Averaged Navier Stokes (RANS) equations are solved using a coupled, unstructured solver [Chakravarthy et al., 2001], which is second-order accurate in space with total-variation-diminishing (TVD) interpolation and a nonlinear Reimann solver, namely HLLC (Harten, Lax and van Lear with Contact discontinuity). The following solver-specific features were invoked in this study: (i) implicit relaxation approach, to avoid time-step restrictions, for both flow and scalar variables, (ii) implicit boundary condition treatment, (iii) dual time stepping for convergence acceleration, (iv) use of algebraic grid approach for convergence acceleration, (v) point-wise implicit relaxation methodology to enable parallel processing capability, (vi) variable thermal and transport properties for all species, and (vii) a realizable k-□ model for modeling turbulence processes. For all the simulations reported here, viscous terms are included because they are considered to be important for the PDE cycle processes. A 2-step reduced chemical mechanism, which considers a total of 8 species (Varatharajan et al. 2001), was used for simulating C_2H_4-O_2-diluent chemical reactions.

COMPUTATIONAL DOMAIN

IDEAL TUBE

The ideal PDE tube configuration used in the present study is a two-dimensional axisymmetric geometry, 1.43 m in length and 0.038 m in diameter. This geometry is the same as the idealized PDE geometry considered in a previous experimental study (Hinckley, 2003) in which performance measurements were reported. The unstructured grid that was used for the ideal tube without obstacles is the same as reported earlier (Tangirala et al., 2003). The computational domain extends to a length of 1.62 m (5 diameters in the axial direction at the exit of the tube) and the maximum radial coordinate of the domain outside the tube is 0.19 m (5 diameters in the radial direction at the exit of the tube). The grid spacing is □x = 0.7 mm and □y = 0.7 mm inside the tube, and the total mesh size is 75000 elements. A dual time-stepping method in which the global CFL number (defined as (u+c)*dt/dx where u is the local convective speed, c is the speed of sound, dx is the spatial grid spacing and dt is the global time step) of 0.1-1.0, was specified for all the simulations reported here.

BENCHMARK TUBE

The benchmark PDE tube configuration used in the present study is a two-dimensional axi-symmetric geometry, 1.27 m in length and 0.051 m in diameter. Figure 2 shows the geometry of the benchmark PDE tube with obstacles. Care was taken to model the upstream geometry with local 3D features in the context of a 2D axisymmetric assumption, while preserving upstream volume and surface-to-volume ratio in the geometric model. For the benchmark tube geometry with internal obstacles (Fig. 2), the blockage ratio, defined as the ratio of obstacle area to the total tube cross-sectional area, is 0.43. The obstacle spacing is one diameter, and there are a total of 20 obstacles evenly distributed downstream of the fuel injector.

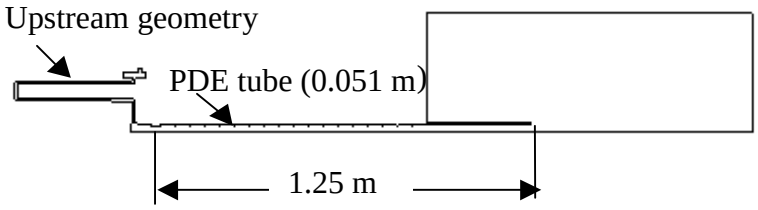

Figure 2: Computational domain (2D-axisymmetric) of the benchmark tube used for simulation of Cases 4, 5, 6 and 7.

An unstructured grid was used for discretization of the computational domain comprising of the benchmark tube with obstacles. The computational domain considered extends to a length of 1.6 m (7 diameters are considered in the axial direction at the exit of the tube) and the maximum radial coordinate of the domain outside the tube is 0.27 m (7 diameters in the radial direction at the exit of the tube). For all the results reported here, grid spacing was $\Delta x = 0.7$ mm and $\Delta y = 0.7$ mm inside the tube, and the total mesh size was 90,000 quadrilateral elements. To estimate grid resolution effects, an additional grid was used in which grid spacing considered was $\Delta x = 0.35$ mm and $\Delta y = 0.35$ mm inside the tube, and the total mesh size was 180,000 quadrilateral elements.

COMPUTATIONAL MODEL

The computational model considers an unsteady Reynold's averaged Navier Stokes (RANS) simulation with a variable property formulation including real gas effects. A realizable k-ε model was used for turbulence, and a 2-step reduced chemical mechanism (Varatharajan and Williams, 2002) was used for simulating C_2H_4-O_2 and C_2H_4-air chemical reactions. Initial conditions of 1.0 atm., 298 K and a stoichiometric C_2H_4-O_2 mixture, are specified for the ideal tube PDE simulations. For the benchmark tube, a steady state solution for a specified inlet air flowrate at an inlet temperature of 298 K serves as the initial condition. The boundary conditions for the domain outside the tube are: the back pressure condition of 1 atm., for the right (downstream) boundary condition in the axial direction and far stream boundary conditions for all other external boundaries. In addition, fuel (C_2H_4) is brought in separately using either a timing valve model (to simulate a fuel valve) at a specified boundary surface or a volumetric source term in a range of interior elements.

For the case of the ideal tube, a shock-induced detonation initiation model is used. This model was described in detail in an earlier investigation of detonation initiation (Tangirala et al., 2003). In the case of the benchmark tube, the simulation of weak/DDT initiation is achieved by adding thermal energy (u''') at a rate of 125 W, as a volumetric source to a range of tagged ignition cells, for a time duration of 2 ms. A parametric study in which u''' is varied by ±50% showed significant effect on DDT run-up distance (by ± 15%), however it had less than ± 5% effect on key predictions of the present investigations namely, thrust, impulse per unit volume, and fuel-specific impulse of the benchmark tube PDE. Similarly, increasing the grid size by a factor of 2 resulted in a decrease of the predicted run-up distance by 20%; however it had less than ± 5% effect on the rest of the key predictions of interest for the benchmark tube PDE.

SUMMARY OF VARIATION OF PARAMETERS

Table 1 shows a summary of the ranges of parameters varied in order to understand the effect of bulk velocity on both fuel-air mixing and the performance parameters, namely thrust (T), impulse per unit volume (I_v) and fuel-specific impulse (I_{spf}). The bulk velocity of the flow through the benchmark PDE is varied by changing the air mass flowrate. A range of 0.0682 – 0.182 kg/s in mass flowrate results in a variation of 30-80 m/s in the bulk velocity. The fuel fill time for 100% fill is determined using the tube length divided by bulk velocity, resulting in a range of 42-17 ms for 100% fill.

Case #	Inlet Air Flowrate (kg/s)	C_2H4_+ Oxidizer	Fuel Fill Time (ms)
1	0	O_2	N/A
2	0	O_2	N/A
3	0	Air	N/A
4	0.0682	Air	50
5	0.0682	Air	42
6	0.125	Air	24
7	0.182	Air	17

Ideal tube
Benchmark tube

Table 1: Summary of tube PDE run conditions, including those chosen to study the effect of bulk velocity of the inlet air flow on PDE cycle operation.

Validation of the Computations for an ideal TUBE PDE
Simulations of an ideal tube PDE fueled with a stoichiometric mixture of C_2H_4-O_2 are used to both validate the computational method and the ability of the 2-step reduced chemical mechanism to model detonation propagation and to obtain performance estimates. A shock-induced ignition of the mixture is simulated by introducing a high temperature and high pressure region (2000 K and 10.0 atm, respectively) 5 mm thick at the closed end of the tube. The C_2H_4-O_2 mixture is initially at 1 atm. (P_0), and 298 K (T_0), and at an equivalence ratio (ϕ_0) of 1.0. Autoignition occurs after an induction delay, which is a strong function of local temperature, in a region between the leading shock wave and the contact surface (Wu and Yang, 2000). Hence, the initial temperature has a strong impact on the occurrence/ non-occurrence of detonation initiation. Subsequent heat release results in pressure waves which couple with the leading shock wave to form a detonation. For lower initiation-region temperatures (Ts < 1000 K), no detonation was initiated. The initiation-region pressure has only a secondary effect through the shock compression of the fresh reactants, which raises the temperature of the fresh mixture and thus influences the initiation of detonation.

Figure 3 shows the predicted variation of normalized combustion wave velocity, normalized with Chapman-Jouguet (CJ) detonation velocity (V_{CJ} ~ 2370 m/s), along the length of the ideal PDE tube. The detonation velocity is calculated from time-of-arrival of pressure peaks at various locations along the length of the tube. During the initial part of the transient (time < 50 μs or x < 0.1 m), the flow near the spark region was found to be unsteady, which is reflected in the predicted time evolution of combustion wave velocity. For x > 0.1 m, the predicted detonation velocity is independent of axial distance (x) or transient time and is in close agreement with the CJ velocity (V_{CJ}). The total time for the detonation to traverse the length of the tube (1.43 m) is 550 μs.

Figure 4 compares the predicted pressure-time traces adjacent to the closed end of an idealized PDE tube with test measurements of the Stanford single shot ideal PDE tube (Hinckley, 2003). Overall comparison shows good agreement between predicted and measured pressure–time traces. Two noteworthy differences are noted as follows. At the beginning of the transient (t ~ 0.0), the deviation of the predicted pressure from the measured value is attributed to the shock-induced initiation model, which was used in the simulations as opposed to spark-induced initiation in the experiments. In addition, the fluctuations in the predicted pressure time trace is not as pronounced when compared to the fluctuations in the measured pressure-time trace. The predicted 'plateau' pressure of 11.5 bar is in close agreement with the test measurements and with the value reported by Kailasanath et al., 2002.

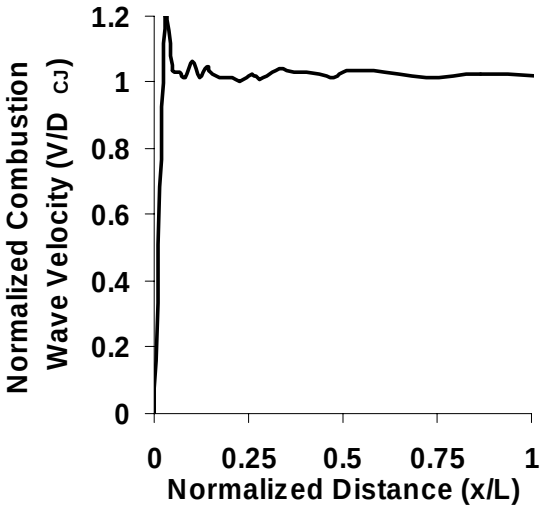

Figure 3: Predicted detonation velocity as a function of normalized axial distance for an ideal PDE tube during the detonation propagation.

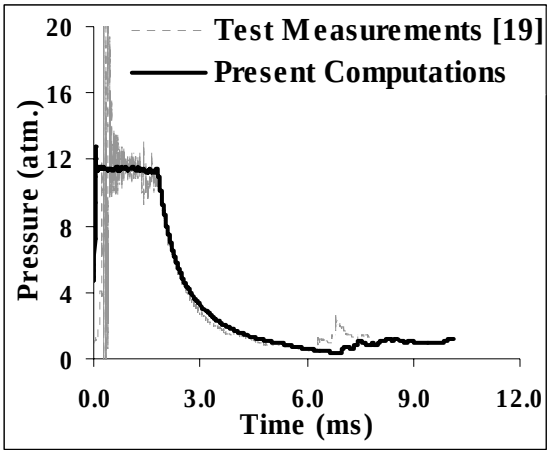

Figure 4: Comparison of predicted pressure at the closed end of the tube as a function of time with Stanford ideal tube PDE test measurements (Hinckley, 2003).

The performance metrics of the ideal PDE tube for the case of stoichiometric C_2H_4-O_2 mixture obtained using the 2-step reduced mechanism are given below. Figure 5 shows the cumulative net impulse during the blowdown process. The predicted net impulse during the blowdown of a single shot PDE cycle is estimated to be 3.2 N.s. The predicted impulse per unit volume (I_v) is 2082 N-s/m3, the predicted mixture-based specific impulse (I_{sp}) is 167s and the fuel-based specific impulse (I_{spf}) is 741 s. Table 2 shows the comparison of the predicted performance parameters with existing data in the literature (Kailasanath et al., 2002; Hinckley, 2003; Cooper et al., 2001). The performance parameters are in close agreement with the performance predictions/measurements reported by Kailasanath et al., 2002; Cooper et al., 2001; Hinckley, 2003. In summary, the computational method using a 2-step reduced chemical mechanism for C_2H_4-O_2 mixture successfully simulates the propagation and blowdown processes of an ideal tube PDE. In the comparisons for the ideal-tube PDE (Table 2), the analytical predictions of I_{spf} (Wintenberger et al., 2001) are a little lower (~ 11%) than the other results because of (i) the modeling assumptions such as direct initiation of detonation and (ii) the uncertainties associated with specification of the analytical model parameters. The performance estimates show good agreement with other existing data in the literature as shown in Table 2.

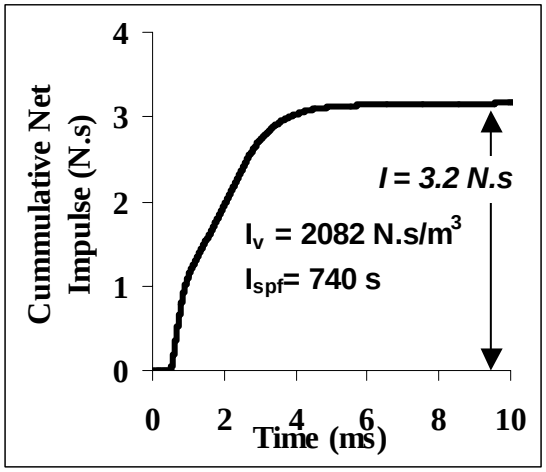

Figure 5: Variation of cumulative impulse as a function of time for an ideal PDE tube using a stoichiometric mixture of C_2H_4 and O_2 during the blowdown.

	P_3 (atm)	I_V (N.s/ m$^{3)}$	I_{spf} (sec)
Test measurements, Hinckley, 2003	11.5	2089	720
Test measurements, Cooper et al. 2001	N/A	2136	758
Analytical predictions, Wintenberger et al. 2001	11.0	1843	668
CFD predictions, Kailasanath et al. 2002	12.0	2100	732
Present CFD predictions	11.5	2082	740

Table 2: Comparison of impulse per unit volume and fuel specific impulse of the ideal tube PDE (Case 2) with results from previous studies.

simulation of Benchmark tube PDE cycle and comparison with experiment

The main processes of the PDE cycle are summarized in Table 3. For both the experiments and calculations in this report, the initial conditions in the PDE tube are stoichiometric ethylene-air at the mixing element during fill, 101.3 kPa outlet pressure, 300 K inlet temperature, 0.068 kg/s average mass flow and an operating frequency of 10 Hz. For these conditions, the approximate duration for each part of the cycle is shown in Table 3.

PDE cycle process	Cycle Time (ms)
Fuel fill	0 - 50.0
Ignition Transition Propagation	50 - 52 52 - 53.2 53.2 - 53.6
Blowdown	53.6 - 58.0
Purge	58.0 - 100.0

Table 3: PDE Cycle Timing for Case 4.

STEADY FLOW

Steady flow calculations reveal the basic features of the flow through the PDE tube. For an average mass flow through the PDE tube of 0.068 kg/s, Fig. 6a shows the axial velocity and pressure through the tube. Due to the pressure drop across each orifice, the velocity increases through the DDT section. For these conditions and a blockage ratio of 0.43, the pressure drop in the DDT section is about 5%. The pressure drop downstream of the DDT section is negligible. This value is in good agreement with the pressure drop measured in the rig at the same conditions.

FUEL FILL

At the upstream mixing element, fuel is added to the air resulting in an initially uniform mixture. As this mixture flows through the DDT section, there is a core flow convecting fresh charge at ~80 m/s as shown in Fig. 6b(ii). This core flow is moving much faster than the bulk velocity of 30 m/s that would occur with no obstacles. If the duration of the fill cycle is timed to achieve one volume change in the tube, then a lean fuel-air mixture will exit the tube before the fill cycle is complete. As a consequence, the fill time would need to be reduced to avoid sending fuel out the end of the tube, resulting in pockets of leaner mixture near the wall between obstacles. The resulting axial and radial profiles of fuel concentration deviate from the goal of achieving a uniform, 100% charge of fresh detonable mixture as shown in Fig. 6b(iv).

DETONATION INITIATION AND PROPAGATION

In the benchmark experiments, the combustion process is initiated via a weak spark (~30 mJ) timed to closely coincide with the end of the fill cycle. The spark plug is located near the head end of the PDE tube. A set of seventeen orifice plates (blockage ratio = 0.43) is used to reduce the run-up distance to detonation. Detonation initiation was visualized by imaging chemi-luminescence through a transparent polycarbonate tube with a high-speed video camera. For the imaging runs, the PDE was fired in short bursts with the valve and spark timing consistent with 10Hz operation. All other parameters (mass flow, inlet temperature and pressure, etc) were kept the same as for Case 4.

Figure 7 shows a series of images of a DDT event where time zero is taken when the spark flash is detected at the head end. The dark sections between obstacles 8 – 9 and beyond obstacle 16 correspond to metal support features outside the tube. The spark is initiated at the end of the fill cycle when the tube is filled with a combustible mixture (Fig. 7(i)). After 2.6 ms, a turbulent flame appears from the left and propagates to the right (Fig. 7(ii)). The flame continues to accelerate, and more intense chemiluminescence is observed at obstacle 12 (Fig. 7(iv)). The frame of Fig. 7(vi) shows a nearly planar detonation emerging from the DDT section, while there is still considerable chemiluminescence from the turbulent combustion region.

The predictions of flame propagation and transition to detonation are shown in Fig. 8. In the numerical simulation, the combustion process is initiated by depositing energy in the same axial location as the spark plug in the PDE experiments. Energy deposition for initiation corresponds to the end of the fuel fill cycle. Figures 8a(i) through 8a(iv) show a turbulent flame propagating through the obstacles. Transition to detonation is observed in Fig. 8a(viii), which shows the formation of a planar shock front, and the wave velocity approaches Chapman-Jouguet (C-J) velocity. The detonation achieves characteristics of a steady-state detonation as it propagates toward the exit of the tube (Fig. 8b). The predicted time of flight (the time interval between the spark initiation and the exit of the detonation wave from the tube) of 3.6 ms agrees very closely with the experimentally measured value of 3.8 ms.

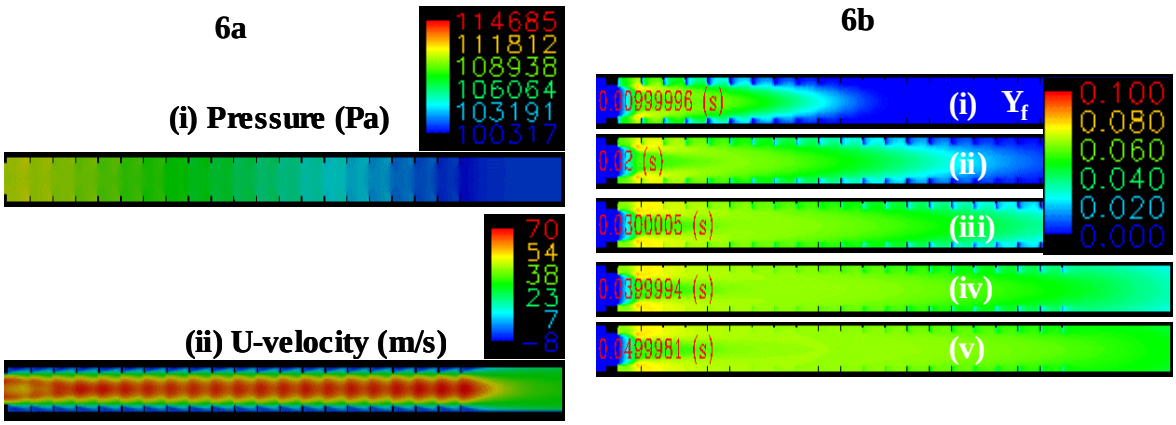

Figure 6: (a) Predicted steady state contours (pressure and U-velocity) through the midsection of PDE tube at steady state flow conditions of P_{in} = 1.15 bar, T_{in}=300K, mair = 0.068 kg/s, and (b) predicted fuel mass fraction contours at various times during the fuel fill process (Case4).

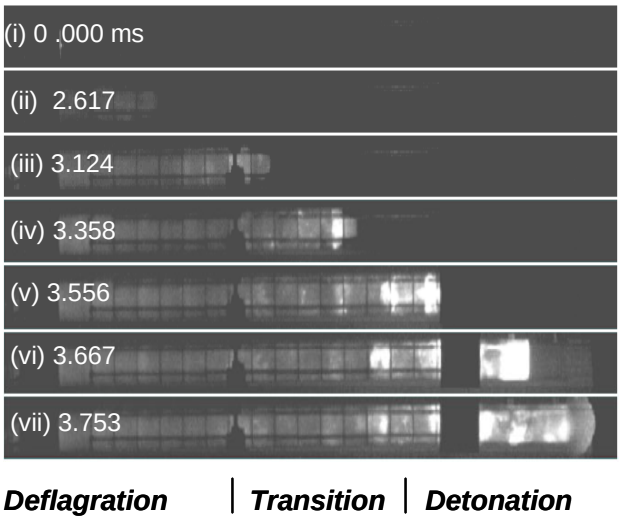

Figure 7: High-speed imaging of ethylene-air DDT in PDE tube at various times of the PDE cycle (Case 4).

BLOWDOWN AND PURGING

Figure 8c shows predicted time evolution of oxygen concentration contours during the purging process. At the end of detonation and blowdown processes, oxygen is completely consumed. As the blowdown is completed, the pressure in the end cap plenum decreases, and the purge flow enters the tube. Figure 8c(i) shows the oxygen mass fraction at the end of the blowdown process, and Fig. 8c(iv) shows the oxygen mass fraction contours at the end of purge process. The purging process is completed approximately 30 ms after the completion of the blowdown process.

The blowdown process is responsible for most of the thrust production. There are three phases of blowdown: emergence of the blast wave, supersonic blowdown, and subsonic blowdown. A comparison of measured and numerical prediction of the initial phase of blowdown is shown in Fig. 9. The numerical predictions are presented as numerical schlieren images produced by post-processing the results. As the detonation emerges from the tube, the reaction front separates from the leading shock wave. The shock wave wraps around the tube and travels both upstream and downstream. The hot combustion products follow the leading shock, but the reaction zone quickly de-couples from the leading shock wave.

PREDICTED AND MEASURED DDT RUN-UP TIME AND DISTANCE

The transition of the deflagration to detonation occurred in the experiment as well as simulation. A key qualitative difference between the measurements and calculations is the axial location where the transition occurs within the benchmark tube. More detailed comparisons between the measurement and calculation of DDT are presented in the X-t diagram (Fig. 10(i)) and the variation of leading wave velocity vs. axial distance diagram (Fig. 10(ii)). In the experiment, the transition occurred (determined as the axial distance at which the abrupt change in the velocity of the leading wave leading to a quasi-steady veloity at/near CJ veloity) at the 17^{th} obstacle while the predictions showed that the transition occurred at the 11^{th} obstacle (as shown in Fig. 10 (ii)) and the difference between these two values is 35%. The measured time of flight of the combustion wave in the benchmark tube (defined as the time at which detonation emerges from the benchmark tube relative to spark initiation time) was 3.8 ms, while the predicted time of flight was 3.6 ms and the difference between these two values is 5% (as shown in Fig. 10(i)). The numerical predictions reveal rapid flame acceleration leading to over-driven detonation and finally relaxing to C-J velocity. This behavior agrees well with experimental observations of the DDT process reported by Cooper et al., 2001.

The ability to predict time scales of detonation initiation and detonation propagation is important to estimate the maxumum operating frequency of the PDE. It also enabled a realistic simulation of all the processes of the repeating cyclical operation of the benchmark tube PDE. The abovementioned discrepancy between the predicted and the measured values of the run-up distance may be attributed to the inadequacy of the combustion model to accurately simulate turbulence-chemistry interactions. However, the applicability of a single combustion model to cover all the regimes of turbulent flames, which are encountered in a confined high-speed deflagration flame transitioning to a detonation (flame ignition regime, turbulent flamelet regime, broken reaction regime during the shock-flame interactions and transition regime (Tangirala et al., 2004)) is yet to be established. Even if such a model were to exist, criteria are yet to be developed for the use of a separate combustion model for each of the turbulent combustion regimes. The discrepancy in the prediction of the run-up distnace (~35%) when compared to the measured value, highlights the need to model the turbulence-chemistry interactions more accurately by resolving the relevant scales of turbulence and reaction. A close agreement in the time of flight in the benchmark tube enabled the simulation of the cyclic operation of the benchmark tube PDE tube in order to assess its performance.

PREDICTED AND MEASURED PRESSURE-TIME TRACES

Figure 11 shows comparisons of predicted and measured pressure-time traces in the end cap cavity. The comparison of the head-end pressure traces shows that the qualitative features of the measured pressure-time traces are captured by the simulations. The predicted mean plateau pressure of 5.0 atm is less than the measured value of 6.6 atm by 25%. The discrepancy between the measured and the predicted values can be attributed to 2D axisymmetric assumption in modeling the upstream geometry of the benchmark tube.

Influence of bulk velocity on thrust and Fuel air mixing

The benchmark tube study includes all the processes of a multi-cycle PDE with realistic geometry. This results in differences in performance between the benchmark tube and the ideal PDE tube. One important parameter in the benchmark PDE study is the bulk velocity of air flow ($V_b = m_{air} / \rho A_e$ where m_{air} is air flow rate (kg/s), ρ is the density of air at initial conditions (kg/m^3), and A_e is the tube exit area (m^2)) during the fuel fill and purge processes. This velocity, V_b, influences gas exchange during purge, fuel-air mixing, DDT and overall thrust production. In this section, the effect of bulk velocity of flow through the benchmark tube on fuel-air mixing and thrust is studied, while keeping all other parameters fixed.

8a

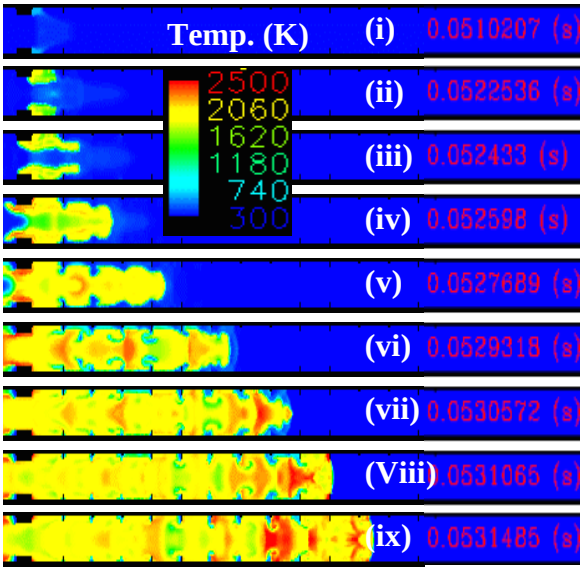

8b

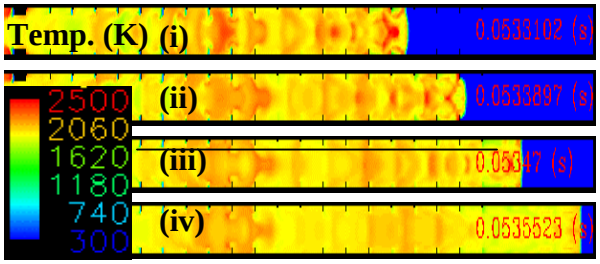

8c

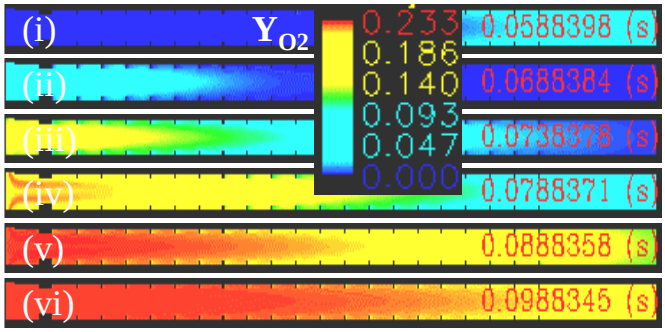

Figure 8: Predicted temperature contours at various times during (a) the detonation initiation process, (b) detonation propagation process, and (c) Predicted oxygen mass fraction contours at various times during blowdown and purge processes (Case 4).

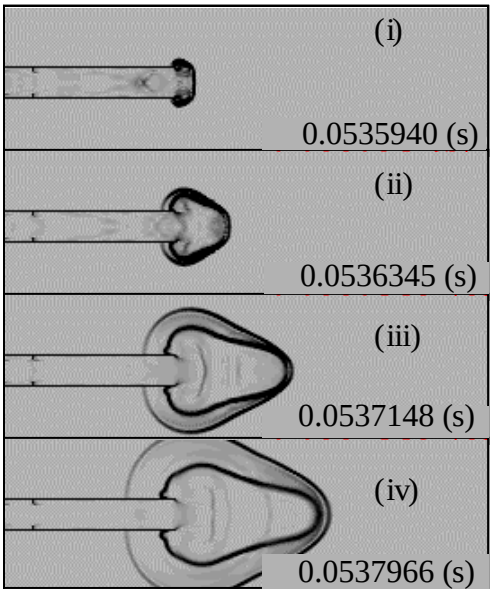

Figure 9: Predicted schlieren contours at various times of the blowdown process (Case 4).

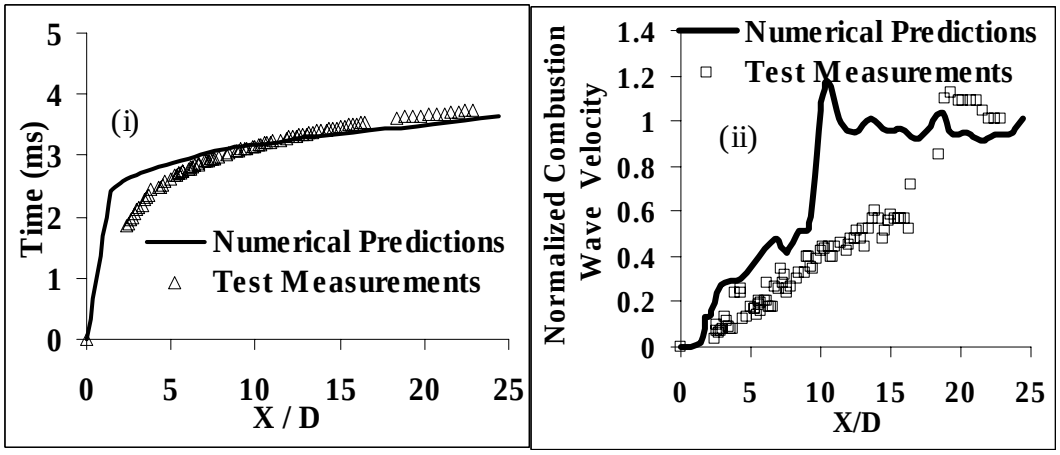

Figure 10: Comparison of numerical prediction and measurement of (i) X-t diagram and (ii) velocity-position

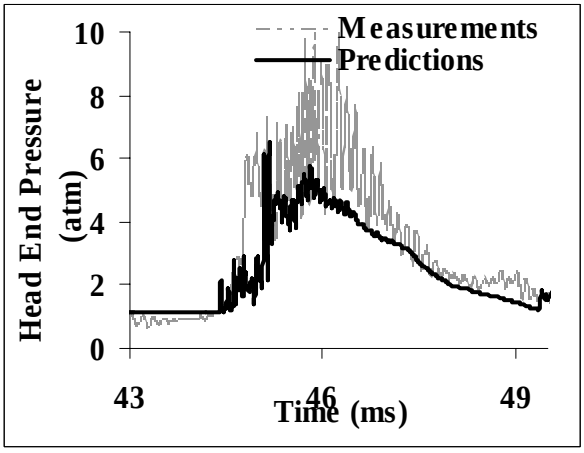

Figure 11: Comparison of predicted and measured pressure-time traces in the end-cap cavity (Case 5).

THRUST ESTIMATION

The key parameters for determining the net impulse over a PDE cycle are momentum flux and pressure forces acting in the axial direction at the tube exit. Here, the thrust calculation is illustrated by using a control volume, as shown in Figure 12.

Figure 12: Control volume used for thrust estimations for Cases 2, 4, 5, 6 and 7.

The impulse generated by the PDE is estimated using the control volume (Fig. 12) and can be written as follows:

$$I = \int_0^{t_{cycle}} \left[\dot{m}_e u_e - P_e A_{id} + P_a A_{od} - P_{e'} A_{tw} \right] dt \rightarrow (1)$$

Where

I: Net impulse generated by the PDE (N.s),

F_x: Instantaneous net forces acting on the control surface (neglecting the accumulation terms) in the x-direction (N)

m_e: mass flow rate at the exit of the tube (kg/s),

u_e: x-velocity component at the exit of the tube (m/s),

P_e tube exit pressure (Pa), A_{id} is the corresponding area (m^2),

$P_{e'}$ exit pressure adjacent to tube walls (Pa), A_{tw} is the corresponding area (m^2),

t_{cycle} = 1/ f, f is the frequency of PDE operation (Hz), and

P_a ambient pressure (Pa) A_{od} is the corresponding area (m^2).

The impulse per unit volume (I_v) is defined as $I_v = I/V$, where V is the volume of the ideal tube PDE. The fuel-specific impulse of the ideal tube PDE is defined below, following Wintenberger et al., 2001.

$$I_{spf} = \frac{I_v}{(\rho . y_F . g)} \rightarrow (2)$$

Where □ is the density of the fuel-air mixture at initial conditions (kg/m^3), y_F is fuel mass fraction in the initial mixture and g is acceleration due to gravity (m/s^2). For the case of a benchmark tube, the fuel-specific impulse is adjusted by fuel fill fraction, FF (defined as the ratio of the mass of fuel at the end of fuel fill process in the tube to the total mass of fuel injected into the tube) as given below.

$$I_{spf} = \frac{I_v}{(FF . \rho . y_F . g)} \rightarrow (3)$$

To estimate cumulative impulse using Eq. 1, knowledge of mass flow rate, velocity and pressure at the exit as a function of time is needed. This information is easily extracted from the unstructured CFD predictions of flow and scalar fields at the tube exit plane. Impulse estimations using control volume 1 and Eq. 1 are obtained for the benchmark cases 2, 4, 5, 6 and 7. A specific correction was applied to the thrust estimated by Eq. 1 for benchmark tube cases (4, 5, 6 and 7). This correction is equal to the impulse generated by the tube operating under steady flow conditions with no chemical reactions and is directly proportional to the square of the mass flow rate of the mixture flowing through the tube.

The cumulative impulse generated by a PDE is the sum of contributions to impulse during the supersonic blowdown and the subsonic blowdown. The exit Mach number for Case 5 during the blowdown is plotted in Fig. 13 and shows the relative

duration of each part of the blowdown. Initially, there is choked supersonic flow for a period of 2 ms (20% of the total blowdown time of 10 ms). The remainder of the blowdown (80%) is a subsonic blowdown. Figure 13 shows that the exit Mach number drops to a minimum after approximately 5 ms into the blowdown process and then increases again. This is caused by variation in depressurization rate from the tube due to obstacles.

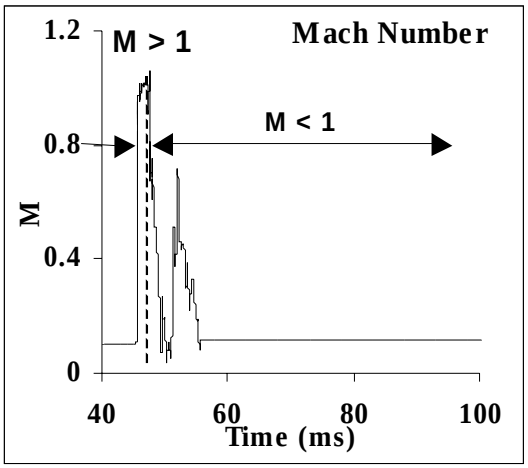

Figure 13: Time variation of the tube exit Mach number (M) during the blowdown (Case 5).

The cumulative impulse generated by the benchmark tube (Case 5) is shown in Fig. 14. It attains a constant value of 1.6 N.s in approximately 19 ms from the start of the blowdown process. This includes a correction of 0.2 N.s for the thrust developed during steady state initial conditions with no reactions. This cumulative impulse translates into a value of 16 N for thrust ($T = I * f$, where T denotes thrust (N)) generated by the benchmark tube operating at 10 Hz and a mass flow rate of 0.068 kg/s, a value of 626 N.s/m3 for impulse per unit volume (I_v) and a value of 947 s for fuel-specific impulse (I_{spf}).

IDEAL TUBE VS. BENCHMARK TUBE

The operation and thrust estimations of an ideal tube PDE are well documented in the literature. The key differences between the simulation of an ideal tube and the simulation of the benchmark tube for obtaining thrust estimates can be summarized as follows: in an ideal tube PDE, the fuel is initially premixed with air, and the fuel-air mixture is well characterized by the initial condition specification. In addition, the ideal tube PDE does not have any internal geometry features, which can cause a pressure drop in the system. For thrust estimation of an ideal tube PDE, it is sufficient to simulate detonation initiation, detonation propagation and blowdown processes.

The benchmark tube can be distinguished from the ideal tube in the following ways. (i) The fuel and air are brought in separately (overall equivalence ratio is 1.0, air flowrate is 0.068-0.18 kg/s) in the mixing segment of the tube, and this results in mixture nonuniformities and leads to local equivalence ratios which are less than or greater than the overall equivalence ratio. For an overall equivalence ratio of 1.0 of the fuel-air mixture, the variation in local equivalence ratios can only lower the impulse produced by the benchmark tube. (ii) The upstream section of the tube is not closed, and air flows through the system continuously except for the time interval during which high-pressure conditions exist in the tube. A strong compression pulse (retonation) is formed during the initiation process and then travels upstream causing back flow in the upstream section of the tube, resulting in a reduction of the net impulse. (iii) The benchmark tube has internal geometry features such as the DDT-promoting obstacles and a mixing element, which result in a pressure drop in the tube. These internal flow resistances can cause substantial reductions in the thrust developed by the benchmark tube.

The performance parameters, namely impulse per unit volume (I_v) and fuel specific impulse (I_{spf}) for the ideal case fueled with C_2H_4-air mixtures (Case 3), obtained using the analytical method (Wintenberger et al., 2001), are 1328 (N.s/m3) and 1839 s, respectively. The corresponding metrics for the benchmark tube (Case 7) are 764 (N.s/m3) and 1109 s respectively. The predicted decrease of 40% in I_{spf} of the benchmark tube (Case 7) when compared to the I_{spf} of an ideal tube (Case 3) may be attributed to (i) pressure drop in the benchmark tube resulting from a realistic simulation of benchmark tube internal geometry (DDT obstacles), (ii) nonuniformities in the mixture composition for the benchmark case as opposed to assumed uniform mixture composition for the case of an ideal tube and (iii) backflows in the inlet

section of the benchmark tube due to a compression wave propagating into the upstream geometry. Further work is required to quantify the contribution of each of these factors.

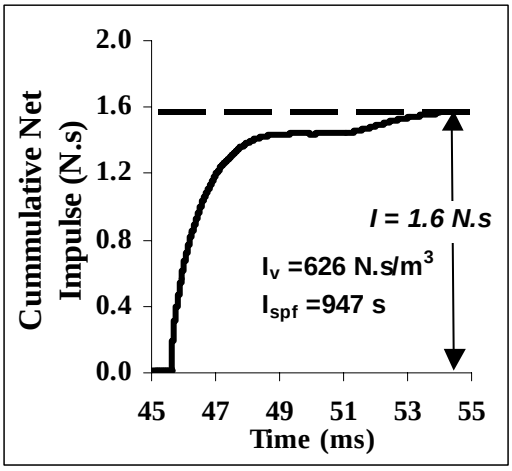

Figure 14: Time variation cumulative impulse for the PDE cycle operation of the benchmark tube (Case 5).

EFFECT OF BULK VELOCITY ON FUEL AIR MIXING

In order to understand the effect of bulk velocity on the fuel air mixing in the benchmark tube, the bulk velocity of the air flow (V_b) is systematically varied from 33 m/s for Case 5 to 85 m/s for Case 7. For all the cases considered, the fuel fill fraction (defined as the amount of fuel injected into the tube divided by the amount of fuel in the tube corresponding to a stoichiometric mixture) is maintained as close to unity as possible by varying the fuel fill time. This resulted in decreasing the fuel fill time from 42 ms (Case 5) to 17 ms (Case 7). Figure 18 shows the axial variation of the centerline fuel mass fraction, at the end of the fuel fill process for varying bulk velocities (33, 59, and 85 m/s). Near the mixing element where the fuel is injected into the air flow, ($x < 0.2$), the predicted fuel mass fraction is higher than the stoichiometric value (0.063). For $x\ 0.2 < x < 1.2$, the predicted fuel mass fraction is lower than the stoichiometric value.

Figure 15 also shows a more pronounced effect of bulk velocity on fuel air mixing for Case 7 (85 m/s) than for Cases 5 and 6 (33 and 58 m/s respectively). The centerline fuel mass fraction decreases more rapidly for Case 7 due to higher core flow velocities. This results in a mixture equivalence ratio of 0.75 near the end of the tube for higher bulk velocity. This nonuniformity in fuel air mixing in the axial direction results in the DDT process occurring upstream in a rich/stoichiometric mixture and the detonation propagation occurring downstream in a leaner mixture.

Figure 16 shows the axial variation of the predicted centerline fuel mass fraction at three distinct normalized radial locations (r/D_t = 0.0, 0.39 and 0.78, where r is the radial position (m) and D_t is the tube diameter (m)). The first two curves denoted by 1 and 2 are located in the core flow, one at the centerline and another off-centerline. The third curve denoted by 3 is radially located inside the obstacle region (as seen by the broken segments of the curve, caused by the presence of obstacles). Figure 16 shows that the radial variation in both the igniter section and the obstacle region of the benchmark tube is very significant as shown by the large radial gradients of the predicted fuel mass fraction in regions outside the core flow. The effect of these nonuniformities of mixture composition in the radial direction are expected to impact the flame acceleration and the detonation initiation processes.

EFFECT OF BULK VELOCITY ON THRUST

Figure 17 shows the effect of varying the bulk velocity on the net impulse generated by the benchmark tube PDE for Cases 5, 6, and 7. For all cases considered, the blowdown time scale (t_b) over which the performance metrics are estimated is set to 10 ms despite the variations in the bulk velocity and the fuel fill time. For all the performance metrics reported in this subsection, an effort was made to maintain a constant value of unity for the fuel fill fraction (*FF*), by using an *a priori* estimation of the fuel fill time ($t_{fill} = L/V_b$, where L is the tube length). However, detailed computations show that the fuel fill fraction (*FF*) is less than unity because a fraction of the fuel leaves the tube before all the fuel is injected during the fuel fill process. The combined effect of the decreased value of fuel fill fraction (*FF*) and the fuel air mixing nonuniformities

(which decrease the average mass fraction of the fuel at high bulk flow velocities) results in a small increase (13%) in the predicted fuel-specific impulse. In summary, the bulk velocity together with fuel fill fraction (*FF*) are predicted to have an impact on the performance metrics by affecting the fuel-air mixing processes in the benchmark tube PDE.

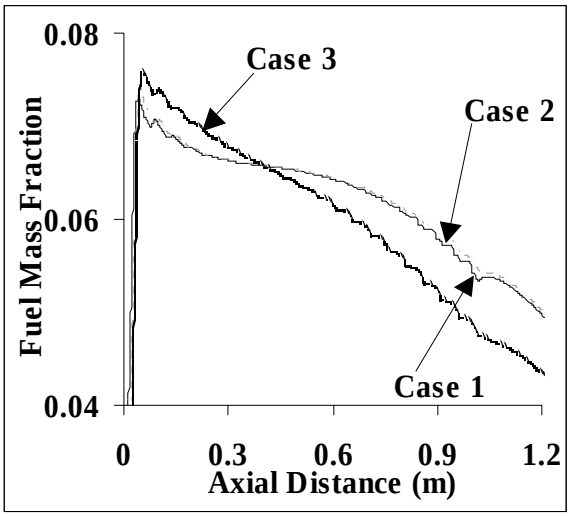

Figure 15: Predicted axial variation of fuel mass fraction at the end of fuel fill process for varying bulk velocities (33, 59, and 85 m/s) of the flow through the benchmark tube.

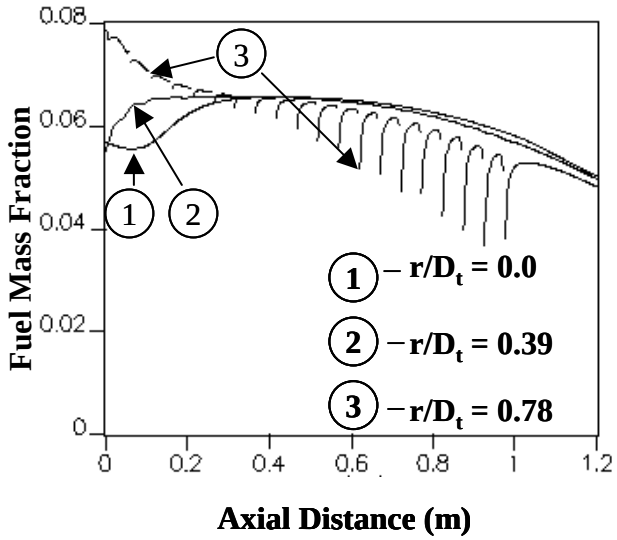

Figure 16: Predicted axial variation of the fuel mass fraction at the end of the fuel fill process at various radial locations for Case 7 (bulk velocity = 80 m/s and D_t = 5.09 cm).

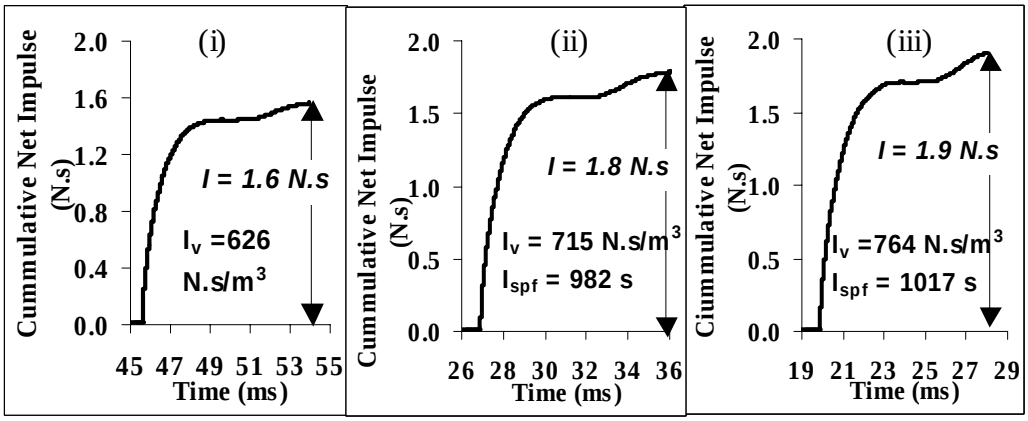

Figure 17: Effect of bulk velocity on predicted cumulative impulse for (i) Case 5, (ii) Case 6 and (iii) Case 7.

	Thrust (N)	I_V ($N.s/m^{3)}$	I_{spf} (sec)
Case 5	16	626	947
Case 6	18	715	982
Case 7	19	764	1017

Table 4: Summary of performance estimates as a function of bulk flow rate through the benchmark PDE tube fueled with C_2H_4-air mixture.

Conclusions

Computational and experimental investigations of performance are reported for a Pulsed Detonation Engine (PDE) operating in a cycle, using ethylene-air mixtures. Simulations are performed for two geometry configurations, namely an ideal tube PDE with a smooth wall fueled with a premixed C_2H_4-O_2 charge, and a benchmark tube PDE with internal geometry and a valveless air supply fueled with a C_2H_4-air mixture. A 2-step reduced chemical mechanism for C_2H_4-air is used to model chemical reactions. The computational method simulates all the processes of the PDE cycle (fill, DDT, detonation propagation, blowdown and purge). Experiments are performed to validate the simulation of the key PDE cycle processes. Experimental measurements include DDT visualizations and dynamic pressure measurements.

Performance estimates namely the fuel-specific impulse of an ideal-tube PDE, obtained using the 2-step reduced mechanism for a C_2H_4-O_2 mixture, are in good agreement with existing test measurements from the literature. The computational method successfully simulates the propagation and blowdown processes of an ideal tube PDE. The performance estimates show good agreement with existing data in the literature.

Simulations of the benchmark tube PDE yield important insights into continuous cycle operation. Comparisons of experimental and computational visualizations shows good agreement in cycle process time scales. However, run-up distance is underpredicted, indicating a need to improve the flame propagation mechanism. The predicted decrease in the I_{spf} for the benchmark tube when compared to the I_{spf} of an ideal tube, may be attributed to nonuniformities in the mixture composition, pressure drop resulting from internal geometry (DDT-promoting obstacles), and backflows in the valveless benchmark tube due to a compression wave propagating into the upstream geometry. Increasing the bulk velocity of the flow through the benchmark tube has an adverse effect on the fuel/air mixing processes. The bulk velocity impacts the performance metrics by affecting the fuel fill processes in the benchmark PDE.

ACKNOWLEDGEMENTS

Authors wish to acknowledge the technical discussions with Dr. J. Shepherd of California Institute of Technology, and Dr. K. Kailasanath of Naval Research Laboratories. Ideal tube data, provided by K. Hinckley of Stanford University is sincerely acknowledged. Authors acknowledge the technical help with experimental setup provided by Dr. A. Rasheed and E. Cornell of General Electric Global Research. Computational support provided by I. Schild of General Electric Global Research and Dr. S. Palaniswamy of Metacomp Technologies, Inc. is sincerely appreciated.

References:

Brophy, C.M., Netzer, D., and Forster, D., (1999) Operation of JP-10/Air for Pulse Detonation Engine, *AIAA-2000-3591*

Chakravarthy, S., Goldberg, U., Batten, P., Palaniswamy, S., and Peroomian, O., (2001), Some Recent progress in Practical Computational Fluid Dynamics, *AIAA-2001-0136*

Cooper, M., Jackson, S., Austin, J.M., Wintenberger, E., and Shepherd, J.E., (2001) Direct Experimental Impulse Measurements for Detonations and Deflagrations, *AIAA 2001-3812*

Eidelman, S., and Grossmann, W., (1999) Pulse Detonation Engine: Experimental and Theoretical review, *AIAA paper 99-1067*

Glassman, I., (2000) *Combustion*, 2nd Edition, McGraw Hill, New York

Hinckley, K., (2003) Stanford Tube PDE Experimental Data, *personal communications*, Mechanical Engineering Department, Stanford University, CA

Kagan, L., and Sivashinsky, S., (2003) The transition from deflagration to detonation in thin channels, *Combustion and Flame*, 134, 389-397

Kailasanath, K., Patnaik, G., and Li, C., (2002) The Flowfield and Performance of Pulse Detonation Engines, *Twenty-ninth (International) Symposium on Combustion*, The Combustion Institute, PA, 29

Kailasnath, K., (2002) Recent Developments in the Research of Pulse Detonation Engines, *AIAA 2002-0470*

Kailasnath, K., Li, C., and Patnaik, G., (2001) Multilevel Computational Studies of Pulse Detonation Engines, AIAA-2001-1172

Khokhlov, A. M., Oran, E. S., and Thomas, G. O., (1999) Numerical Simulation of Deflagration to Detonation Transition: the Role of Shock-flame Interactions in Turbulent Flames, *Combustion and Flame*, 117, 323-339

Kline, R., (2000) Flame Acceleration and Deflagration to Detonation Transition in Nuclear Safety, *OECD Nuclear Energy Agency Report* NEA/CSNI/ R, (2000) 7

Lee, J. H. S., (2001) Detonation Waves in Gaseous Explosives, *Hand Book of Shock Waves*, 3, Academic Press, 2001

Mohanraj, R., Merkle, C. L., and Ebrahimi, H. B., (2001) Modeling of Pulse Detonation Engine Operation," *AIAA 2001-0475*

Oran, E. S., and Khokhlov, A. M. (1999) Deflagrations, hot spots and the transition to Detonation, *Phil. Trans. R. Soc. Lond. A* (1999) 357, 3539-3551

Povinelli, L. A., and Youngster, S., (2003) Real Gas Effects on the Performance of Hydrocarbon-fueled Pulse Detonation Engines," *AIAA 2003-0712*

Shepherd, J. E., and Lee, J. H. S., (1992) On Transition from Deflagration to Detonation," *Major Research Topics in Combustion*, Springer Verlag, Hampton, VA

Tangirala, V., B. Varatharajan, B., and Dean, A. J., (2003) Numerical Simulations of Detonation Initiation, *AIAA-2003-0716*

Tangirala, V., B. Varatharajan, B., Pinard, P. F., and Dean, A. J., (2004) Application of Reduced Chemical Mechanisms for PDE Initiation, *AIAA-2004-1209*

Varatharajan, B. and Williams, F. A., (2002) Ethylene Ignition and Detonation Chemistry, Part 2: Ignition Histories and Reduced Mechanisms, *Journal of Propulsion and Power*, Vol. 18, No. 2, pp. 352-362, 2002

Varatharajan, B., Petrova, M., Williams, F. A., and Tangirala V. E., (2004) submitted to *Proc. 30th Symp. (Int'l) Combust.* The Combustion Institute, PA

Wintenberger, E., Austin, J .M., Cooper, M., Jackson, *S.*, and Shepherd, J.E., (2001) An Analytical Model for the Impulse of a Single-cycle Pulse Detonation Engine, *AIAA 2001-3811*

Y. Wu and V. Yang, (2000) Numerical Simulation of Detonation with Detailed Chemical Kinetics Using the Space Time Method, *AIAA 2000-0317*

REFERENCES

1. Eidelman, S, Grossmann, W, (1992) Pulse detonation Engine: Experimental and Theoretical Review, AIAA-1992-3168

2. Glassman I (2000) Combustion 2nd Edition, McGraw Hill, New York

3. Brophy, C, Netzer, D, Forster, D, (1998) Detonation Studies of JP-10 with Oxygen and Air for PDE Development, 34th JPC, Cleveland: AIAA-1998-4003

4. Shepherd, J, Lee J, (1992) On the Transition From Deflagration to Detonation, Major Research topics in Combustion, Springer-Verlag, Hampton, Va

5. Chan, C, Dewit, W, (1996) Deflagration-To-Detonation Transition in End Gases, 26th Symposium (International) on Combustion, The Combustion Institute, pp. 2679-2684

6. Peraldi, O, Knystautas, R, Lee, J, (1986) Criteria for Transition to detonation in Tubes, 21st Symposium (International) on Combustion, The Combustion Institute, pp. 1629-1637

7. Kuznetsov, M, Alekseev, V, Yankin, Y, Dorofeev, S (2002) Slow and Fast Deflagrations in Hydrocarbon-Air Mixtures, Combustion Science and Technology, Volume 174, No. 5, pp.157-172

8. Ciccarelli G (2003) Effect of Obstacle Size and Spacing on the Initial Stage of Flame Acceleration in an Obstacle Laden Tube, Queens University, Canada

9. Ciccarelli, G, Boccio, J, Ginsberg, T (1996) The Influence of Initial Temperature on Flame Acceleration and Deflagration-To-Detonation Transition, 26th Symposium (International) on Combustion, The Combustion Institute, pp. 2973-2979

10. McManus, K, Furlong, E, Leyva, I, Sanderson, S, (2001) MEMS-Based Pulse Detonation Engine For Small-Scale Propulsion Applications, AIAA-2001-3469\

11. Meyer, T, Hoke, J, Brown, M, (2002) Experimental Study of Deflagration-To-Detonation Enhancement Techniques In A H_2/Air Pulsed-Detonation Engine, AIAA-2002-3720

12. Tangirala, V, Dean, A, Chapin, D, Pinard, P, Varatharajan, B, (2003) Investigations of Cyclic Pulsed Detonation Processes: Experiments and Calculations, 19th ICDERS

13. Tangirala, V, Dean, A, Rasheed, A, Chapin, D (2003) Performance Estimates of a Pulsed Detonation Engine, ISABE-2003-1215

14. Shultz, E, Wintenberger, E, Shepherd J, (1999) Investigation of Deflagration to Detonation Transition for Application to Pulse Detonation Engines Ignition Systems, 16th JANNAF Propulsion Symposium

15. Kailasnath, K, (2002) Recent Developments in the Research of Pulse Detonation Engines, Reno: AIAA-2002-0470